BRNO UNIVERSITY OF TECHNOLOGY
VYSOKÉ UČENÍ TECHNICKÉ V BRNĚ

FACULTY OF MECHANICAL ENGINEERING
FAKULTA STROJNÍHO INŽENÝRSTVÍ

INSTITUTE OF AEROSPACE ENGINEERING
LETECKÝ ÚSTAV

ANALYSIS OF AERONAUTICAL COMPOSITE STRUCTURES UNDER STATIC LOADING
ANALÝZA KOMPOZITNÍCH LETECKÝCH KONSTRUKCÍ PŘI STATICKÉM ZATÍŽENÍ

DOCTORAL THESIS
DISERTAČNÍ PRÁCE

AUTHOR — Ing. Jakub Cejpek
AUTOR PRÁCE

SUPERVISOR — doc. Ing. Ivo Jebáček, Ph.D.
ŠKOLITEL

BRNO 2017

Abstract

Relatively large number of private companies in the Czech Republic are producing light sport aircraft. Significant number of these airplanes use composite landing gear springs. These springs are either smaller parts that absorb energy (nose and tail gear springs) or they can be used for the main landing gear.

All these types of springs share very similar characteristics: they are made mostly of unidirectional composite of significant thickness, the main loading character is bending moment and large deformations are expected. In fact the wing main spar shares similar characteristic.

How are these products designed and analysed? Generally there are two possibilities. First possible way, to design such product, is to make just a simple analysis (closed-form solution, perhaps some spreadsheet table). The drawbacks of this method are limited capabilities and inflexible application. Second option is to perform an analysis study, perhaps even optimization loops in a professional dedicated finite element program. Of course the drawback is the price (for the program and for the engineer).

This dissertation thesis aims to develop a computer program, that will offer third possibility: thorough analysis of given products without expensive software. This program will simplify and speed up the design and strength analysis. It will allow user to quickly test different variants. Specifics of the targeted products (such as large deformations, local through-thickness stress concentrations and wrap plies) will be taken into account.

From the user's point of view the program should be simple to work with. Minimum input data with clear graphical user interface layout ensures comfortable use. Having a stand alone program (executable without any supplementary software) improves the distribution potential.

Keywords

Composite component analysis, finite element analysis, beam theory, landing gear spring, wing spar.

Abstrakt

Poměrně velké množství soukromých firem v České republice vyrábí lehká sportovní letadla. Značná část těchto letadel využívá kompozitní pružiny ve svých přistávacích zařízení. Tyto pružiny jsou buďto menší díly, absorbující energii (na přídové noze či ostruze), anebo jde celé pružnice hlavního podvozku.

Všechny tyto pružiny sdílí základní charakteristiky: jsou vyrobeny převážně z jednosměrného kompozitu s významnou tloušťkou, hlavním druhem zatížení je ohybový moment a jsou očekávány velké deformace. Podobnou charakteristiku můžeme použít i při popisu hlavního nosníku křídla.

Jak vypadá návrh a analýza takovýchto dílů? V zásadě jsou dvě možnosti. První z nich je poměrně jednoduchá analytická analýza, případně naprogramovaná v tabulkovém výpočetním prostředí. Nevýhody tohoto řešení jsou limitované možnosti výpočtu a jeho nízká flexibilita. Druhou možností je využít komerční konečno-prvkový systém pro analýzu, případně i pro optimalizaci. Pochopitelnou nevýhodou této možnosti je cena programu a obsluhy.

Cílem této disertační práce je vytvořit program, jež nabídne třetí možnost, která umožní provádět zevrubnou analýzu řešených produktů bez nutnosti pořizovat nákladný software. Tento program zjednoduší a urychlí návrh a pevnostní kontrolu. Umožní uživateli rychle analyzovat více návrhových variant. Program dále bude zohledňovat specifika analyzovaných produktů (například velké deformace a lokální koncentrace napětí kolmo na vlákno).

Z pohledu uživatele by program měl být jednoduchý na ovládání. Minimum množství vstupních dat a přehledné grafické rozhraní zajistí komfortní používání. Samostatně spustitelný program (bez instalace a bez podpůrného softwaru) zlepšuje rozšiřitelnost programu.

Klíčová slova

Analýza kompozitních komponent, konečnoprvková analýza, nosníková teorie, pružina podvozku, nosník křídla.

CEJPEK, J. *Analysis of aeronautical composite structures under static loading.* Brno University of Technology, Faculty of Mechanical Engineering, 2017. 90 p. Supervised by doc. Ing. Ivo Jebáček, Ph.D.

Declaration

This thesis is a presentation of my original research work. Wherever contributions of others are involved, every effort is made to indicate this clearly, with due reference to the literature, and acknowledgement of collaborative research and discussions.

Contents

1 Introduction

For many decades the composite materials were used extensively in aviation industry for primary structures of sport airplanes. Pursuing the weight saving design the first military and commercial airplanes started to use composite materials for small surfaces (flaps, ailerons, tail units) in the 1960'[40]. In past decade even the largest wide body airliners introduced by Airbus and Boeing are benefiting on the materials specifically designed for the intended shape and loading.

These new generation airliners brought the technology of design process, manufacturing and assembly to the state of the art. These companies used their extensive experience gained in military aviation industry, scaled-up the size and put all together in a new concept.

Large structures, such as those of A350 and B787, require ultimate knowledge and track of design and manufacturing process. Any possible imperfections must be thought of and compensated for in the fail-safe approach. This approach however is quite not possible with the small airplanes.

Let's focus on the LSA and CS-22 category as representatives of the small airplanes. The automated manufacturing can not be applied for economical reasons in these categories. Same problem concerns the design stage: usually only small engineering teams are involved in the design, using mostly analytical approaches and very limited computer software.

1.1 Life stages of a composite structure

Any structure begins it's life on a design board of an engineer. When the product is tested and certified, the serial production may proceed. When produced and installed, the service life starts. Life of the part can be terminated either in destruction or by completing pre-determined mission (number of cycles for example). These life stages are shown on figure 1.1.

Figure 1.1: Life stages of aeronautical structure.

When focusing on the product properties, the first two stages play the most significant role. Therefore, design means and methods and manufacturing process will be discussed further.

Airplane category, this dissertation focuses on, is manufactured by hand laminating process. Naturally, men is no machine, each part is little bit different. There are three main issues associated with hand-laminating:

1. precision (to lay down the straight fibre on the right places under the desired angle),
2. quality (even distribution, baubles and foreign particles,...),
3. material (strength, stiffness and chemical properties such as wettability for example).

Very important aspect of the manufacturing stage is the choice of technology. The choice is very important in terms of final material properties - most importantly the fibre volume fracture and thus the final stiffness. For hand lamination (no automated machines or prepregs), there are two basic techniques [28], [82]. These techniques are pressure systems (vacuum bagging and pressure moulds) or two-sided moulds.

Figure 1.2 shows the connection between the design and manufacturing stages. It explains the following process:

1. given inputs are: geometry, loading, material and available manufacturing technology,
2. technology and material provide the material properties (volume fracture, stiffness and strength),
3. according to the available material data, the proper failure criteria is chosen (limit, interactive, physically based),
4. first lay-up design is made,
5. analysis of the design will determine whether it is sufficient or re-design is required,
6. when the design is found to be sufficient, the manufacturing starts.

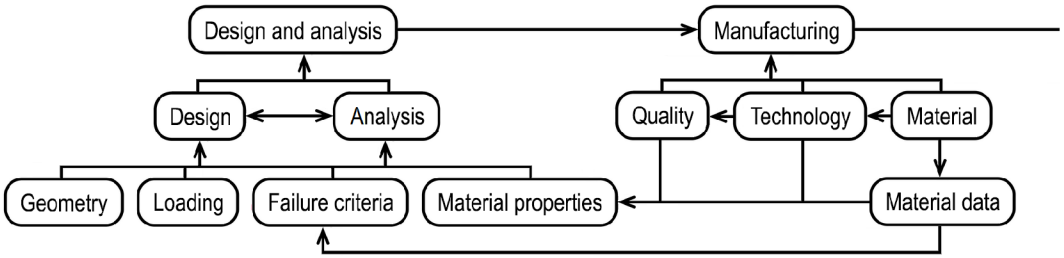

Figure 1.2: Aspects of design and manufacturing life in composite product.

During the design and analysis period a number of simplifications is usually made in order to approximate the problem by easy-to-solve sub-problems and/or by neglecting some of the aspects.

Simplification is proportionally linked with the means of structural analysis. This analysis may use closed-form formula solutions or the finite element method can be employed. Both ways offer their advantages as well as drawbacks.

The engineer must consider number of specific problems that come hand to hand with anisotropic nature of the composite. This concerns not only failure modes but it also affects the deflection.

1.2 Motivation

As an example of a typical composite aeronautical structures, wing and landing gear spring can be given, both shown on figure 1.3.

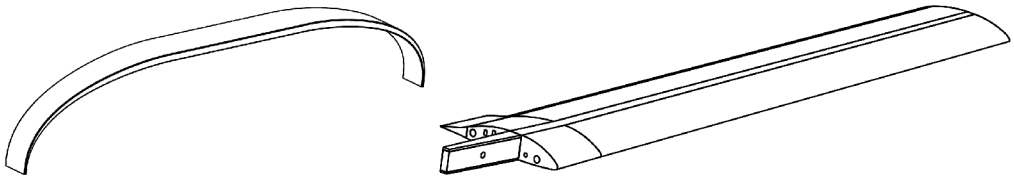

Figure 1.3: Example of aeronautical structures: wing and landing gear spring.

Since 2004, the Institute of Aerospace Engineering (IAE), has participated [71] on the G304S glider project in area of structural design and airworthiness certification. This includes, among others, a large number of material tests, wing quasi-static tests and segment fatigue characteristics (results are presented in table 1.2). Neither of the specimen survived the required quasi-static loading.

Segment #	X-01	X-02	X-03	X-04	X-05
Failure at [%]	123	144.6	149.1	203	154
Goal to meet [%]	225	225	225	225	187.5

Table 1.1: List of static tests results.[68], [70]

Later segments (X-06 through X-07) were tested in fatigue cycles, therefore it is not comparable in the table above. Sample X-08 has been also a quasi-static test of the whole wing. Last tested sample, segment X-09, was damaged during fatigue cycles.

The wing segment has been analysed in NASTRAN by the author. A number of scenarios has been simulated on different types of models (1D beam elements, 2D shell elements up to 3D volume elements with glue layer and contact function). These simulations were published in [74] in an article that focused on the build-up of inter-laminar shear stresses in the flanges.

The author is drawing experience from his former employer, the TechProAviation company,

based in Olomouc. One of the tasks, appointed to the author, was the development of composite landing gear parts for in-house designed and built sport airplanes (figure 1.4).

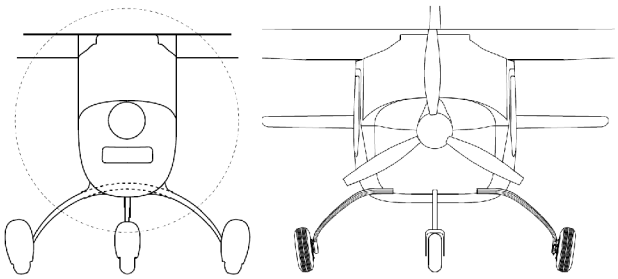

Figure 1.4: Example of airplanes using composite landing gear spring.

1.3 Summary

Airbus and Boeing companies have introduced their new wide body CS-25 category airliners made mostly from composite materials (Airbus 350 features 53% of CFRP [56], Boeing 787 features 50% of CFRP [57]). Manufacturing of these airframes is computer-controlled every step of the way, thus achieving maximum precision and repeatability of the process. For this reason a thorough analysis must have been included in the design process. The background of these large companies allows extensive bottom-up testing of coupons, parts, sub-assemblies and assemblies. A large amount of data from these tests allows designers to use advanced failure criteria, which require different material limits (this requirement is due to the composite anisotropy that can appear in all three dimensions: longitudinal, lateral and through thickness, and also in the tension/compression direction).

Not only material data are provided from these test. Having a precisely controlled manufacturing process and results from the tests of parts and higher assemblies opens a great opportunity to validate the finite element models and, in general, different boundary conditions, loading conditions, failure modes and many other aspects of the simulations.

The situation in the world of small airplanes is different. Usually, in companies producing LSA or CS-22 airplanes, the manufacturing is based on man power rather than computer controlled machines. Quality, therefore, is much lower, compared to category CS-25. Also the design and analysis and testing work is limited mostly to available resources (closed form equations or simple finite element analysis).

This thesis's goal is to suggest and provide the means for better analysis of composite parts, namely the landing gear springs. In chapter 2 a state of the art in respect to the chosen airplane category will be presented on the following topics:

1. composite landing gear and wing spar design,
2. material properties,
3. specifics of thick composite structures,
4. failure criteria,
5. analysis tools,
6. verification and validation of a simulation.

Based on the research of the topics mentioned above a set of goals will be presented in chapter 3. Fulfilling of these goals will take place in the following chapter. Last chapter 6 will provide author's conclusion on the problematic.

2 Literature review

This chapter provides a state of the art overview in respect to the chosen airplane category. The objective of the dissertation and the means to achieve the objectives will be formulated (in chapter 3) according to this overview.

2.1 Composite landing gear and wing spar design

Thick composites used in the airplanes (LSA and CS-22 category) are represented by landing gear springs and wing spars.

Edwin Spencer: optimization strategy for composite landing gear

Mister Spencer's work [58], presented in 2012 at MSC 2012 Regional User Conference, describes a procedure of design and optimization of a composite landing gear by means of NASTRAN solution sequence SOL200.

In the first step, he suggests to built a model consisting of tapered rectangular beam elements. On these elements only geometry will be optimized in terms of thickness and width, thus achieving an optimal cross-section at each node along the length of the mid-fibre (which defines the global shape of the landing gear).

The second step builds on the element geometry and defines the number of layers in 0° and ±45° direction.

On a plus side, Mr. Spencer offers both, the design and optimization solution. The NASTRAN solver will give the optimal cross-section for given shape and loading. And in the second stage, by using quadrilateral shell elements for composite materials a lay-up will be devised.

However on the other side, the solution is dependent on a very sophisticated and expensive software. The results are quite dependent on the actual manufacturing methods. It is worth mentioning, that the lay-up of the landing gear (as well as wing flanges) is made out of 0° unidirectional plies. Only several outer layers are added for the minor loading modes. Therefore the application of special elements and 3D-orthotropic material is unnecessary.

Amit Goyal: Design, Analysis and Simulation of a composite landing gear

Mr. Goyal emphasises the kinematics of landing gear deformation as a result of energy absorption process. Because of achieving large deformations, he suggests to use non-linear analysis techniques.

He also points out the advantage of using fibre reinforced plastics for their properties, such as:

- high strength,
- lightweight,
- medium stiffness and
- high elastic strain energy storage capacity.

The capacity of the unidirectional composite material to store the elastic strain energy is 13.6 times better than steel material [59]. For this reason the glass fibre reinforcement constituent is suggested.

In the article an example design is shown. The aim is to design composite main landing gear for a light sport airplane of $m_{TOW} = 350kg$. The employed theory for deformation and stress analysis is the membrane theory with additional bending theory to account for discontinuities in the stress distribution. FE model uses shell elements with Tsai-Wu failure criterion to account for multi-axial stress state.

The loading is introduced only for vertical and tangential directions. Side loads are mentioned, but for the relative minority (compared to the vertical and tangential loads) and already too complex problem are neglected.

Finally two ideas worth mentioning: Wheel axle is modelled also. Carbon steel with high

module of elasticity is used. The non-linear analysis applies the loading gradually in different sub-steps.

Ivana Ilic: Analysis of landing gear for UAV

Unmanned aerial vehicles (UAV) are quickly expanding group of flying vehicles. More than manned airplanes the UAVs benefit from the advantages of composite materials.

This article [60] describes the development of the main landing gear (figure 2.1) for such a vehicle. First, the global geometry is defined. Along the length a total of 8 control points are chosen. In these points the strains are evaluated and compared to strain gages reading from the laboratory test.

The numerical analysis used 2D shell elements with 2D orthotropic material definition. Interesting fact is the lay-up that was used. Typically outer layers are made of 4 plies $\pm 45°$ fabric, whereas the flanges are made of unidirectional $0°$ plies of carbon fibre. The interesting part is the core. Core, in between the carbon flanges, is made out of unidirectional $0°$ plies of glass fibre. The number of all carbon plies is equal along the whole length. However the number of glass fibre plies varies from 32 - 50 and thus the variable thickness is achieved.

Both, the numerical analysis and the laboratory experiment has reached only the level of 50% of limit load. This is probably due to other intention with the specimen but to destroy it. This fact however does not allow to verify the ultimate strength. The only comparison that may be done is the deflection characteristic.

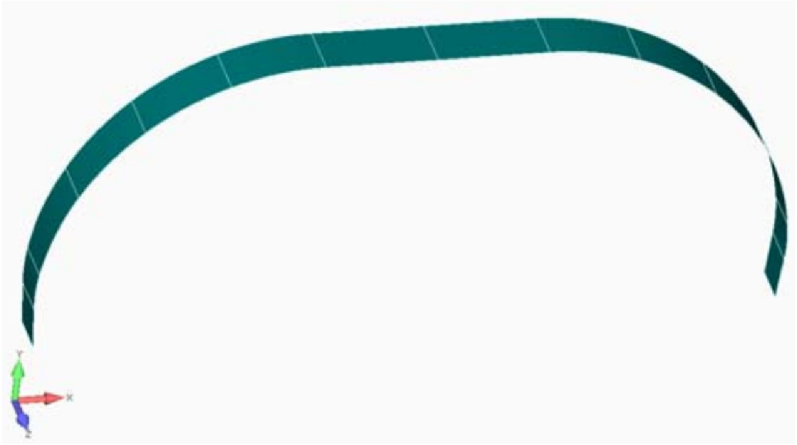

Figure 2.1: Landing gear designed for an UAV. [60]

Akshay Kumar: Automotive Composite Leaf Spring

Not only aeronautical but also automotive industry seeks ways to benefit from composite materials. This article [61] describes design, analysis, manufacturing and testing of a car leaf spring.

The authors introduce existing steel spring and it's parameters. Further analytical and FE analysis are shown in order to evaluate the original steel and new composite (glass-epoxy) design.

After manufacturing the composite leaf spring the quality is evaluated through testing with satisfying results. Moreover the authors claim a great weight savings.

2.2 Material Properties

The following text concerns composite material properties in terms of stiffness, Posisson's ratios and allowed stresses and strains. All these parameters are referring to the material coordinate system (figure 2.2). Understanding the direction is of great importance when dealing with the failure criteria later in this section.

Historically, there are two sets of denotations: German [52], based on geometric symbols and

American [53], based on alphabetical description of the direction. In this thesis, the American denotation is used. An example of ultimate strength denotation is shown in table 2.1.

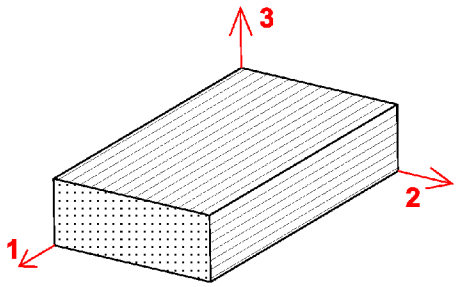

Figure 2.2: Material coord system. Axis 1 along the fibres, Axis 3 through the thickness.

Direction	Orientation	US denotation	German denotation
longitudinal	compression	X_C	$R_{\parallel}^{C}$
longitudinal	tensile	X_T	$R_{\parallel}^{T}$
transverse	compression	Y_C	$R_{\perp}^{C}$
transverse	tensile	Y_T	$R_{\perp}^{C}$
in plane	shear	S_{12}	$R_{\perp\parallel}^{C}$

Table 2.1: Ultimate strength denotation for US and German version.

Harris: From Fibre to Composite

Final properties of a composite is calculated from the properties of individual constituencies (fibre and matrix). The input parameters are fibre modulus E_F, matrix modulus E_M and fibre volume fracture V_F.

Fibre volume fracture defines the volumetric amount of fibre in the cross-section. There are two commonly used examples of fibre packing: square and tight, shown on figure 2.3. Assuming circular cross-section of the fibre and each fibre is touching it's neighbours, the highest volume ratio is $V_F = 90.7\%$. For square packing, the volume ratio is exactly $V_F = 78.5\%$.

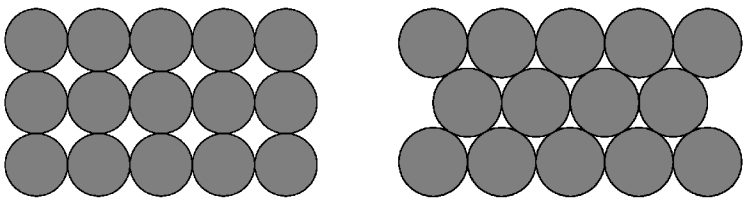

Figure 2.3: Fibre packing in cross-section. Square Array ($V_F = 78.5\%$) and Close Packing ($V_F = 90.7\%$).

There are several theories developed for determining the resulting properties. Table 2.2 shows four methods of calculating longitudinal and transversal (E_1 and E_2) stiffness, based on volume fracture, matrix and fibre stiffness.

	Iso-strain condition	simplified	Reuss estimate	Halpin-Tsai
E_1	$E_F \cdot V_F + E_M \cdot (1 - V_F)$	$E_F \cdot V_F$	$E_F \cdot V_F + E_M \cdot (1 - V_F)$	$E_F \cdot V_F + E_M \cdot (1 - V_F)$
E_2	$\frac{E_F \cdot E_M}{E_M \cdot V_F + E_F \cdot (1 - V_F)}$	$\frac{E_M}{1 - V_F}$	$\frac{E_F \cdot E_M}{E_M \cdot V_F + E_F \cdot (1 - V_F) \cdot (1 - \mu_M^2)}$	$E_M \cdot \frac{1 + V_F \cdot \eta \cdot \zeta}{1 - \eta \cdot V_F}$

Table 2.2: Composite E_1 and E_2 estimation [37].

Halpin-Tsai used two parameters empirically determined in their predictions. Factor ζ reflects material, shape and reinforcement distribution. Ratio η is defined through fibre and matrix stiffness and factor ζ: $\eta = \left(\frac{E_F}{E_M} - 1\right) \cdot \left(\frac{E_M}{E_F + \zeta \cdot E_M}\right)$.

Kaw: Mechanics of Composites

In [41] Mr. Kaw estimates the limit stresses and strains of a composite:

- Ultimate longitudinal tensile strain

For glass fibre, the generally accepted value of limit tensile strain is $\epsilon_1^{ult} = 3\%$ [69]

- Ultimate transversal tensile strain

According to the [41], the ϵ_2^{ult} can be roughly estimated from the matrix tensile strain and volume ratio:

$$\epsilon_2^{ult} = \epsilon_M^{ult} \cdot \left(1 - \sqrt[3]{V_F}\right)$$

- Ultimate longitudinal compression stress

According to the [41], the ultimate stress along the fibre can be estimated as a minimum value of the following:

$$X_C^{extension} = 2 \cdot \left[V_F + (1 - V_F) \cdot \frac{E_M}{E_F}\right] \cdot \sqrt{\frac{V_F \cdot E_M \cdot E_F}{3 \cdot (1 - V_F)}} \qquad X_C^{shear} = \frac{G_M}{1 - V_F}$$

The extension and shear modes of compressive failure are also explained in [34], figure 2.4.

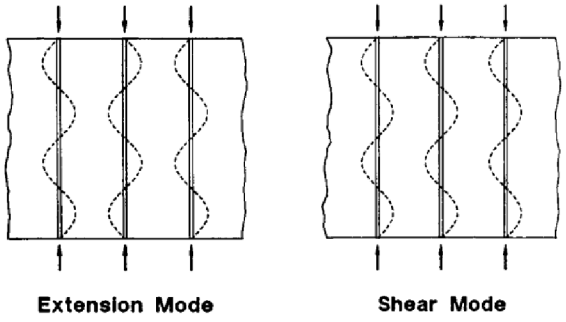

Figure 2.4: Two modes of compression failure in consideration. [34]

Military Handbook 17

The handbook describes mathematical formulation of stress-strain relation for 2D and 3D cases of the unidirectional laminates :

$$\text{2D:} \qquad \begin{Bmatrix} \epsilon_1 \\ \epsilon_2 \\ \gamma_3 \end{Bmatrix} = \begin{bmatrix} \frac{1}{E_1} & -\frac{\mu_{21}}{E_2} & 0 \\ -\frac{\mu_{21}}{E_2} & \frac{1}{E_2} & 0 \\ 0 & 0 & \frac{1}{G_{12}} \end{bmatrix} \begin{Bmatrix} \sigma_1 \\ \sigma_2 \\ \tau_3 \end{Bmatrix}$$

$$\text{3D:} \qquad \begin{Bmatrix} \epsilon_1 \\ \epsilon_2 \\ \epsilon_3 \\ \gamma_{23} \\ \gamma_{31} \\ \gamma_{12} \end{Bmatrix} = \begin{bmatrix} \frac{1}{E_1} & -\frac{\mu_{21}}{E_2} & -\frac{\mu_{31}}{E_3} & 0 & 0 & 0 \\ -\frac{\mu_{12}}{E_1} & \frac{1}{E_2} & -\frac{\mu_{32}}{E_3} & 0 & 0 & 0 \\ -\frac{\mu_{13}}{E_1} & -\frac{\mu_{23}}{E_2} & \frac{1}{E_3} & 0 & 0 & 0 \\ 0 & 0 & 0 & \frac{1}{G_{23}} & 0 & 0 \\ 0 & 0 & 0 & 0 & \frac{1}{G_{31}} & 0 \\ 0 & 0 & 0 & 0 & 0 & \frac{1}{G_{12}} \end{bmatrix} \begin{Bmatrix} \sigma_1 \\ \sigma_2 \\ \sigma_3 \\ \tau_{23} \\ \tau_{31} \\ \tau_{12} \end{Bmatrix}$$

Also there are three reciprocal relationships connecting Es' and μs':

$$\frac{\mu_{12}}{E_1} = \frac{\mu_{21}}{E_2} \qquad \frac{\mu_{13}}{E_1} = \frac{\mu_{31}}{E_3} \qquad \frac{\mu_{23}}{E_2} = \frac{\mu_{32}}{E_3}$$

Andrew Makeev: Shear Behaviour of UD Composites

Study [42] of three point bend test combines numerical investigation and practical tests of carbon unidirectional composite samples. Unidirectional composite material is considered to be a transversely isotropic material. Authors confirmed the same material behaviour in both perpendicular-to-fibre directions (directions 2 and 3). This effectively means:

- Elastic modulus $E_2 = E_3$,
- Shear modulus $G_{12} = G_{13}$,
- Poisson's ratios: $\mu_{12} = \mu_{13}$ and
- Constitutive relations: $\frac{E_1}{E_2} = \frac{\mu_{12}}{\mu_{21}} \qquad \frac{E_1}{E_3} = \frac{\mu_{13}}{\mu_{31}} \qquad \frac{E_2}{E_3} = \frac{\mu_{23}}{\mu_{32}}$

Makeev and He also claim that experiments confirmed the following relation:

$$G_{23} = \frac{E_2}{2 \cdot (1 + \mu_{23})}$$

Chamis Christos: Unequal Tensile and Compression Properties

This NASA technical report introduces mechanical property called *'modular ratio'* (denoted as MR). This is defined as tensile-to-compression modulus ratio. A mathematical apparatus is developed to evaluate the three-point-bend test of a material with unequal material properties. As on of the conclusions Chamis claims:

"The maximum flexural deflection is sensitive to MR. The simple beam formula underestimates the maximum deflection by 25% *when the* $MR = 1.5$ *and overestimates it by 25% when* $MR = 0.5$. *The correction to maximum tensile and compressive stress can be as large as* 25% *compared to a material with equal modulus."* [35]

These findings are of importance in composite analysis. Chamnis quantified the error of omitting the tensile / compression differences.

Isaac Daniel: 3D Behaviour of Textile Composites

The report [36] deals with material and failure investigation of carbon-fabric/epoxy composite and compares the results with unidirectional carbon/epoxy composite that has the same type of fibre and matrix.

First in-plane tensile, compression and shear properties are investigated. Same types of properties were tested in out-of-plane direction. Authors describe significant difficulties in specimen and jig manufacturing for these tests.

Obtained failure data were analysed by different theorems: maximum stress, Hashin-Rotem, Tsai-Wu and Tsai-Hill.

José Almeida: shear behaviour of GFRP

Paper [48] presents a study of the lay-up configuration influence on inter-laminar shear properties of glass fibre epoxy composites. There are three different lay-up configurations, most notable unidirectional 0° and also unidirectional 90°. Authors employ different testing methods for determining the properties:

1. V-notched ASTM D7078-12,
2. Iosipescu ASTM D5379-12,
3. Double-notched ASTM D3846-08,
4. Short beam ASTM D2344-13.

The specimens used are E-glass ($300g \cdot m^{-2}$) and epoxy matrix (LY1316 epoxy resin and Aradur 2969 hardener), The fibre volume fraction is $V_F = 36 \pm 2\%$. Each specimen lay-up is 5 plies. Manufacturing procedure includes matrix vacuum intrusion and curing at $80°C$. Results of the shear tests are indicated in table 2.3.

Ply configuration [°]	V-notched	Iosipescu	Double-notched	Short beam
0	23.0 ± 1.3	20.7 ± 1.3	27.5 ± 0.6	34.4 ± 1.2
90	22.3 ± 0.6	14.3 ± 1.9	14.1 ± 0.9	17.9 ± 1.4

Table 2.3: Shear strength values for GFRP, different testing methods.

The shear trough thickness strength ranges from 20 to 35MPa, depending on the test method. Similar study [49] presents the results of short beam tests. Specimens are made from E-glass and Epoxy/Aradur matrix; volume fracture is not given. The authors claim to achieve maximum shear strength of $\tau_{31} = 32.7MPa$.

The study also presents the results of shear modulus. For the given composite the results are $G_{31} = 2500MPa$ and $G_{23} = 1800MPa$.

2.3 Thick Composite Structures

One of the most important characteristics, identifying thick composites, is that the through-thickness stress is not zero. Predicting the failure of a thick section, using conventional two-dimensional analyses may be misleading [33].

Other characteristic that denotes structure to be thick is the geometry (according to the Mindlin–Reissner plate theory [14] the thickness is $T > 10\%$ of the width) or the number of plies (15 plies of fabric reinforcement [41]) or the thickness is $T > 25.4mm$ [17].

Zimmermann: Testing and Analysis of Ultra Thick Composites

In their work [46], Zimmermann at al. describe the development of a composite main landing gear fitting made of CFRP. The fitting is as thick as 60mm - therefore it is described as ultra thick composite.

On page 8 the material properties used in simulation are described. The author himself admits insufficient knowledge of the material constants. The only known contacts are E_1, E_2, G_{12} and μ_{12}. Mr Zimmermann assumes the following:

$$E_3 = 0.7 \cdot E_2 \quad G_{13} = G_{12} \quad \mu_{31} = \mu_{12} \quad G_{23} = \frac{E_2}{2 \cdot (1 + \mu_{23})}$$

Goering: Lug analysis

McDonnell aircraft corporation has participated in a NASA initiative called *"Innovative Composite Aircraft Primary Structures"* with an article describing higher order, sub-parametric, laminated, 3-D solid finite element analysis of the very thick laminated composite plates.

The authors stressed out that *"The complex stress distributions that may develop through the thickness require that the model be capable of predicting three dimensional stress fields"* [17]. Typical analysis usually employs elements that are based on classical laminated plate theory. Advantage of these elements is that they are simple to use. On the other hand these elements assume out-of-plane stresses are negligible.

To work-around this drawback of the classical plate definition is to use multiple elements in the through-thickness direction. Having multiple elements stacked in this way allows accurate through thickness integration but for a high price (large number of degrees of freedom, longer computation times).

Davallo: Properties of Hand Lay-up Moulding laminates

Paper by Mr. Davallo at all. presents a study [47] of mechanical behaviour of thick unidirectional composite under flexural and tensile loading. The composite samples are hand-made polymer matrix - E-glass bars.

Flexural modulus calculated from the tests slightly varied just as the fibre-to-matrix ratio did.

The author uses mass fibre fraction instead of more usual volume. All the samples of flexural test exhibited same failure: delamination.

2.4 Composite Failure Criteria

In order to evaluate the extend to which the material properties are being used a failure criteria must be employed. In case of isotropic materials the history of failure criteria is long and well established. This is due to two reasons: firstly, the extend of metallic materials application over a long period of time and secondly, the relatively limited number of failure modes.

In mid 20^{th} century the composite materials (mostly glass a carbon reinforced plastics) emerged and new approaches were needed. In the first wave the established concepts for isotropic materials were developed for composites. This led to quite a successful application of the micro-mechanics estimates of effective elastic properties, homogenization and laminate plate theory.

The result of failure criteria is either the Reserve Factor (RF) or the Failure Index (FI). These scalars indicate the extent to which the material properties are exploited. Both are indicating the same, just in inverse relation:

$$RF = FI^{-1}$$

Following paragraphs provide a quick overview on the topic of failure analysis of isotropic materials and composites.

Failure Criteria of Isotropic Materials

First and very important note about failure analysis of isotropic material is the index denotation. While the index in non-isotropic materials indicates the material direction (see figure 2.2), for the isotropic materials the index indicates the magnitude of the principal stresses ($\sigma_1 \geq \sigma_2 \geq \sigma_3$).

Equivalent tensile stress, also known as von Mises stress [2], σ_{RED} is a scalar stress value that is computed:

$$\sigma_{RED} = \sqrt{\frac{1}{2} \cdot \left[(\sigma_1 - \sigma_2)^2 + (\sigma_2 - \sigma_3)^2 + (\sigma_3 - \sigma_1)^2 \right]}$$

The calculated reduced stress is confronted with the allowed (for example yield stress Re) value for given material and the FI or RF is obtained:

$$RF = \frac{Re}{\sigma_{RED}}$$

In similar manner the Tresca maximum shear stress is calculated. In comparison with von Mises the Tresca is more conservative.

$$\tau_{MAX} = \frac{1}{2} \cdot max \left\{ (\sigma_1 - \sigma_2), (\sigma_2 - \sigma_3), (\sigma_1 - \sigma_3) \right\}$$

Limit Failure Criteria

Limit criteria deal with each direction separately. There are two kinds of limit criteria: maximum stress and maximum strain. The principle of these criteria is to compare the actual stress (or strain) to the allowed stress (or strain) in a given direction.

Main problem with these criteria is the assumption that there is no interaction between the stresses in different direction (the stresses are completely separate). Despite this fact, they are often used because of their simplicity and minimal need for material data.

As an example the reserve factor in longitudinal tension is presented:

$$RF = \frac{X_T}{\sigma_1}$$

Interactive Failure Criteria

The main disadvantage of the limit criteria is the interaction between the stresses in different directions. Inspired by von Mises yield failure criterion the Tsai-Hill formula has been proposed in 1965 by Azzi and Tsai [43]:

$$\frac{1}{RF} = \left(\frac{\sigma_1}{X}\right)^2 + \left(\frac{\sigma_2}{Y}\right)^2 - \frac{\sigma_1 \cdot \sigma_2}{X^2} + \left(\frac{\tau_{12}}{S}\right)^2$$

where the X and Y depends on the orientation of the σ_1 and σ_2 stress respectively:

$$X = \begin{cases} X_T \ if & \sigma_1 > 0 \\ X_C \ if & \sigma_1 < 0 \end{cases}$$

$$Y = \begin{cases} Y_T \ if & \sigma_2 > 0 \\ Y_C \ if & \sigma_2 < 0 \end{cases}$$

Tsai-Hill criterion is derived from a theory of yielding material and therefore doubts exist about its validity because of the different failure mechanisms of composite materials [50]. Closer to the reality is the Tsai-Wu criterion. It has been developed as an ellipsoid envelope.

$$\frac{1}{RF} = \frac{\sigma_1^2}{X_T \cdot X_C} + \frac{\sigma_2^2}{Y_T \cdot Y_C} + \left(\frac{\tau_{12}}{S}\right)^2 + \sigma_1 \cdot \frac{X_C - X_T}{X_T \cdot X_C} + \sigma_2 \cdot \frac{Y_C - Y_T}{Y_T \cdot Y_C} - \frac{\sigma_1 \cdot \sigma_2}{\sqrt{X_T \cdot X_C \cdot Y_T \cdot Y_C}}$$

Physically based Failure Criteria

Successful failure criteria is to recognize the different modes of failure of the composite materials. Puck's failure criterion [52] recognized seven failure modes depending on the position of the fracture plane relative to the fibre. The theory introduces a large number of empirical constants. Some of these constants, mostly associated with the matrix failure, are difficult to determine, even for a unidirectional composites [51].

Similar approach is used in the family of NASA failure criteria developed in Langley Research Center.

2.5 Finite Element Analysis

Bo Torstenfelt: FEM from the early beginning to the very end

"The text to come is written by an engineer for engineers" [4]. Mr. Torstenfelt indeed presents this difficult topic in a very understandable manner. All is explained in step-by-step fashion with practical examples.

Just like in the school seminars start with pure tension, here the bar elements are introduced. All the equations are described in a consequential order so that the reader can easily orient him or her self. From a single two-node element a larger model is shown. Examples of a 2D and 3D truss problems are presented with solutions.

From bars are derived beams. Unlike bars, beams can be loaded by other kinds of load than just pure tension/compression. Mr. Torstenfelt explains the formulation of strong formulation, which is transformed into weak form for an Euler-Bernoulli beam. After that a two kinds of formulations are presented: the Galerkin and Matrix. The final formulation of a 2-node element is shown for 2D and 3D space.

Antonio Ferreira: Codes for FEA

Fundamental source for anyone, who wishes to write own FEA code. The book [1] is intended as a practical guide with many examples and working Matlab codes.

First, a short introduction to Matlab provides necessary understanding of the scripting language. Other, more universal languages, even open-source free languages exist (such as C++,

Fortran, etc.). However using Matlab for explaining the FEA is a great choice. Matlab syntax is easy to understand, working with matrix is straight forward (other languages use rather clumsy arrays and lists) and it is usually available at the university.

Chapter two explains simple problems, such as rigid bar connecting three springs. By writing all the equations and making notes in process, the reader is likely to understand the logic behind.

Following chapters are devoted to bars, 2D and 3D trusses, Bernoulli and Timoshenko beams, 2D and 3D frames and finally plates. In each of these chapters several examples are shown. These examples are provided also as a Matlab script files. From these source codes more understanding can be extracted.

Hasan Mehmet: FE analysis of thick composite

The authors [20] are using 8-node brick element when dealing with thick composite model. The problem, they are addressing is the homogenization of the properties of different plies in order to obtain single element describing these plies as a whole. For this purpose two averaging techniques for calculating element material properties are introduced:

1. the arithmetic average,
2. the weighted average.

The arithmetic average method sums the multiples of the thickness and the property. This sum is then divided by total thickness:

$$\bar{P} = \frac{1}{T} \cdot \sum P_i \cdot (k_i - k_{i-1})$$

Whereas the weighted average considers the moment of area of the ply:

$$\bar{P} = \frac{1}{3 \cdot J_J \cdot B} \cdot \sum P_i \cdot \left(k_i^3 - k_{i-1}^3\right)$$

The meaning of the used symbols: P arbitrary property, T total thickness, k through-thickness coordinate of the ply border, B total width of the element, J_J is the moments of area of a cross-section.

A test case is shown on a plate and a beam under two different types of loading: compression and three-point bending. The results are compared with analytical solution. The authors have concluded that:

- the arithmetic-average method provides satisfactory results for in-plane loading,
- the weighted-average method gives better results for transverse loading.

Primary result of this study is a proof, that it is not necessary to model one element per ply. It is possible to model several plies by one element.

Håkan Petersson: An Industrial Survey

Mr. Petersson presents an industrial survey, taken in late 2014, between design and analyst engineers. He describes a traditional company, where the design and analysis departments exist separately. The task of a design department is *"to develop concept, product architecture or detailed design solution"*[6]. Then the work shifts to analysis department, where the typical tasks are:

- FEM - finite element method analysis,
- CFD - computational fluid dynamics,
- MBS - multi-body system analysis,
- OPT - optimisations (shape, topology, etc.).

This politics, however, may lack the dynamic needed to succeed on the ever faster market. In order to speed up things the designers are now performing some analysis tasks in a specific supervised form. This is allowed and supported by developing CAD-CAE system (for example SolidWorks).

Petersson argues, that designers lack in level of knowledge and experience as design analysts.

This may diminish the positive contribution of this politics. Peterson also stressed out the need for support, supervision, and larger number of expensive software licenses.

A study [7] from 2013 claims that the trend is to make the analysis available to designers and less experienced users. This is achieved by special tutorial[1], training programs and support by senior analyst.

Even the current trend of putting as much analysis on the shoulders of a designer does not mean, that the analyst position will be shut down. The analyst needs to be more specialized to perform a thorough analysis for which the designer does not have the experience or time.

The survey is based on 282 participants, from 77 countries and 71 different companies. The following lists the percentage of those who:

- 85% perform linear static FEA,
- 52% perform non-linear FEA,
- 76% validate the product on physical testing and/or advanced simulation by a design analyst.

Zhang: FEA of laminated plates

Article [18] written by authors from Australian universities summarises the recent history of finite element analysis of composite plates. The article lists theories that are generally used:

- Equivalent Single Layer theories (ESL)
  - Classical Lamination Theory (CLT)
  - First-Order Shear Deformation Theory (FSDT)
  - Higher order Shear Deformation Theory (HSDT)
  - Layer-wise Lamination Theory (LLT)
- Continuum based 3D elasticity theory

CLT comes from Kirchhoff plate theory, neglects shear deformation. However it is the simplest one. FSDT accounts for shear within it's limits. It suits for thin and moderately thick plates. FSDT does not account for ILSS. Higher order theories overcame this problem. LLT can predict inter-laminar stresses accurately however the complexity of the calculation grows with the number of plies. Similar problem with computational cost concerns the 3D models as well.

In the conclusion, the authors list several topics that - in their opinion - should be followed in more detailed studies in years to come. Very first topic listed by the authors is the problematic of material non-linearity. One of the material non-linearities is the difference between tension and compression.

2.6 Material properties and FEM

What is user allowed to use in Finite Element Analysis

Current FEM programs typically offer three basic types of material: isotropic, 2D orthotropic and 3D orthotropic. The variables (dependant and independent) are:

- Isotropic material: E, μ, G.
- 2D orthotropic material: $E_1, E_2, \mu_{12}, G_{12}, G_{23}, G_{13}$.
- 3D orthotropic material: $E_1, E_2, E_3, \mu_{12}, \mu_{23}, \mu_{31}, G_{12}, G_{23}, G_{31}$.

First problem here is that the software does not allow user to directly define different properties for tension and compression. This problem may be overcome in two ways:

1. define stress / strain curve of given material (see figure 2.5), [54], [55],
2. use different material for tension / compression areas (example shown on figure 2.6).

[1] Guidelines that define for example the mesh, boundary condition and solver that is to be used. What results are to be extracted and evaluated.

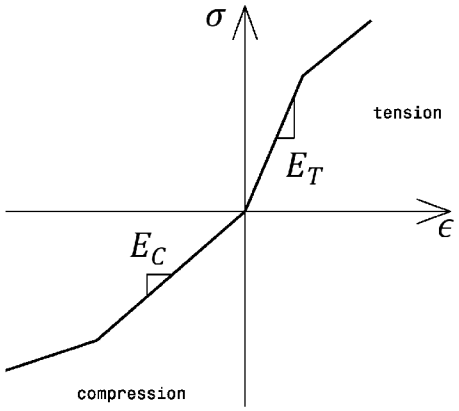

Figure 2.5: Stress-strain curve with different tensile and compression moduli.

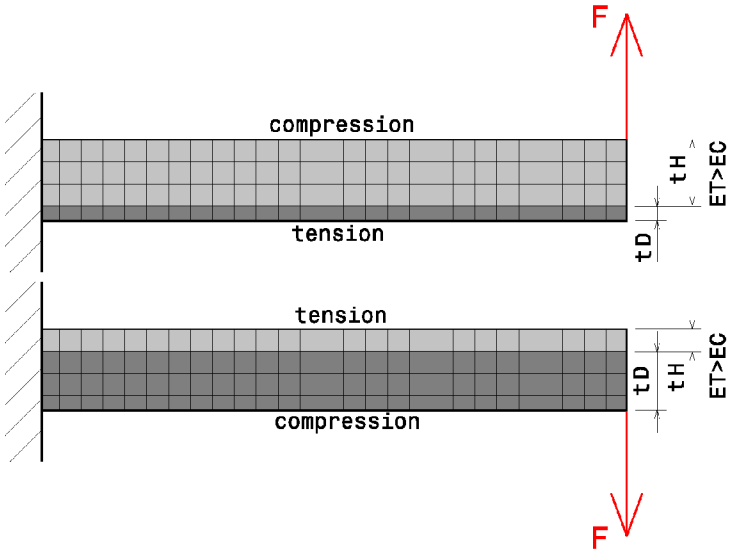

Figure 2.6: Different properties for two regions of the cantilever beam.

Other problem occurs in case of 2D element representing a composite. Each layer is defined separately, but the element still can have only one total parameter. One of the possibilities of homogenization is explained in classical laminate theory (CLT) [16]. Different homogenization process is used in [19].

2.7 Beam Theories

The main interest of this thesis lies with the wing spars and landing gear springs. These products can be seen as beams. For this reason an overview of the beam theories is given below. The following text is based on [1], [9], [10], [13], [25] and [26].

Euler-Bernoulli Beam Theory

The basic theory of a beam structure, first introduced in the mid 18^{th} century. Well known product, developed on the Euler-Bernoulli beam theory, is the Eiffel Tower in Paris.

The theory is based on a second order differential equation. By adding boundary condition

while integrating this equation a function of the rotations and displacements is obtained.

$$\frac{d^2U}{dx^2} = \frac{M(x)}{E(x) \cdot J(x)}$$

The assumptions are:

1. Cross-section is absolutely rigid in it's own plane.
2. Cross-section remains plane after deformation.
3. Cross-section remains perpendicular to the deformed beam axis.

The assumption that cross-section remains perpendicular to the longitudinal axis necessarily implies that shear strain is zero. The only load that results in zero shear force is constant bending moment and thus Euler-Bernoulli theory is acceptable only for long slender beams.

Timoshenko Beam Theory

In early 20^{th} century a generalized form of Euler-Bernoulli beam formulation has been introduced by Stephen Timoshenko. A shear correction factor is introduced, therefore accounting for shear deformation and rotational bending effects. The theory effectively lowers the stiffness of the beam and this results in larger deflections compared to Euler-Bernoulli formulation. The difference becomes more pronounced in vibration problems (compared to static problems). In closed-form formulation, the Timoshenko beam is:

$$\frac{d^2U}{dx^2} - \frac{d\gamma}{dx} = \frac{M(x)}{E(x) \cdot J(x)}$$

Timoshenko beam theory is higher order than the Euler-Bernoulli theory, it is known to be superior in predicting the transient response of the beam. The superiority is more pronounced for beams with a low aspect ratio. Shear deformation effects are significant for beams which have a length-to-depth ratio less than 5 [9].

The introduced shear correction factor is the ratio of the average shear strain on a section to the shear strain at the centroid. For solid rectangular sections $\alpha \approx \frac{6}{5}$ and for solid circular sections $\alpha \approx \frac{10}{9}$ [9].

Second Order Theory

This theory introduces an element called a beam-column. The name describes it's function: a column is a structural element where axial compression predominates, while beam is a structural element where bending predominates. Therefore the combination beam-column element refers to a structural element that is subjected to both, axial tension or compression force and bending moment. The interaction of the axial force and bending moment may result to a non-linear behaviour of the element. The assumptions are:

1. The material is linearly elastic.
2. Rotations are small and can be neglected.
3. The beam-column is prismatic.
4. Shear deformation is neglected.
5. The frame members are two-dimensional and subjected to in-plane forces and deformations only.

Following figure 2.7 illustrates the deflection caused by bending moment (first-order) and by axial force.

Summary

Three beam theories were presented. Other theories exist, but these are the most known. The similarities are illustrated on the element stiffness matrix formulation. First, the Euler-Bernoulli formulation, than modification accounting for shear deformation in Timoshenko formulation and finally the Second order theory accounting for the effects of axial forces .

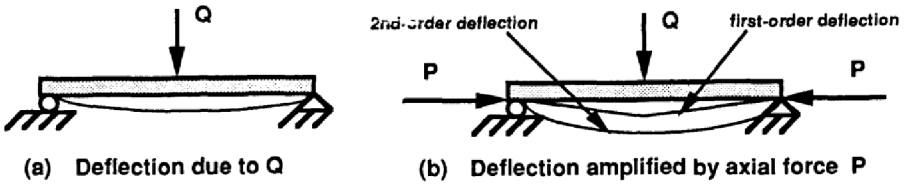

Figure 2.7: Illustration of 2nd order deflection. [10]

$$[LS] = \begin{bmatrix} \frac{A\cdot E}{L} & -\frac{A\cdot E}{L} & 0 & 0 & 0 & 0 \\ -\frac{A\cdot E}{L} & \frac{A\cdot E}{L} & 0 & 0 & 0 & 0 \\ 0 & 0 & 12\cdot\frac{E\cdot JJ}{L^3} & -12\cdot\frac{E\cdot JJ}{L^3} & 6\cdot\frac{E\cdot JJ}{L^2} & 6\cdot\frac{E\cdot JJ}{L^2} \\ 0 & 0 & -12\cdot\frac{E\cdot JJ}{L^3} & 12\cdot\frac{E\cdot JJ}{L^3} & -6\cdot\frac{E\cdot JJ}{L^2} & -6\cdot\frac{E\cdot JJ}{L^2} \\ 0 & 0 & 6\cdot\frac{E\cdot JJ}{L^2} & -6\cdot\frac{E\cdot JJ}{L^2} & 4\cdot\frac{E\cdot JJ}{L} & 2\cdot\frac{E\cdot JJ}{L} \\ 0 & 0 & 6\cdot\frac{E\cdot JJ}{L^2} & -6\cdot\frac{E\cdot JJ}{L^2} & 2\cdot\frac{E\cdot JJ}{L} & 4\cdot\frac{E\cdot JJ}{L} \end{bmatrix}$$

Element Stiffness Matrix: Euler-Bernoulli.

$$[LS] = \begin{bmatrix} \frac{A\cdot E}{L} & -\frac{A\cdot E}{L} & 0 & 0 & 0 & 0 \\ -\frac{A\cdot E}{L} & \frac{A\cdot E}{L} & 0 & 0 & 0 & 0 \\ 0 & 0 & \frac{12}{1+\Phi}\cdot\frac{E\cdot JJ}{L^3} & \frac{-12}{1+\Phi}\cdot\frac{E\cdot JJ}{L^3} & \frac{6}{1+\Phi}\cdot\frac{E\cdot JJ}{L^2} & \frac{6}{1+\Phi}\cdot\frac{E\cdot JJ}{L^2} \\ 0 & 0 & \frac{-12}{1+\Phi}\cdot\frac{E\cdot JJ}{L^3} & \frac{12}{1+\Phi}\cdot\frac{E\cdot JJ}{L^3} & \frac{-6}{1+\Phi}\cdot\frac{E\cdot JJ}{L^2} & \frac{-6}{1+\Phi}\cdot\frac{E\cdot JJ}{L^2} \\ 0 & 0 & \frac{6}{1+\Phi}\cdot\frac{E\cdot JJ}{L^2} & \frac{-6}{1+\Phi}\cdot\frac{E\cdot JJ}{L^2} & \frac{4+\Phi}{1+\Phi}\cdot\frac{E\cdot JJ}{L} & \frac{2-\Phi}{1+\Phi}\cdot\frac{E\cdot JJ}{L} \\ 0 & 0 & \frac{6}{1+\Phi}\cdot\frac{E\cdot JJ}{L^2} & \frac{-6}{1+\Phi}\cdot\frac{E\cdot JJ}{L^2} & \frac{2-\Phi}{1+\Phi}\cdot\frac{E\cdot JJ}{L} & \frac{4+\Phi}{1+\Phi}\cdot\frac{E\cdot JJ}{L} \end{bmatrix}$$

Element Stiffness Matrix: Timoshenko.

$$[LS] = \begin{bmatrix} \frac{A\cdot E}{L} & -\frac{A\cdot E}{L} & 0 & 0 & 0 & 0 \\ -\frac{A\cdot E}{L} & \frac{A\cdot E}{L} & 0 & 0 & 0 & 0 \\ 0 & 0 & 12\cdot\frac{E\cdot JJ}{L^3}\cdot s_1 & -12\cdot\frac{E\cdot JJ}{L^3}\cdot s_1 & 6\cdot\frac{E\cdot JJ}{L^2}\cdot s_2 & 6\cdot\frac{E\cdot JJ}{L^2}\cdot s_2 \\ 0 & 0 & -12\cdot\frac{E\cdot JJ}{L^3}\cdot s_1 & 12\cdot\frac{E\cdot JJ}{L^3}\cdot s_1 & -6\cdot\frac{E\cdot JJ}{L^2}\cdot s_2 & -6\cdot\frac{E\cdot JJ}{L^2}\cdot s_2 \\ 0 & 0 & 6\cdot\frac{E\cdot JJ}{L^2}\cdot s_2 & -6\cdot\frac{E\cdot JJ}{L^2}\cdot s_2 & 4\cdot\frac{E\cdot JJ}{L}\cdot s_3 & 2\cdot\frac{E\cdot JJ}{L}\cdot s_4 \\ 0 & 0 & 6\cdot\frac{E\cdot JJ}{L^2}\cdot s_2 & -6\cdot\frac{E\cdot JJ}{L^2}\cdot s_2 & 2\cdot\frac{E\cdot JJ}{L}\cdot s_4 & 4\cdot\frac{E\cdot JJ}{L}\cdot s_3 \end{bmatrix}$$

Element Stiffness Matrix: 2nd order beam-column.

2.8 Plate Theories

By extending the beam theories into two dimensions a plate theory is devised. The basic theories are:

- the Kirchhoff-Love theory of plates, also known as *"classical plate theory"*,
- the Mindlin-Reissner theory of plates, also known as *"first-order shear plate theory"*.

The need to describe more phenomenons in the thick structures higher order theories, based on Mindlin-Reissner were formulated.

This section is based on the following sources:[21], [22], [30], [31] and [32].

Kirchhoff-Love Theory of Plates

Kirchhoff-Love theory of plates has been developed from Euler-Bernoulli beam theory. Similar assumptions are made as in case of Euler-Bernoulli beam theory:

1. Cross-section is absolutely rigid in it's own plane (plate thickness remains the unchanged after deformation).
2. Cross-section remains plane after deformation.
3. Cross-section remains perpendicular to the deformed mid-surface.

The very assumptions limit the theory to thin plates only, because $\sigma_3 = \tau_{13} = \tau_{23} = 0$. The typical thickness / width ratio is less than 10%.

Mindlin-Reissner Plate Theory

Similar concept, as the Timoshenko Beam theory, has been developed from Kirchhoff-Love Theory of Plates. The Mindlin-Reissner Plate Theory takes into account shear deformations through-the-thickness of the plate. In this theory, the cross-section does not necessarily remains perpendicular to the mid surface.

The shear stresses are accounted for: $\tau_{13} \neq 0$ and $\tau_{23} \neq 0$. However the $\sigma_3 = 0$. The bending stresses σ_1 and σ_2 are linear, while the shear stress is quadratic through the thickness of the plate.

Disadvantage of this theory is that it requires shear correction factor.

Higher Order Plate Theories

These theories employ higher order polynomials in the equations describing displacement through the thickness. This allows avoiding the need for shear correction factors.

These Higher Order Plate Theories offer the most in terms of thick composite analysis.

Summary

From the beam theories a number of two-dimensional derivatives were devised. These theories are called plate theories. There are different theories suiting for different applications. Thin laminates (thickness is less than 10% of the width) can be successfully analysed by Kirchhoff-Love Plate theory. Should the thickness be more than 10% of the width first or higher order theories should be employed.

The need for larger quantities of input data comes hand to hand with the advanced theories. Just the geometry definition is of a single linear element is twice more demanding compared to the beam (4 nodes instead of 2, figure 2.8).

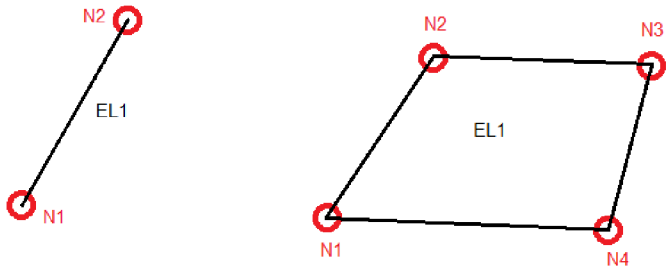

Figure 2.8: Linear plate element has twice as many nodes as linear beam element.

2.9 Verification and Validation of the Simulation

Verification and Validation is of great importance in the simulation process. It assures that the simulation results are trustworthy and further decision, based on these results, will have solid ground.

Dave Conover: Verification and Validation

Any text on finite element method topic informs reader that the obtained solution is not exact but merely an approximation. Mr Conover's presentation [62] draws attention to a very important topic of how trustworthy is the answer given by the FEA. Verification and validation are defined as follows:

Verification: *'Did I construct the models right?'*
Validation: *'Did I construct the right models?'*

Robert Sargent: Verification and Validation of simulation models

Very extensive text on validation, verification and accreditation of a computerized model is presented in [63]. The definition of the VV terms is:

Model **verification** ensures that the model and its implementation are correct.
Model **validation** ensures that the model is used within its domain of applicability.

2.10 Static vs. Dynamic Loading

Generally all the loads are dynamic: landing or taxiing force impulses happen at considerable speeds. However all the regulations [64], [65], [66], [67] prescribe exact force the landing gear is required to withstand. This effectively changes the character of the loading to quasi-static. All the loads in this thesis are therefore considered quasi-static.

2.11 Summary

Findings of previous sections, together with the author's own experience, are the base for the state of the art summary that follows. This summary is the starting point for the main work, which is presented in the following chapters.

2.11.1 Product

The author is employed by TechProAviation company. Services, that the company offers include airplane design, manufacturing and strength testing for certification of microlights, ultralights and LSAs, categories according to the regulations [65], [66], [64].

Another task the author has been appointed while at the university was a finite element simulation of wing segment of a glider (regulation [67]).

Author's first hand experience concerns beam-like products - that is wing spar and landing gear spring. Therefore these objects are chosen to be the focus of this work.

2.11.2 Material

The wing spar (flanges) and landing gear springs are classified as thick composite structures. For this reason the focus of this thesis is on the thick composite material, based on unidirectional lay-up.

One definition of *thick* is based on the Mindlin–Reissner plate theory, which is through the plate thickness-to-width ratio greater than 10%. Another definition marks the composite as *thick*, if it contains over 15 plies.

An important property of the thick composite, compared to the thin structures, is the out-of-plane stress. By through-thickness loading new phenomena occur, such as ILSS. Therefore the appropriate attention should be given to the analysis of such effects.

- **Material properties**

Total of five independent material constants are needed for strain vector determination. The following suggestion defines E-glass fibre unidirectional composite in terms of these constants.

- Lateral and through thickness modulus

It has been established, that $E_2 \equiv E_3$. In the beginning of the analysis, with no better data, the elastic modulus of the matrix can be used. Typical value of epoxy-matrix elastic modulus is $E_M = 3.5GPa$. Hence it can be assumed $E_2 \equiv E_3 = E_M = 3.5GPa$.

- Longitudinal modulus

Longitudinal modulus is mostly based on the fibre volume fracture and fibre elastic modulus. Let's assume fibre volume fraction $V_F = 60\%$ and E-glass fibre. Typical elastic modulus (in tension) is $E_F^T = 73GPa$ [69]. From knowing the matrix elastic modulus the final E_1 can be determined.

$$E_1 = E_F \cdot V_F + E_M \cdot (1 - V_F) = 73 \cdot 0.6 + 3.5 \cdot (1 - 0.6) = 45.2GPa$$

- Poisson's ratios

Typical value of isotropic metal material is $\mu = 0.3$. Similar values are usually published for composites: $\mu_{12} = \langle 0.23 \div 0.30 \rangle$ [33], [38].

Poisson's ratio in the plane, perpendicular to the longitudinal direction, can be approached in similar way as out-of-plane elastic modulus: only the matrix matters. Therefore $\mu_{23} \equiv \mu_M$. Investigation [45] of Poisson's ratio of epoxy resin determined the value to be $\mu_M = \langle 0.43 \div 0.47 \rangle$.

Authors in [48] investigated the through thickness shear moduli of E-glass unidirectional composite of $V_F = 35\%$: $G_{31} = 2500MPa$ and $G_{23} = 1800MPa$.

- **Engineering vs True values**

All FE codes consider the material properties as the *"true stress value"*. Change in the cross-section is accounted for. The difference is explained on figure 2.9 and table 2.4.

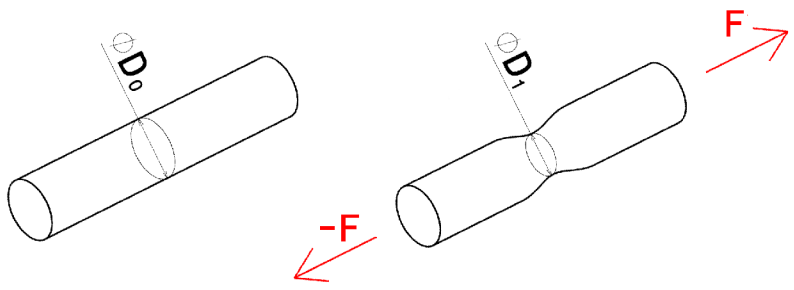

Figure 2.9: Engineering and true stress differs in the cross-section.

Engineering stress	$\sigma_{ENG} = \frac{4 \cdot F}{\pi \cdot D_0^2}$
True stress	$\sigma_{TRU} = \frac{4 \cdot F}{\pi \cdot D_1^2}$

Table 2.4: Engineering and true stress differs in the cross-section.

This concept is important in plastic region of stress-strain curve. The material considered (Glass or Carbon fibre) is assumed to be ideally linear until break. An assumption can be made:

$$\sigma_{TRU} \equiv \sigma_{ENG}$$

- **Hook's law for thick unidirectional composites**

Hook's law defines the relationship between stresses and strains of the material. Unidirectional composites are considered to be transversely isotropic. This reduces unknown material constants from nine down to five. The unknown material properties are $E_1, E_2, G_{12}, \mu_{12}$ and μ_{23}. The Hook's law in vector form is defined:

$$\begin{Bmatrix} \epsilon_1 \\ \epsilon_2 \\ \epsilon_3 \\ \gamma_{23} \\ \gamma_{13} \\ \gamma_{12} \end{Bmatrix} = \begin{bmatrix} \frac{1}{E_1} & -\frac{\mu_{12}}{E_1} & -\frac{\mu_{12}}{E_1} & 0 & 0 & 0 \\ -\frac{\mu_{12}}{E_1} & \frac{1}{E_2} & -\frac{\mu_{23}}{E_2} & 0 & 0 & 0 \\ -\frac{\mu_{12}}{E_1} & -\frac{\mu_{23}}{E_2} & \frac{1}{E_2} & 0 & 0 & 0 \\ 0 & 0 & 0 & \frac{2 \cdot (1+\mu_{23})}{E_2} & 0 & 0 \\ 0 & 0 & 0 & 0 & \frac{1}{G_{12}} & 0 \\ 0 & 0 & 0 & 0 & 0 & \frac{1}{G_{12}} \end{bmatrix} \begin{Bmatrix} \sigma_1 \\ \sigma_2 \\ \sigma_3 \\ \tau_{23} \\ \tau_{13} \\ \tau_{12} \end{Bmatrix}$$

After the analysis, which compares actual numbers for the intended application (that is landing gear springs and wing flanges), the following simplification can be made:

$$\epsilon_1 = \frac{1}{E_1} \cdot \sigma_1$$

- **Unequal tensile and compression properties**

The nature of composites is to have different properties in compression compared to the tension. Studies are providing the data so that a realistic assumption can be made as to what moduli ratio MR should be considered for materials, such as E-Glass / epoxy, HM carbon / epoxy or HS carbon epoxy composites.

Other practical impact of this study is the shift in neutral axis position in the laminate cross-section. This influences the peaks in the normal and shear stresses as illustrates on figure 2.10.

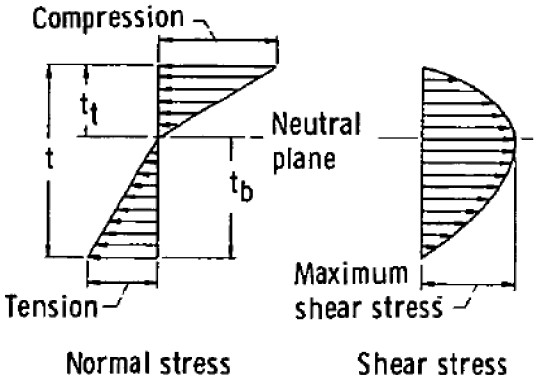

Figure 2.10: Position of neutral axis shifts away from the mid-fibre if $MR \neq 1$. [35]

A short assessment of the MR ratio follows in table 2.5. The overview should provide some insight to the extend of tensile / compression nonconformity.

Type	V_F [%]	E_1^C $[GPa]$	E_1^T $[GPa]$	X_C $[MPa]$	X_T $[MPa]$	MR $[-]$
GFRP	50.0	42	43	900	1100	1.02
GFRP	67.6	34.2	36.0	523	658	1.05
GFRP	58.7	49	48	820	1023	0.98
CFRP	53.0	104	110	900	1337	1.05
CFRP	60.0	113	150	1300	2000	1.02

Table 2.5: Overview of relevant tensile and compressive properties of commonly used composite materials. Data collected from [69], [44],[39] and [33]

This overview in table table 2.5 suggests that the difference in tensile and compression moduli is between $2 - 5\%$. This difference is quite low. However the author feels that this difference should not be omitted in the analysis.

- **Failure criteria**

On one hand, thick composites do require the usage of interactive failure criterion. On the other hand, the aviation industry producing small sport airplanes does not usually have the required material characteristics available.

The most common material test is the three-point-bend test. These tests are cheap and easy to do. Such test suits perfectly for monitoring of production quality. Flexural modulus and strength can be obtained quite easily. With some difficulties even tensile and compression modulus can be determined approximately. An inter-laminar shear strength can be obtained from a very similar test, even using the same, already damaged samples.

The absence of multiple material values usually leads to rough estimation based on published values for similar materials.

With respect to the data available and manufacturing possibilities one has to conclude that even the best interactive failure criterion will give unreliable answers, when the inputs are not correct.

When designing a new product - for example the main landing gear - a good question is what failure is likely to occur? It is shown on figure 2.11, that the loading bears similar[2] character as the tree-point-bend test.

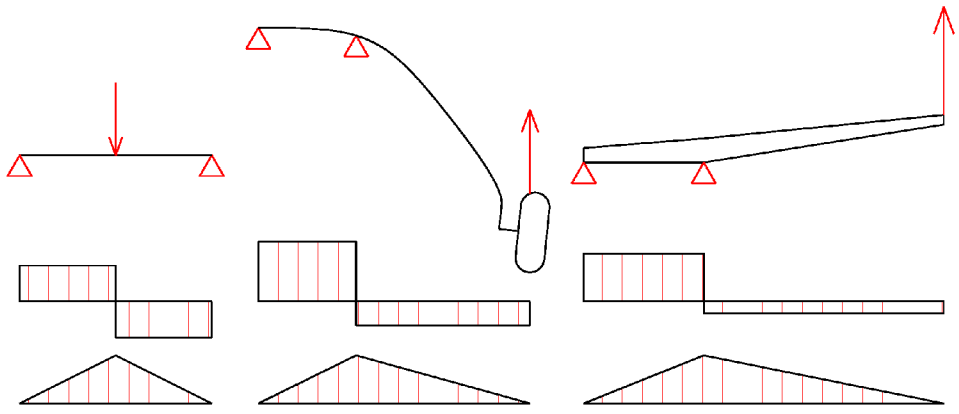

Figure 2.11: The similarity between three-point-bend test, landing gear and wing loading character.

Mr. Davallo [47] performed a number of flexural tests of hand-made laminates. All of these samples have failed in the same way: delamination. A number of failed landing gear springs at TechProAviation exhibits this very same failure. Other common failure observed during the drop tests is the result of through-thickness stresses. These failures are shown on figure 2.12.

[2]For the illustrative purposes only the dominant force is considered.

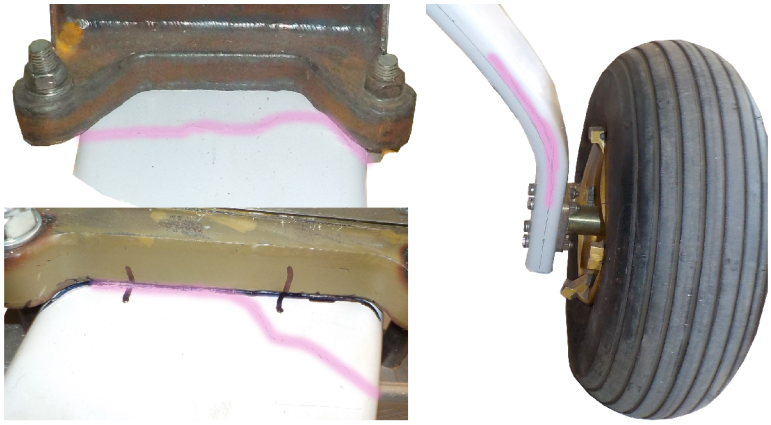

Figure 2.12: Typical landing gear failure: delamination and through-thickness crashing.

This thesis focuses on the products that are mostly loaded by simple bending. For this loading maximum strains or maximum stress will be adequate failure criteria. However, just like in three-point-bend test, there is an area where extensive through-thickness force is introduced. At this point a special analysis considering the through-thickness stress will take place. Also the issue of delamination exist, especially in the curved (small radius) areas.

- **Laboratory test experiments**

Laboratory tests of the coupons will only provide characteristics for certain type of loading. Only through a number of different test the material properties can be described. Moreover the airworthiness regulations require the actual product to be tested. These are the reasons why in so many cases the manufacturer chooses to produce a prototype (final product) and test it to the intended loading directly. This practice is used more often, if previous experience with similar product exists. From this standpoint of view, the coupon tests are redundant, expensive and impractical.

This practice however brings some drawbacks. The product must be designed and manufactured first, tested second, then analysed with a risk of re-design. Potential deficiencies may require significant changes in the design (different layup or even new mould). Yet still this practice may be cheaper and faster than obtaining the material data through different coupon testing.

The article [60] illustrates another drawback of omitting the coupon testing. Only 50% load has been applied during the laboratory test. The reason for this is that the specimen must not be destroyed. Probably, the specimen will be later used for the drop test of the whole airplane. Such test provides only the stiffness characteristic (force-deflection dependency). Not achieving the failure results in the lack of failure data for the material. Thus no validation of failure criterion can be evaluated, because no relevant material data were obtained.

2.11.3 Computer Aided Design and Engineering

Old schema of a company with separate design and analysis departments has changed during the last decade. New trend shifts the basic conceptual analysis directly to the design department, while the analysis department focuses on special, more thorough studies.

This shift has been enabled by combining CAD and CAE system into a single program distribution. Well known leading companies are Dassault Systèmes and Siemens. Their programs allow user to interact with 3D model and FEM in real time.

There are two other types of FEA programs. Both are dedicated only to analysis (there is either no 3D modeller at all or one with very limited capabilities). First types are the universal FEA programs, such as Abaqus, ANSYS and NASTRAN. Other programs are specialized and far less sophisticated, for example Ministatik. Figure 2.13 illustrates the hierarchy of three structural analysis software classes. With increasing capabilities of the software, the price grows.

In the author's experience it is not very common for FEM software to allow deformed geometry exports in a format, that can be used for perturbation or clearance analyses. To some extend the CAD built-in CAE modules allow these tasks. But only recent version (for example ANSYS 17 [15]) introduced a functionality that exports STL or STA file with deformed geometry.

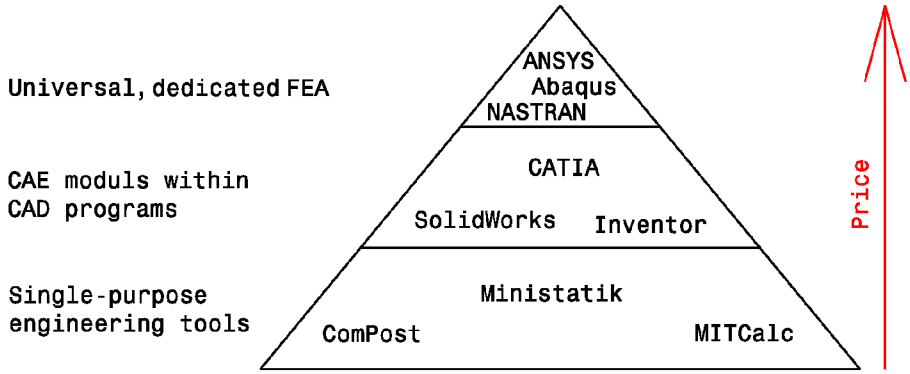

Figure 2.13: Three types of software for structural analysis.

- **Beam and Plate Theories**

Three theories were presented: the oldest and most basic Euler-Bernoulli formulation, advanced Timoshenko formulation and quite complicated second order formulation. Similar situation is with the plate theories, which were developed from the beam theories.

Even though the plate theories, especially the higher order theories, offer great features in thick composite analysis, they are not suitable for achieving the goal of this thesis. The reason are:

- The plate is more difficult to formulate than the beam is. This thesis aims to develop a software that is easy and flexible to use for quick design assessment. Beam elements suit this need far better.
- The intended analysis is two-dimensional, where the element's width is perpendicular to this plane. The plate element would have to be turned 90°. The mathematical formulation would not work within it's definition limits in this case.
- The beam elements and analysis will be modified to account for the most important stresses in order to compensate for the shortcoming of the theory.

Both, the Euler-Bernoulli and Timoshenko theories are suitable for the beam elements, where deflection is caused by bending moment (which is the primary loading that is expected in the landing gear springs and wing spars). Timoshenko accounts for shear deformation and therefore shows much better results on elements with low aspect ratio ($AR < 5$).

The second order theory accounts for deflection caused by axial loading on top of the bending moment. Theoretically, this should give better results. However the intended area of interest lies in the deflection caused by bending moment, only Euler-Bernoulli and Timoshenko theories are used thereafter.

- **Programming language**

Mr. Ferreira [1] uses Matlab scripting language for it's easy-to-understand appearance and capability to work easily with matrixes.

Indeed Matlab is very useful language with many practical capabilities. However several issues exclude Matlab from being used in this thesis do exist:

- stand-alone,
- GUI,
- price.

Matlab is not a freeware, actually it is quite expensive software. In 2016 the commercial licence price is 71.980Kč (approx. 2665€) annually [81].

Second problem concerns GUI. In order for a software to spread into public general use, it

must be user-friendly. One of user-friendliness keystones is the graphical user interface. That requires simple and clear data input. Large pieces of data may be imported through spreadsheet datafile. Other data can be inputted via textboxes. For settings the checkboxes and radioboxes are ideal choice. Each input must have its own description or hint.

Even though Matlab does include these GUI functions, the author does not consider these satisfactory.

Stand-alone capability (executable program) is very important to any software. It allows simply run the application on any computer without having to think about other supporting programs.

Python language is very popular among engineers lately [72]. It provides large libraries, such as Numpy [77] specialized to mathematical operations. GUI can be built easily with WX-Python library [78]. And Py2EXE library [79] can be used to develop a stand-alone executable application.

- **Deformation, Deflection and Displacement**

The author makes an effort throughout this text to use these terms in the meaning explained bellow. The explanation is based on [29]. Figure 2.14 shows the difference between deflection and displacement.

Deflection is the distance that an object bends or twists from its original position. Deflection is a general term that refers to a shape that the object transforms to when external loading is introduced.

Displacement is a vector that quantifies the deflection. In general, there are six constituents of a displacement vector (three translations and three rotations).

Elastic **deformation** is a resulting distortion in the material. It is the result of the force introduced externally. Deformation is equivalent to the term **strain**.

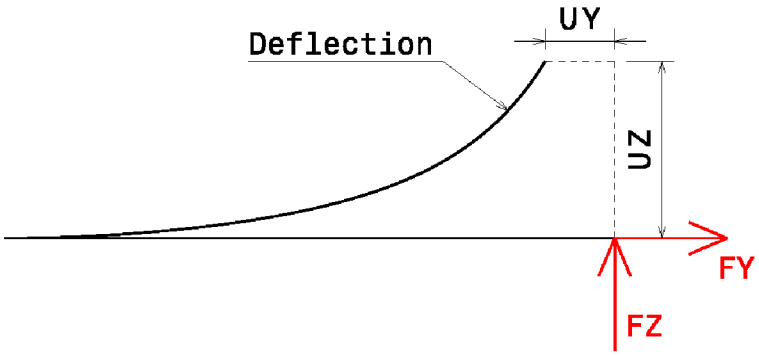

Figure 2.14: Deflection and $[U_Y, U_Z]$ displacement.

- **Non-linearity**

After studding various textbooks and presentations, for example [8] and [24], on the topic of non-linear analysis, the following summary can be concluded:

There are several types of non-linear behaviour, that may affect the solutions:

1. material (plasticity, creep),
2. boundary conditions and loads (springs, etc),
3. geometry.

It has been established in previous paragraph, that material behaviour is linear up to destruction. Also boundary conditions are rigid and linear behaviour is expected.

Geometrical non-linearity is in the context of this thesis of most interest. Large deformations are expected in case of main landing gear. There are two ways the geometry and its deformation may affect the loading. Both types are shown on figure 2.15.

Deformed geometry may change the vector of the loading force (figure 2.15, left) or the position of the loading force may shift as the structure deforms (figure 2.15, right). This thesis is focussed on main landing gear. Only the second type of non-linearity can be expected. This

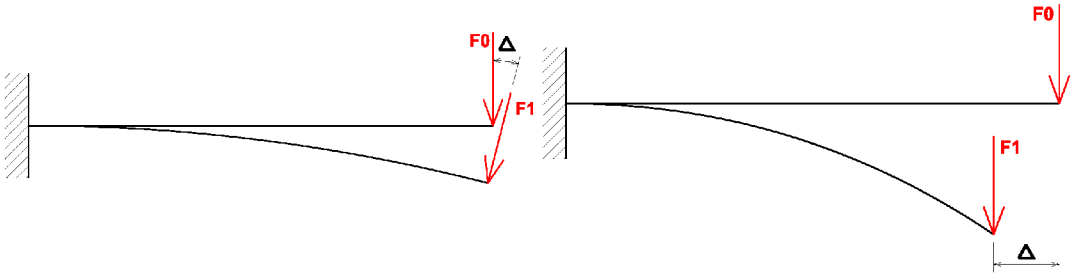

Figure 2.15: Non-linearity due to geometrical displacements and rotations.

expectation is illustrated on figure 2.16 showing a drop-test of Merlin 100 airplane. This figure is composed from a picture with un-deformed landing gear and the maximum deformation. The direction of the loading may not change (flat surface). However the arm of the force changes with the displacement.

Figure 2.16: Composed picture of main landing gear during drop test. Un-deformed and maximum deformation. Courtesy of TechProAviation, s.r.o.

For analysis of the intended products the non-linear analysis may be important. Progressive deformation will be taken into account in this thesis.

- **Verification and Validation**

Any mathematical model needs to be validated and verified in order to be considered credible. Verification of a finite element analysis confirms, that the used model is correct. Typical example of verification is the mesh check for element aspect ratio (figure 2.17). If the aspect ratio is too high, the mathematical model of the element does not work correctly.

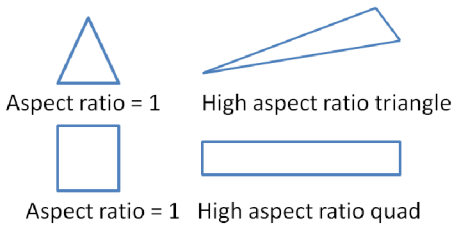

Figure 2.17: Example of verification: element aspect ratio [27].

For the purpose of KuFEM verification, the following definition is adopted:

"KuFEM is considered to be verified if the calculated results are same or very close to closed formula results and NASTRAN outputs."

Usually, validation of a mathematical model is achieved through the calibration. Which is a comparison of the model and actual measurement. This effectively means:

"KuFEM is considered to be validated if the calculated results are close to actual laboratory measurement."

This definition may proof to be controversial. It expects a perfect product and perfect measurement. Therefore multiple measurements will have to be made in order to obtain statistically significant results.

3 Industry problems and Goals of the Dissertation Thesis

3.1 Current problems

The Czech Republic is a large producer of small sport airplanes. Even though most of these airplanes are made of sheet aluminium, there are some typical components, that are made of fibre reinforced composites. These parts are usually non-structural wing-tips and variety of covers. Great number of these airplanes are designed with non-retractable undercarriage. For these kinds of landing gear composite springs are used with great success. Nose and tail gears often benefit from the composite springs as well.

Typical composite spring used for the undercarriage, regardless main, nose or tail gear, is a thick unidirectional beam with some kind of wrap layers. Similar kind of layup can be used in automotive leaf spring and sport equipment.

Manufacturing of these composite parts is a manual process, usually with the benefit of precise moulds with good control over the volume fracture. Even though computerized manufacturing could be employed, it is not common practice. It is due to the quantity of the productions (usually no more than one or two hundreds pieces annually). Such production can not afford extensive investments in manufacturing automation.

Further steps are based on assumption, that the moulds are precisely manufactured and are similar to forging moulds (lower container and upper lid). Described manufacturing assumptions have significant impact on determining the fibre volume fracture of the final composite. Having control over the volume fracture effectively means to control the mechanical properties of the final product. This allows accurate predictions of deflection, stress and strain.

Consider a typical landing gear spring. The most significant loading and boundary condition work in one plane. Similar situation can be found while exploring the loading and boundary conditions of a wing. However out-of-plane loading can be also found in both products. Yet no significant displacement is expected in the out-of-plane direction. That is other commonality that shall be exploited.

Focus of this thesis lies with thick composite products in aeronautical industry of the Czech Republic. This environment may not afford to buy expensive CAE programs. Quite often the engineers have insufficient knowledge of composite problematic, because most engineers must be in CAD departments and CAE departments are understaffed, if they exist at all. This can lead into two possibilities: new design is a) devised externally or b) in-house engineer among other duties must deal with the problem (either on his own or under some supervision of a senior structural engineer).

Imagine the engineer and his possibilities. In order to design new thick composite spring he can use closed-form solutions - perhaps even pre-programmed in spreadsheet tables. Or alternatively he can use dedicated FEM program or a module (now commonly available in CAD distributions). This however expects him to have such software available and more importantly to be able to use it correctly and efficiently.

Neither possibility is optimal. Closed form solutions are slow to be solved, design iteration is problematic and generating deformed shape CAD file is practically impossible. The other possibility expects some investment into software and the engineer to operate it. In aviation the NASTRAN solver is an established brand. Any changes in geometry are not easily propagated to the solver. The more complex model, the less flexible changes.

Products, that are considered in this thesis are expected to exhibit large displacements. Non-linear analysis should be available. One of the problems, connected to the large deflection, is the possibility of clashes with other parts of the assembly. Current FEM programs do not fully support export of deformed shape that could be easily included in the assembly, which prevents any clash checks.

- Industry problem:

1. The Czech Republic is a large producer of small sport airplanes.
2. These airplanes commonly use thick unidirectional composite components for landing gear.
3. Practically all composite parts in this sector are hand-made.
4. Hand made composites are far from perfect.
5. Thick composite parts can be manufactured in precise moulds with good control over the volume fracture.
6. If the volume fracture can be controlled reliably, the stiffness can be determined accurately.
7. Stiffness of the composite affects the deformation characteristics.
8. Landing gear springs exhibit large deformations in one plane.
9. Means of analytical analysis are not sufficient and effective tools in the landing gear design.
10. Small companies rarely own software and know-how deep enough to do effective landing gear design.

- Commercial Structural Analysis Software:

1. Available software[3] is universal.
2. It takes a long time to understand and operationally use such software.
3. This kind of software is expensive.
4. The time to built, evaluate and optimize a FE model is too long.
5. The more precise the model, the less flexible it becomes.
6. Exporting of the deformed shape is not a native function to current software.

3.2 Goals

Czech aviation industry must deal with both metal and composite structures. Special case are thick composite structural members, such as springs and wing spars. Both have similar problems, boundary conditions and loading. Very similar products can be found in automotive industry and sport equipment. For the purpose of design and optimization of these parts a special software is required, because closed-form solutions are not suitable and dedicated FEM programs have their specific problems.

New program must fit the needs for a simple, easy-to-use user friendly design tool. It must reflect the typical boundary conditions of intended application. First operation must be to determine the deflected shape of the beam. On this deformed shape a force and moment analysis shall be performed. From the known forces and geometry stress should be determined. According to the simplified Hook's law the strains shall be determined.

In order to help the user to orient himself in the results, simple output must be produced. This output contains the input recapitulation, deformed geometry, forces and moments, stresses and strains. User must be given the option to export the deformed geometry in universal CAD file in order to perform clash analysis.

Optional output shall be the NASTRAN input file. This should allow user to verify the program results with the established solver.

- Develop a program, that will:

1. be used in design and analysis of typical thick composite parts,
2. predict displacements in one plane,
3. calculate the element loads, stresses and strains,
4. export these results in understandable fashion,
5. be easy and flexible to use,
6. allow user to export geometry of deformed body,
7. allow user to export NASTRAN BDF file.

- Verify and validate the software

[3]This point considers dedicated FEM softwares (Ansys, Abaqus, etc).

4 KuFEM

Previous chapters revealed that thick composite structural parts are commonly used for small airplanes. Whether it is main landing gear, nose or tail gear spring or even main wing spar, all the parts are similar in terms of material behaviour, loading and deflection characteristics. In each case there is one dominant direction of loading and deflection. In this direction the largest and most significant displacement exists. Also the boundary conditions are similar (three-point bending is often encountered). Forces and displacements, perpendicular to the main loading direction, do exists. But these are not as significant as those of primary direction. For this reason only planar deformation analysis should be sufficient enough.

State of the art summary in chapter 2 concluded, that in present time Czech companies developing light sport airplanes may take an advantage of a cheap program dedicated to thick composite parts design. Therefore this thesis goal is to offer software of this kind.

4.1 What is KuFEM?

KuFEM is a program with a graphical user interface (see figure 4.1) for predicting deformed shape of a structural part and evaluating the stresses and strains. It is being developed with composite specifics in mind in order to evaluate more than just simple tension/compression. KuFEM allows simple export of deformed geometry (shown on figure 4.3) so the user can quickly evaluate collisions in his 3D model.

The software is based mostly on [1], [2], [3], [4], [5] and [9].

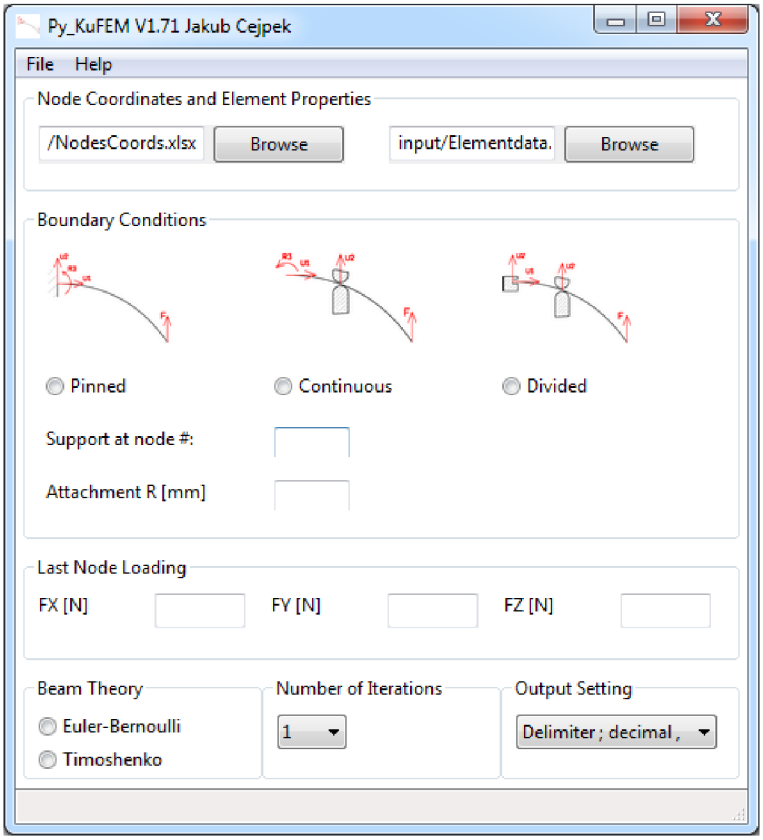

Figure 4.1: Graphical User Interface (GUI) of Python-built version of KuFEM.

Principle, how the program works, is shown on diagram 4.2. User is supposed to prepare the analysis input data, which consist of:

- geometry,
- boundary conditions,
- loading,
- calculation setting.

Based on these data, provided in the form of a spreadsheet tables, field inputs and radio-boxes in the GUI the deformed shape is predicted. Upon this deformed shape the forces and moments are calculated along the length of the model. Then the stresses and strains are calculated. When the program is finished with the calculation, the results are exported. These results are presented in three forms:

- detailed text file (with notes for easier understanding),
- spreadsheets (for quick plot generation and user failure criteria evaluation),
- IGES outputs (3D representation of deformed and un-deformed 3D shape).

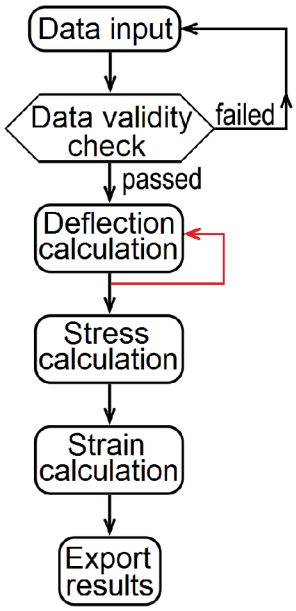

Figure 4.2: Basic diagram of the program.

User is also allowed to generate a BDF file (NASTRAN input file) that allows him to run very similar analysis in NASTRAN solver. This option provides an opportunity to verify the KuFEM results.

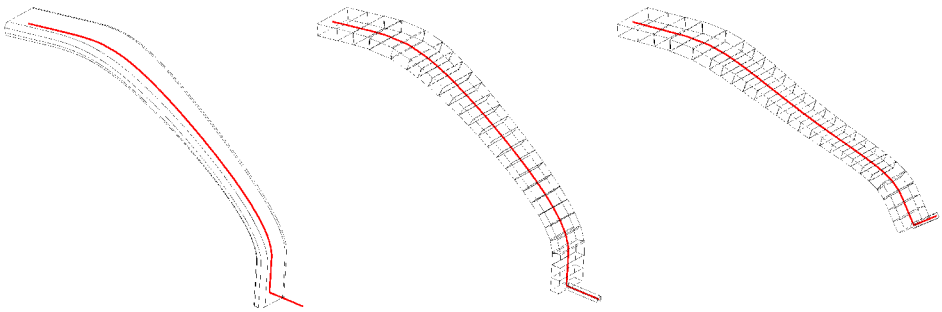

Figure 4.3: Original geometry. Meshed un-deformed geometry. Predicted deformed geometry.

4.2 User input

Program inputs are in two forms: spreadsheet files describing geometry and various settings and values in the graphical user interface (GUI). All inputs are described in detail in the following paragraphs.

4.2.1 NodesCoords spreadsheet

First, user is required to define the mid-fibre of the model. The mid-fibre is created as an intersection of two planes representing geometrical centre of the thickness and width along the length. In case of the main landing gear the last node is the centre of the wheel.

Having the mid-fibre defined, user must mesh the curve. Keep in mind that there should be node at each significant area, such as boundary condition, geometry change or different properties (this may be even more significant for composite structures as a stiffness may rapidly change). Node coordinate input can be found on figure 4.4

Total number of nodes should be high enough to represent the curved geometry and yet low enough for user's sake. For example main landing gear for Dusty and Merlin airplanes used 25 and 31 nodes respectively. In similar analysis [58] a total of 33 nodes were used.

	A	B
1	Y [mm]	Z [mm]
2	347,5	110,3
3	399,1	110,3
4	441,8	110,2
5	484,4	109
6	542,3	99,8
7	584,8	83,6
8	611	69,8

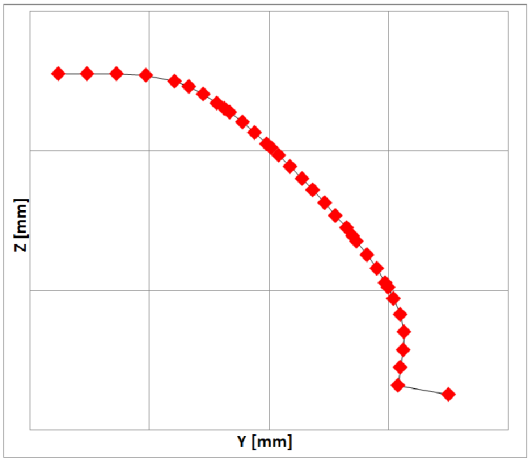

Figure 4.4: Spreadsheet example. Graphical representation of the spreadsheet values.

The size of the array is 2 x noNod, where noNod is a variable denoting the total number of nodes.

4.2.2 ElementData spreadsheet

Each two neighbouring nodes form one beam element (shown on figure 4.5). Therefore:

$$noEl = noNod - 1 \tag{1}$$

ElementData spreadsheet defines the geometrical and mechanical properties of each element (explained on figures 4.6 and 4.7). These values are:

- $B[mm]$ width,
- $T[mm]$ thickness,
- $t_H[mm]$ upper flange thickness,
- $t_D[mm]$ lower flange thickness,
- $E_H[MPa]$ upper flange stiffness,
- $E_D[MPa]$ lower flange stiffness,
- $t_O[mm]$ wrap thickness.

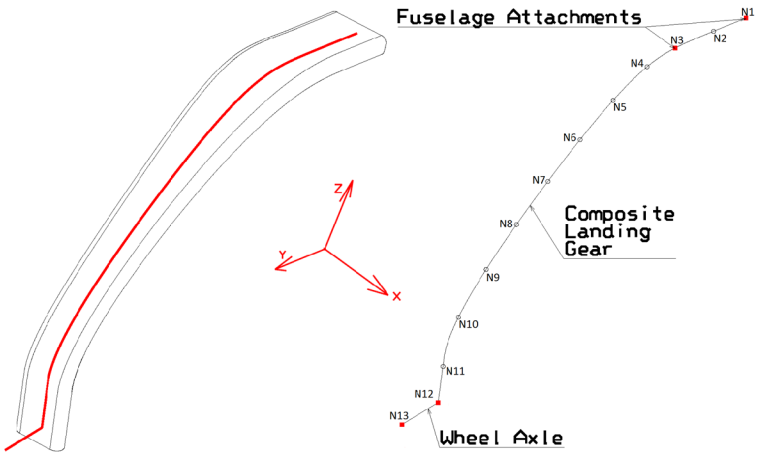

Figure 4.5: Nodes and elements iso-view.

	A	B	C	D	E	F	G
1	B [mm]	T [mm]	TH [mm]	TD [mm]	EH [MPa]	ED [MPa]	tO [mm]
2	98,38	26,48	8,2	8	52500	68000	0,99
3	98,81	26,46	8,2	8	52500	68000	0,99
4	101,47	26,39	8,2	8	52500	68000	0,99
5	105,86	26,33	8,2	8	52500	68000	0,99
6	106,78	26,29	8,2	8	52500	68000	0,99
7	103,87	26,12	7,8	7,6	52500	68000	0,99
8	100,33	25,79	7	6,8	52500	68000	0,99
9	96,57	25,38	6,6	6,4	52500	68000	0,99

Figure 4.6: Element data spreadsheet table.

4.2.3 Boundary conditions

User can choose from three different boundary conditions. This option increases the potential of the program. User can choose from the following boundary conditions:

1. pinned,
2. continuous,
3. divided.

These boundary conditions represent the most typical clamping and support combinations encountered in relation to the wings and landing gear springs. Further description follows in section 4.3.4.

4.2.4 Loading

Last node loading allows user to input the vector of forces in X, Y and Z direction. As the analysis is only 2D in terms of deformation, but 3D in terms of stress (strain) distribution. Force in the X direction will produce no deflection in this model.

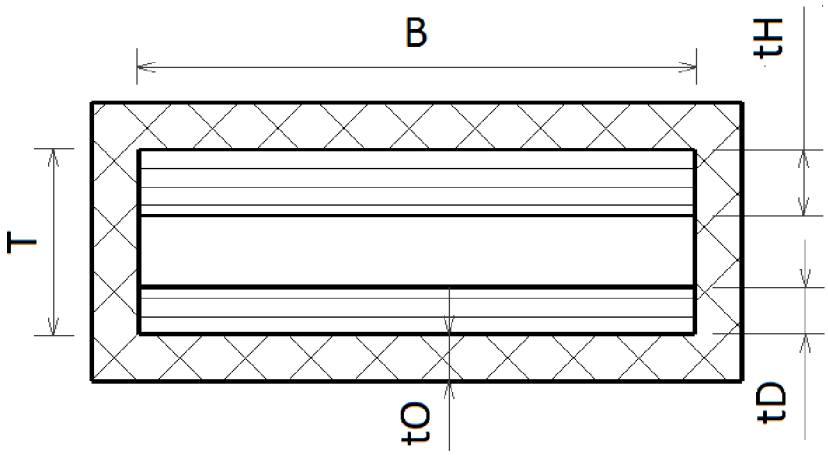

Figure 4.7: Cross-section geometry of an element.

4.2.5 Beam theory

Two beam theories are available for user to choose from. The choice will only affect the deflection (Timoshenko definition introduces shear effects. Therefore it is not as stiff as Euler-Bernoulli).

Choice of beam theory has no direct influence on stress / strain values. Further information on the beam theory implementation is given in section 4.3.2.

4.2.6 Number of iterations

Section 2.11.3 shows that the landing gear deflection is extensive and geometrically linear analysis may not be suitable for this kind of problem. For this reason a simple procedure of step-by-step load increase and geometry update is introduced. User may choose either linear (1 iteration) or non-linear analysis (multiple iterations). Further information about the non-linear procedure is given in section 4.3.3.

4.2.7 Output setting

KuFEM exports number of spreadsheet tables after the calculation is successfully finished. In order to help the user with the post-processing, the delimiters can be adjusted. This should avoid any potential problem user might face with his computer setting.

4.3 Analysis work-flow and equations

Principle, how KuFEM calculates the analysis is shown on diagram 4.8. Firstly, the geometry data processing is explained. Next section describes displacement vector determination. Other sections are focused on forces, stresses and strains calculation.

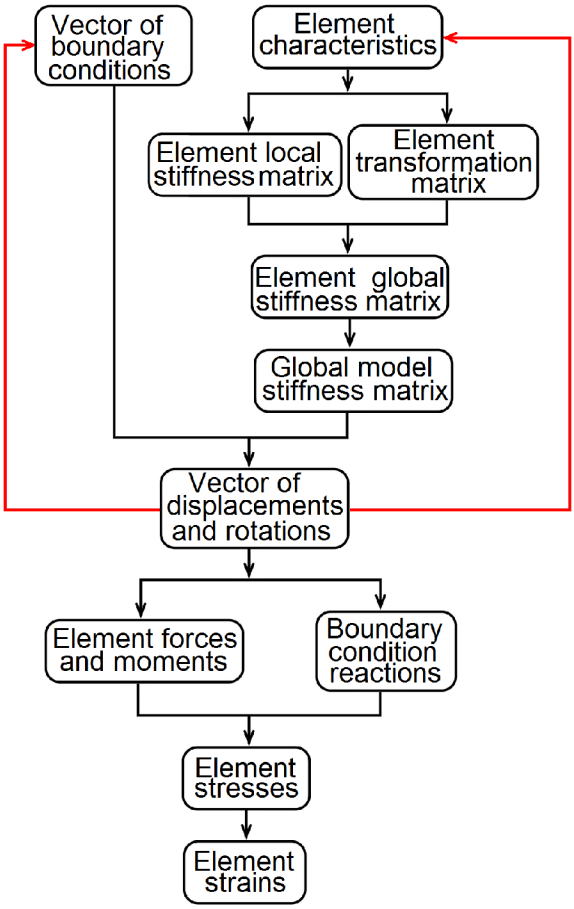

Figure 4.8: Diagram of calculation algorithm including non-linear procedure (red lines).

4.3.1 Geometry data processing

At this point, user has successfully loaded the geometry, element properties and filled out the boundary conditions. After pressing on *Run calculation* button, the data input is processed by determining the number of degrees of freedom:

$$no_{DOF} = 3 \cdot no_{Nod} \tag{2}$$

All elements are defined through the upper and lower flange (thickness and elastic modulus). However the mathematical formulation of beam elements does not accept this definition. For this purpose an effective properties will be calculated. This effective elastic modulus serve as a reference value to which the properties are transformed.

- element effective elastic modulus:

$$E_{EFi} = \frac{t_{Hi} \cdot E_{Hi} + t_{Di} \cdot E_{Di}}{t_{Hi} + t_{Di}} \tag{3}$$

First parameter of the element is the cross-section area, perpendicular to the mid-fibre:

- cross-section area:

$$A_i = t_{Hi} \cdot B_i \cdot \frac{E_{EFi}}{E_{Hi}} + t_{Di} \cdot B_i \cdot \frac{E_{EFi}}{E_{Di}} \tag{4}$$

Next step is to calculate the position of neutral axis. Neutral axis (figure 4.9) is determined from the total thickness of the element and from the thickness and stiffness of the flanges.

$$NO_i = \frac{1}{2} \cdot t_{Di} + t_{Hi} \cdot E_{Hi} \cdot \frac{T_i - \frac{1}{2} \cdot (t_{Di} + t_{Hi})}{t_{Di} \cdot E_{Di} + t_{Hi} \cdot E_{Hi}} \tag{5}$$

The 2^{nd} moment of area of the element cross-section needs to be calculated. It is calculated as a sum of upper and lower flange moment of area. Upper flange moment is denoted as JJ_{Hi} whereas the lower flange moment is denoted as JJ_{Di}.

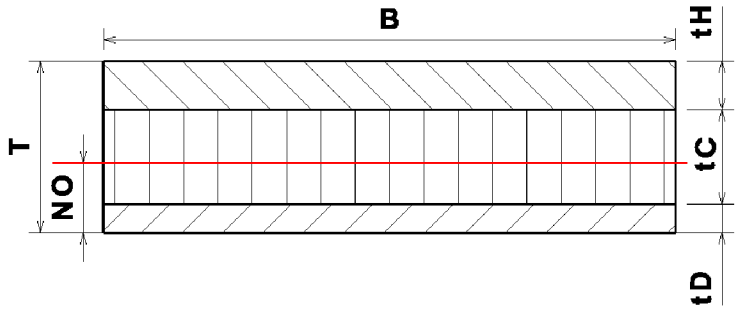

Figure 4.9: Neutral axis of a cross-section.

- 2^{nd} moment of area, upper flange to neutral axis:

$$JJ_{Hi} = \frac{1}{12} \cdot \left(B_i \cdot \frac{E_{EFi}}{E_{Hi}} \right) \cdot t_{Hi}^3 + \left(B_i \cdot \frac{E_{EFi}}{E_{Hi}} \right) \cdot t_{Hi} \cdot \left(T_i - NO_i - \frac{1}{2} \cdot t_{Hi} \right)^2 \tag{6}$$

- 2^{nd} moment of area, lower flange to neutral axis:

$$JJ_{Di} = \frac{1}{12} \cdot \left(B_i \cdot \frac{E_{EFi}}{E_{Di}} \right) \cdot t_{Di}^3 + \left(B_i \cdot \frac{E_{EFi}}{E_{Di}} \right) \cdot t_{Di} \cdot \left(NO_i - \frac{1}{2} \cdot t_{Di} \right)^2 \tag{7}$$

- total 2^{nd} moment of area to lateral axis:

$$JJ_i = JJ_{Hi} + JJ_{Di} \tag{8}$$

- 2^{nd} moment of area to through-thickness axis:

$$JK_i = \frac{1}{12} \cdot \left(B_i \cdot \frac{E_{EFi}}{E_{Hi}} \right)^3 \cdot t_{Hi} + \frac{1}{12} \cdot \left(B_i \cdot \frac{E_{EFi}}{E_{Di}} \right)^3 \cdot t_{Di} \tag{9}$$

Now only the geometrical parameters length and angle are calculated:

- length of an element is calculated from node coordinates:

$$L_i = \sqrt{(Y_i - Y_{i+1})^2 + (Z_i - Z_{i+1})^2} \tag{10}$$

- sinus value:

$$sin_i = \frac{Z_{i+1} - Z_i}{L_i} \tag{11}$$

- cosin value:

$$cos_i = \frac{Y_{i+1} - Y_i}{L_i} \tag{12}$$

At this point the stiffness matrix and transformation matrix of each element can be formulated.

4.3.2 Deformation

This calculation is based on an assumption, that the X-direction displacement is not significant in comparison to the Y and Z directions. Assuming $UX = 0$ significantly reduces difficulty of the problem. Only two translations and one rotation for each node will be calculated (see figure 4.10).

For a two-dimensional beam problem the Timoshenko or Euler-Bernoulli beam theories are adopted. User chooses the theory before running the calculation. Euler-Bernoulli theory assumes that un-deformed plane sections remain plane under deformation (cross-section remains constant). A shear correction factor is introduced to the element stiffness matrix. This changes Euler-Bernoulli beam element definition to the the Timoshenko beam element formulation.

The difference between the two beam theories is the element stiffness matrix. Equation 17

shows the LS matrix for Timoshenko beam. By giving $\Phi = 0$ the matrix is reduced to the Euler-Bernoulli theory. The parameter Φ gives the relative importance of the shear deformations to the bending deformations.

$$\Phi_i = 24 \cdot \alpha_i \cdot (1 + \mu) \left(\frac{r_i}{L_i} \right)^2 \tag{13}$$

where the parameter α is shear area coefficient. It reduces the cross-section area to account for the non-uniform distribution of shear stresses in the cross section. For rectangular cross-section, according to Cowper's [12] approach:

$$\alpha_i = \frac{12 + 11 \cdot \mu}{10 \cdot (1 + \mu)} \tag{14}$$

For the wide flange cross-section the coefficient can be approximately determined:

$$\alpha_i = \frac{1.2 \cdot T_i}{t_{Hi} + t_{Di}} \tag{15}$$

The r parameter is the *radius of gyration* of the cross-section:

$$r_i = \sqrt{\frac{JJ_i}{A_i}} \tag{16}$$

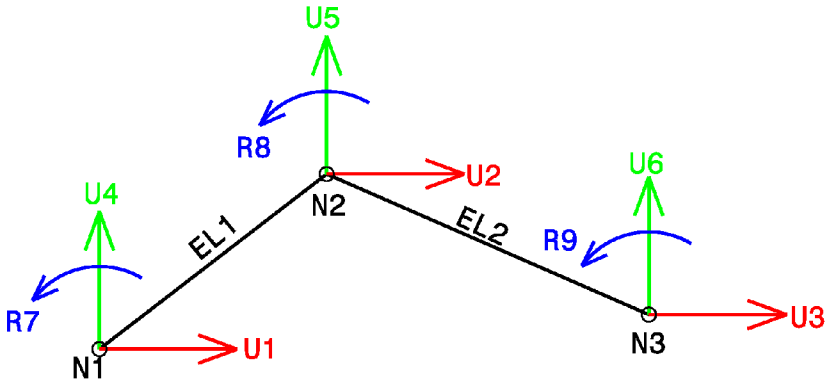

Figure 4.10: Degrees of freedom numbering (U=translation, R=rotation, N=node and EL=element).

Local stiffness matrix is calculated for each element[4][5]:

$$[LS] = \begin{bmatrix} \frac{A \cdot E}{L} & -\frac{A \cdot E}{L} & 0 & 0 & 0 & 0 \\ -\frac{A \cdot E}{L} & \frac{A \cdot E}{L} & 0 & 0 & 0 & 0 \\ 0 & 0 & \frac{12}{1+\Phi} \cdot \frac{E \cdot JJ}{L^3} & \frac{-12}{1+\Phi} \cdot \frac{E \cdot JJ}{L^3} & \frac{6}{1+\Phi} \cdot \frac{E \cdot JJ}{L^2} & \frac{6}{1+\Phi} \cdot \frac{E \cdot JJ}{L^2} \\ 0 & 0 & \frac{-12}{1+\Phi} \cdot \frac{E \cdot JJ}{L^3} & \frac{12}{1+\Phi} \cdot \frac{E \cdot JJ}{L^3} & \frac{-6}{1+\Phi} \cdot \frac{E \cdot JJ}{L^2} & \frac{-6}{1+\Phi} \cdot \frac{E \cdot JJ}{L^2} \\ 0 & 0 & \frac{6}{1+\Phi} \cdot \frac{E \cdot JJ}{L^2} & \frac{-6}{1+\Phi} \cdot \frac{E \cdot JJ}{L^2} & \frac{4+\Phi}{1+\Phi} \cdot \frac{E \cdot JJ}{L} & \frac{2-\Phi}{1+\Phi} \cdot \frac{E \cdot JJ}{L} \\ 0 & 0 & \frac{6}{1+\Phi} \cdot \frac{E \cdot JJ}{L^2} & \frac{-6}{1+\Phi} \cdot \frac{E \cdot JJ}{L^2} & \frac{2-\Phi}{1+\Phi} \cdot \frac{E \cdot JJ}{L} & \frac{4+\Phi}{1+\Phi} \cdot \frac{E \cdot JJ}{L} \end{bmatrix} \tag{17}$$

[4]The lower index *'i'* is omitted for the sake of clarity.

[5]The elastic modulus of the element is marked as 'E', however the effective stiffness from equation 3 is used. More information on this topic in section 4.4.1.

Each element is positioned at a different angle, relative to the YZ axis. In the next step a transformation matrix of goniometric functions is calculated:

$$[T] = \begin{bmatrix} cos_i & 0 & sin_i & 0 & 0 & 0 \\ 0 & cos_i & 0 & sins_i & 0 & 0 \\ -sin_i & 0 & cos_i & 0 & 0 & 0 \\ 0 & -sin_i & 0 & cos_i & 0 & 0 \\ 0 & 0 & 0 & 0 & 1 & 0 \\ 0 & 0 & 0 & 0 & 0 & 1 \end{bmatrix} \tag{18}$$

By multiplying these two matrices (T and LS) for each element a global stiffness matrix is obtained:

$$[GS_i] = [T_i]^{-1}[LS_i][T_i] \tag{19}$$

Combining all Global Stiffness matrices together creates Global Stiffness of the whole Model (GSM). This is ruled by the DOF number for each node.

$$[GSM] = \sum_{i=1}^{noEl} [GS_i] \tag{20}$$

Those DOF that were removed by boundary conditions are reflected in the GSM matrix and also in Loading Vector F. Final vector of displacements and rotations is obtained by multiplying the GSM matrix and Force vector:

$$\{U\} = [GSM]\{F\}^{-1} \tag{21}$$

Also the reactions can be determined by multiplying global stiffness matrix and transposed displacement vector:

$$\{R\} = [GSM] \cdot \{U\}^T \tag{22}$$

4.3.3 Geometrically non-linear analysis

Especially main landing gear is expected to achieve large deformations when dampening the landing shock force. Mr. Goyal emphasises the need for a non-linear analysis [59]. For this reason user can choose non-linear calculation by increasing the number of iterations.

Established procedure of non-linear analysis is based on Newton-Raphson technique. Each iteration involves formulation and solution of linearised equilibrium equations (updated stiffness matrix and solving the system).

Non-linear calculation reflects progressive deformation as a response to the increasing load. This is illustrated on figure 4.11 where linear and two-step non-linear calculation is illustrated. User may choose 5, 10 or 20 steps.

Diagram 4.8 illustrates the iteration loop by red lines.

4.3.4 Forces and Moments distribution in global coordinate system

KuFEM offers three different types of boundary conditions. The forces and moments at the centre of each element must be calculated in accordance to these conditions.

Pinned BC

Loading is introduced at node L. At node A all degrees of freedom are removed (UY, UZ, RX). Figure 4.12 shows the influence lines and table 4.1 provides the equations.

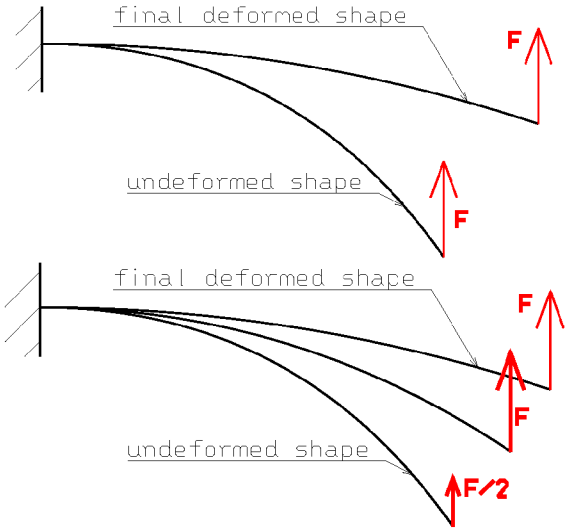

Figure 4.11: Difference between linear (1 step) and non-linear (2 steps) calculation.

For nodes	Direction	Forces	Moments
from A	X	$TX_i = FX$	$MX_i = FY \cdot (Z_i - Z_L) + FZ \cdot (Y_L - Y_i)$
to	Y	$TY_i = FY$	$MY_i = FX \cdot (Z_L - Z_i)$
to L	Z	$TZ_i = FZ$	$MZ_i = FX \cdot (Y_i - Y_L)$

Table 4.1: Influence lines equations for pinned BC.

Continuous BC

Loading is introduced at node L. At node A one rotation and one translation is removed (UY, RX). Node N removes the remaining degree of freedom (UZ). Figure 4.13 shows the influence lines and table 4.2 provides the equations.

For nodes	Direction	Forces	Moments
from A	X	0	$MX_i = F_Y \cdot (Z_N - Z_L) + F_Z \cdot (Y_L - Y_N)$
to	Y	$TY_i = FY$	$MY_i = 0$
to N	Z	0	$MZ_i = FX \cdot (Y_N - Y_L)$
from N	X	$TX_i = FX$	$MX_i = FY \cdot (Z_i - Z_L) + FZ \cdot (Y_L - Y_i)$
to	Y	$TY_i = FY$	$MY_i = FX \cdot (Z_L - Z_i)$
to L	Z	$TZ_i = FZ$	$MZ_i = FX \cdot (Y_i - Y_L)$

Table 4.2: Influence lines equations for continuous BC.

Divided BC

Loading is introduced at node L. At node A two translations are removed (UY, UZ). Node A removes the remaining degree of freedom (UZ). Figure 4.14 shows the influence lines and table 4.3 provides the equations.

User should be aware of the fact, that the MX component caused from FY may not always be in correspondence with the actual geometry. However the described model ensures the calculation to be on a safe side.

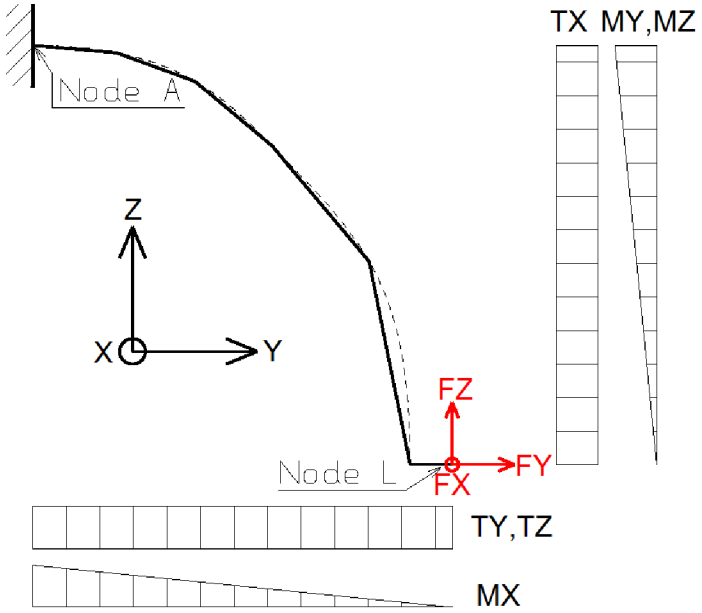

Figure 4.12: Influence lines for the pinned boundary condition.

For nodes	Direction	Forces	Moments
from A	X	$TX_i = -FX \cdot \frac{Y_L - Y_N}{Y_N - Y_1}$	$MX_i = FZ \cdot (Y_L - Y_N) \cdot \frac{Y_i - Y_1}{Y_N - Y_1} + FY \cdot (Z_N - Z_L) \cdot \frac{Y_i - Y_1}{Y_N - Y_1}$
to	Y	$TY_i = FY$	0
to N	Z	$TZ_i = -FZ \cdot \frac{Y_L - Y_N}{Y_N - Y_1}$	$MZ_i = FX \cdot (Y_N - Y_L) \cdot \frac{Y_i - Y_1}{Y_N - Y_1}$
from N	X	$TX_i = FX$	$MX_i = FY \cdot (Z_i - Z_L) + FZ \cdot (Y_L - Y_i)$
to	Y	$TY_i = FY$	$MY_i = FX \cdot (Z_L - Z_i)$
to L	Z	$TZ_i = FZ$	$MZ_i = FX \cdot (Y_i - Y_L)$

Table 4.3: Influence lines equations for divided BC.

4.3.5 Forces and Moments on Element

The forces and moments in global coordinate system are calculated at the centre of each element (figure 4.15). These forces and moments are transformed into the local element coordinate system, unique to each element.

It has been described in previous section that the whole geometry is located in one plane; therefore the geometry is two dimensional. An angle between the element longitudinal axis $\overrightarrow{I}$ and global horizontal axis $\overrightarrow{Y}$ can be calculated. According to this angle (figure 4.16) all forces and moments are transformed into the element coordinate system.

- characteristic angle is also calculated from node coordinates:

$$\theta_i = arctan\left(\frac{dZ}{dY}\right) = arctan\left(\frac{Z_{i+1} - Z_i}{Y_{i+1} - Y_i}\right) \tag{23}$$

- element longitudinal force is calculated from element centre coordinates:

$$FI_i = FY_i \cdot cos\,(\theta_i) + FZ_i \cdot sin\,(\theta_i) \tag{24}$$

- element lateral force does not change:

$$FJ_i = FX_i \tag{25}$$

- element through-thickness force:

$$FK_i = FZ_i \cdot cos\,(\theta_i) - FY_i \cdot sin\,(\theta_i) \tag{26}$$

- element twisting moment:

$$MI_i = MY_i \cdot cos\,(\theta_i) + MZ_i \cdot sin\,(\theta_i) \tag{27}$$

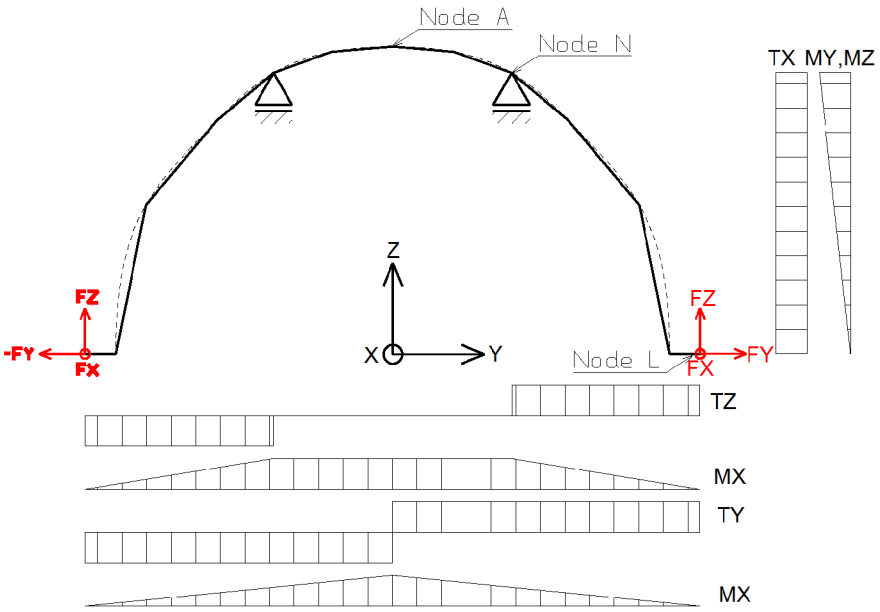

Figure 4.13: Influence lines for the continuous boundary condition.

- element lateral bending moment

$$MJ_i = MX_i \tag{28}$$

- element bending moment:

$$MK_i = MZ_i \cdot cos\left(\theta_i\right) - MY_i \cdot sin\left(\theta_i\right) \tag{29}$$

4.3.6 Stress analysis

General FEM approach to determine stresses and strains is to solve strains through strain-displacement matrix and than obtain the stresses by multiplying the strain vector by stiffness matrix:

$$\{\epsilon\} = [B]\{u\}$$

$$\{\sigma\} = [GSM]\{\epsilon\}$$

Where the matrix $[B]$ is the strain displacement matrix. It represents a function of the partial derivatives of shape functions with respect to the global XYZ coordinate system. This leads to Jacobian introduction. Jacobian matrix relates derivatives of the function in local coordinate system to derivatives in global coordinate system.

For KuFEM this approach will be substituted by more intuitive approach, based on geometry and already known element forces. Another advantage of suggested approach is that it is not limited by planar definition of the displacement calculation described above. Suggested approach follows simple idea, familiar to all engineering students:

$$\frac{Force}{Area} \rightarrow Stress \quad and \quad \frac{Stress}{Stiffness} \rightarrow Strain$$

Another advantage of this approach uses the element definition from section 4.2.2. This element definition allows to account for unsymmetrical flanges (geometry and material). Method is based on [11].

Each element is loaded by three forces and three moments. These forces and moments were determined in previous sections. At this point, stresses are going to be calculated. Four locations in the cross-section are picked as the most loaded points. These points are denoted as C, D, E and F. In rectangular cross-section these points are the vertexes as shown on figure 4.17. These points are equivalent to NASTRAN solutions. [3, 3049-3056]. Dimensions are defined on figures

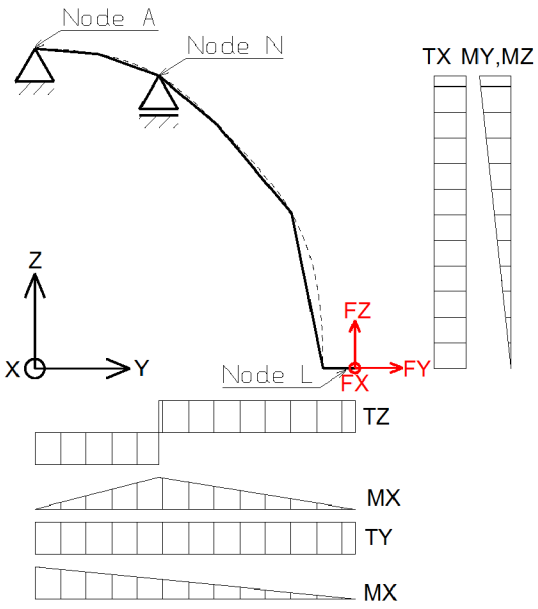

Figure 4.14: Influence lines for the divided boundary condition.

4.6 and 4.7. Figure 4.18 shows the cross-section stress loading by given force or moment, whereas figure 4.19 shows the shear flow in the wrap.

The following stresses are calculated for the flanges:

- normal tensile/compression[6] stress:

$$\sigma I_i = \frac{FI_i}{B_i \cdot (t_{Hi} + t_{Di})} \tag{30}$$

- bending stress at CF edge[7]:

$$\sigma J_{CFi} = \frac{MJ_i}{JJ_i} \cdot (T_i - NO_i) \tag{31}$$

- bending stress at DE edge:

$$\sigma J_{DEi} = \frac{MJ_i}{JJ_i} \cdot NO_i \tag{32}$$

- bending stress due to MK [8]:

$$\sigma K_i = \frac{MK_i}{JK_i} \cdot \frac{1}{2} \cdot B_i \tag{33}$$

- total stress at point C:

$$\sigma_{Ci} = \sigma I_i + \sigma J_{CFi} + \sigma K_i \tag{34}$$

- total stress at point D:

$$\sigma_{Di} = \sigma I_i + \sigma J_{DEi} - \sigma K_i \tag{35}$$

- total stress at point E:

$$\sigma_{Ei} = \sigma I_i - \sigma J_{DEi} - \sigma K_i \tag{36}$$

- total stress at point F:

$$\sigma_{Fi} = \sigma I_i - \sigma J_{CFi} + \sigma K_i \tag{37}$$

Standard beam elements do not support stress and strain calculation in form required for the intended analysis. Following approach is applied.

[6]Tensile / compression stress component does not require recalculation due to different elastic modulus, because of the assumption that both flanges are made from the same material and both are loaded in the same direction.

[7]Different tensile / compression module is incorporated into the Neutral axis position NO.

[8]Tensile / compression stress component does not require recalculation due to different elastic modulus, because of the symmetrical arrangement of the flanges.

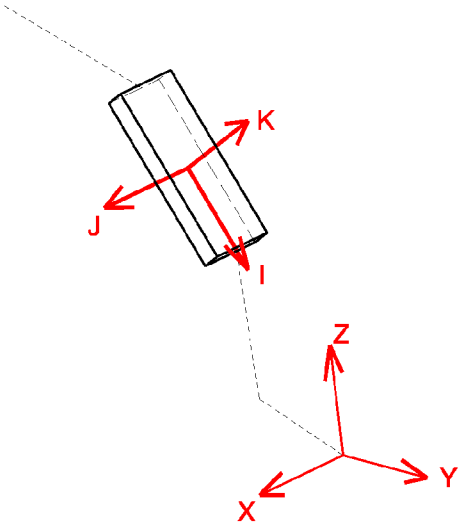

Figure 4.15: Element geometry and loading.

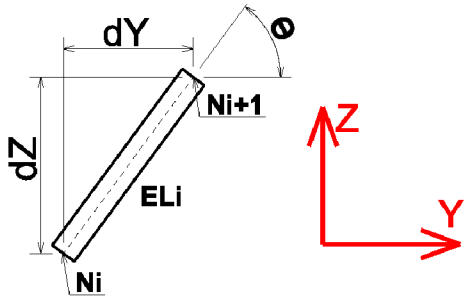

Figure 4.16: Characteristic angle θ.

- shear flow from torsion:

$$q_{Oi} = \frac{MI_i}{2 \cdot T_i \cdot B_i} \tag{38}$$

- shear stress from torsion:

$$\tau_{Oi} = \frac{q_{Oi}}{t_{Oi}} \tag{39}$$

4.3.7 Normal stress through thickness

When using the divided or continuous boundary condition, important problem is the through-thickness stress in the area of the outer hinge. For this reason is user required to input the attachment width R. Width B is an average value between the two neighbouring elements.

- through-thickness stress:

$$\sigma_{TT} = \frac{2}{R \cdot (B_{N-1} + B_N)} \cdot F_Z \cdot \frac{Y_L - Y_N}{Y_N - Y_1} \tag{40}$$

4.3.8 Shear stress through thickness

This section has been developed as a part of KuFEM's later versions. Therefore new definitions are necessary in order to describe the calculation of the shear stress through thickness (figure 4.20).

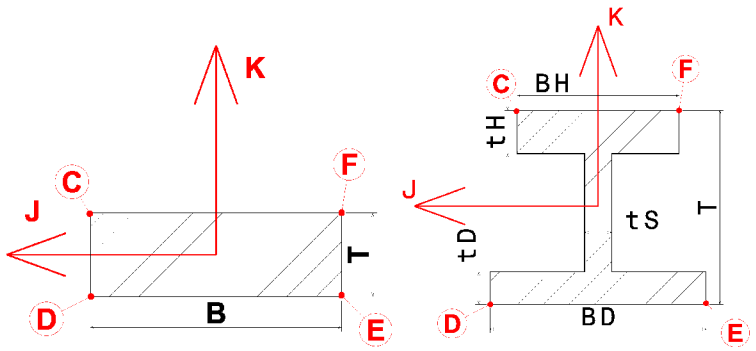

Figure 4.17: Cross-section points for stress calculation. Rectangular and I cross-section.

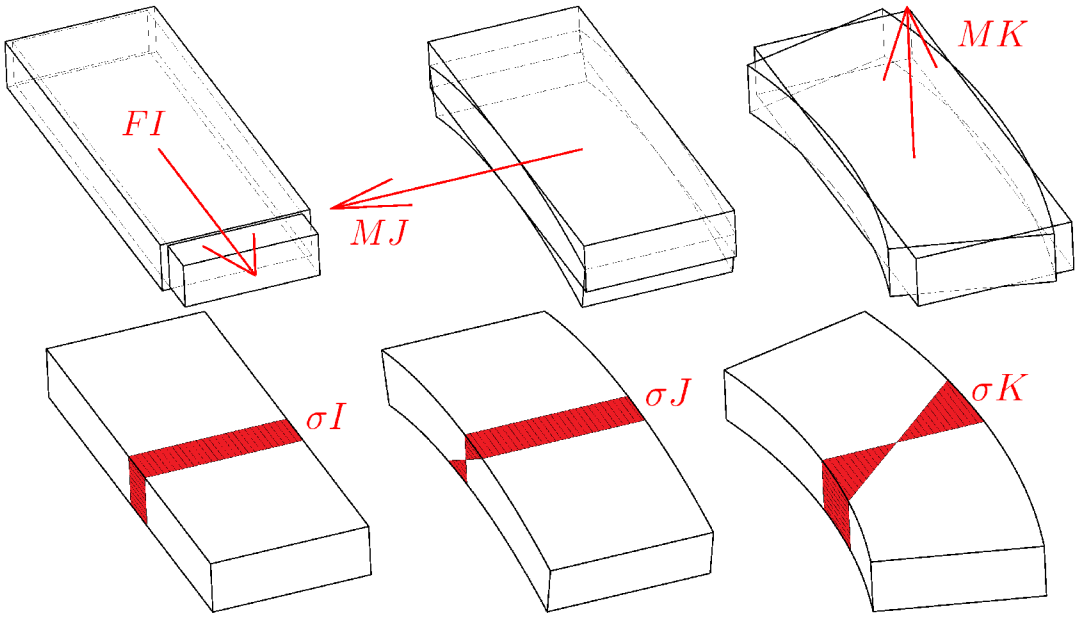

Figure 4.18: Force FI causes stress σ_I. Moment MJ causes stress σ_J. Moment MK causes stress σ_K.

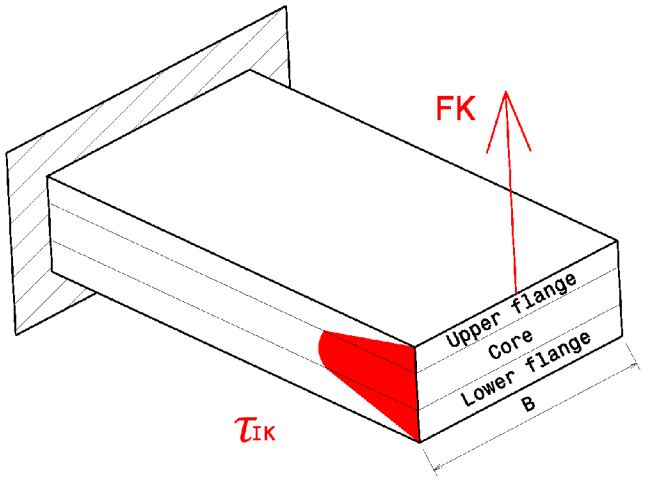

Figure 4.20: Shear stress through thickness of the element.

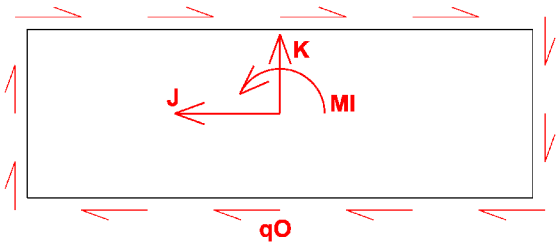

Figure 4.19: Moment MI causes stress τ_O.

Shear stress through thickness is based on [19], a simpliffied method introduced by Mr. Bednarcyk in 2008.

In general, the calculation expects the cross-section to consist of three plies: upper and lower flange and the core. Each cross-section constituent has it's own stiffness modulus.

Since the KuFEM is now focussing also on the core a change in the input data seemed reasonable. Original input set of data describing the thickness was T, t_H and t_D (section 4.2.2). Now it has been changed to more logical t_H, t_C and t_D. Each constituent is also described by it's stiffness: E_H, E_C and E_D.

First the basic parameters are determined:

- Total thickness:

$$T = t_H + t_C + t_D \tag{41}$$

- Effective stiffness (upgraded equation 3):

$$E_{EF} = \frac{t_H \cdot E_H + t_C \cdot E_C + t_D \cdot E_D}{T} \tag{42}$$

- Neutral axis position (upgraded equation 5):

$$NO = \frac{1}{T \cdot E_{EF}} \cdot \left[\frac{1}{2} \cdot E_D \cdot t_D^2 + t_C \cdot E_C \cdot \left(t_D + \frac{1}{2} \cdot t_C\right) + t_H \cdot E_H \cdot \left(t_D + t_C + \frac{1}{2} \cdot t_H\right)\right] \tag{43}$$

The shear flow through the thickness is calculated from the width of the element.

- Shear flow:

$$q_{IK} = \frac{F_K}{B} \tag{44}$$

Further equations determine the 2^{nd} moment of area of the cross-section:

- Upper flange: see equation 6.
- Lower flange: see equation 7.
- Core:

$$JJC = B \cdot \frac{E_{EF}}{E_C} \cdot t_D \cdot \left[\frac{1}{12} \cdot t_C^2 + \left(NO - \frac{1}{2} \cdot t_C - t_D\right)^2\right] \tag{45}$$

- Total (upgraded equation 8):

$$JJ = JJH + JJC + JJD \tag{46}$$

Next objective is to divide the cross-section into several slices[9] (figure 4.21) and calculate the first moment of area:

- Slice addition to the first moment of area:

$$\Delta S_{\Omega i} = \frac{1}{2} \cdot B \cdot \frac{E_C}{E_{EF}} \cdot \left(k_i^2 - k_{i+1}^2\right) \tag{47}$$

- First moment of area at K:

$$S_K = \sum_{k=-NO}^{k=K} \Delta S_\Omega \tag{48}$$

And finally the distribution of the shear stress through thickness can be calculated:

[9] KuFEM pre-set value is 50 slices regardless the total thickness T.

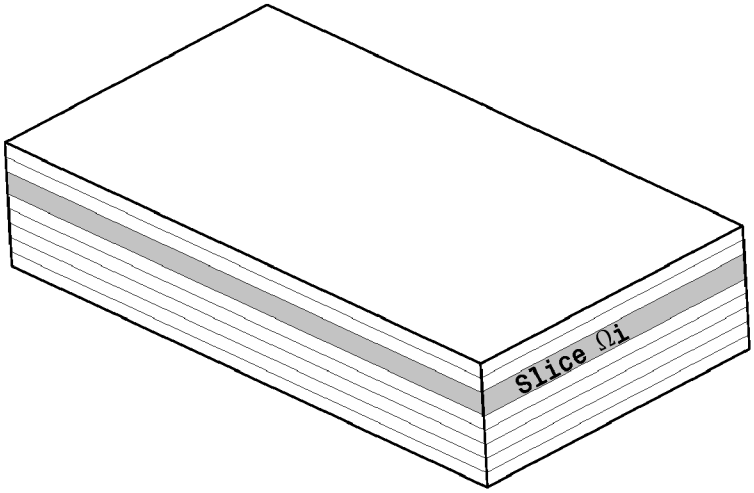

Figure 4.21: Element has been divided to several slices in through-thickness direction.

- Shear stress distribution on a cross-section:

$$\tau_{IK} = \frac{q_K}{JJ} \cdot S_K \tag{49}$$

The resulting shear stress distribution may look similar to figure 4.22.

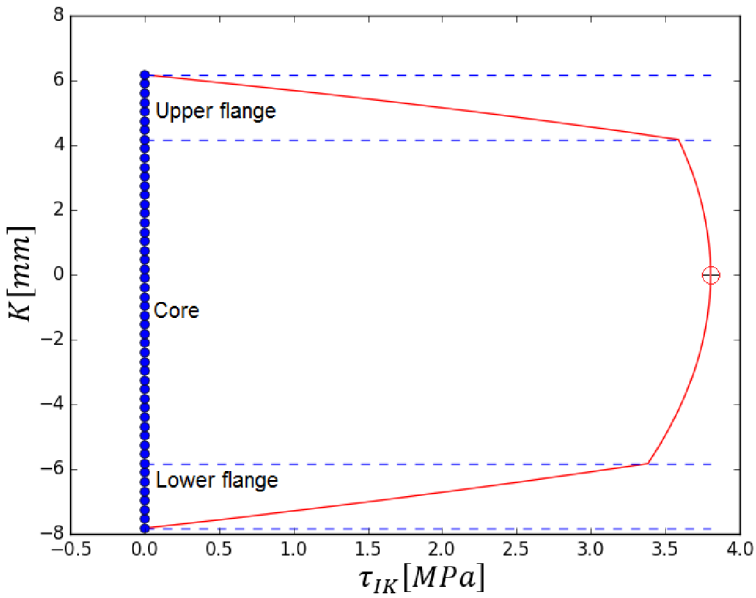

Figure 4.22: Typical distribution of shear stress on a cross-section made out of two flanges and core.

KuFEM output of this calculation for each element is only the maximum shear stress and it's position.

4.3.9 Strain analysis

Having determined the normal stresses at points C,D,E and F, now the simplified Hook's law is used to determine the actual strain:

$$\epsilon_{ji} = 100 \cdot \frac{\sigma_{ji}}{E_{ji}} \tag{50}$$

where the index i denotes the number of element and index j denotes the location in the element. In this manner the difference between compression and tensile modulus is taken into account. The strain is given in [%] for user comfort. For example typical fibre glass, used for structural parts, is to withstand about 3.5% of strain [69] before destruction. This gives fast and easy reference how well the material's potential is used.

4.4 Output functions

4.4.1 BDF Output

User can generate a BDF output file based on the inputs made previously. A short description of BDF follows. Important note concerns the element stiffness is presented. BDF file description has been used from [80] and the quick reference guide [3].

First problem to solve is the cross-section characteristics. KuFEM input includes total thickness and upper and lower flange thickness. Therefore there is the possibility that:

$$T > t_H + t_D \tag{51}$$

For this reason, the BDF export function first determines what cross-section shall be used. The rectangular cross-section is used unless following condition is true:

$$T - t_H - t_D \leq 0.1 \tag{52}$$

Margin of 0.1mm is applied. If this condition is satisfied, the I-cross-section to be exported to BDF is chosen. As only one E can be recorded, the E_{EF} is chosen. For this reason the width of the flanges of the I will be adjusted accordingly:

$$\begin{aligned} B_D &= B \cdot \frac{E_{EF}}{E_D} \\ B_H &= B \cdot \frac{E_{EF}}{E_H} \end{aligned} \tag{53}$$

Flange thickness remain unchanged. At this point, the element properties can be recorded to the BDF file.

BDF file is an ASCII record with 80 characters per line of code. One line consists of 10 slots (8 characters each). The code is divided into the following sections:

1. Job information record,
2. Elements and Element Properties record,
3. Material Records,
4. List of Nodes,
5. Boundary condition record.

Example element of a rectangular cross-section is described as $B = 20.50mm$, $T = 10.00mm$. It is made of material 'MAT1' ($E = 72000MPa$ and $\mu = 0.3$). The element is defined through points $[0, 25.1, 50.15]$ and [0,20.4,40.25]. Node 1 is pinned. Node 2 is loaded by $F_Z = -1000N$.

```
PBARL          1       1       BAR
           10.00   20.50
CBAR           1       1       1       2       1.      0.      0.
```

Listing 1: BDF example code, Elements with Rectangular cross-section.

In case of the I cross-section only one line is different. An example shows BDF code of an element similar to that above, except the cross-section is defined: $T = 10.00mm$, $B_H = 20.50mm$, $B_D = 15.75mm$, $t_H = 2.11$ and $t_D = 4.31$. Web thickness t_S is chosen to be 10% of the width B[10].

[10]This value has been set by trial-and-error method and is therefore generally unreliable. In future KuFEM versions more suitable quad elements shall be used, instead of beam elements. The web thickness will be defined by user directly.

```
PBARL           1       1           I
              10.00   15.75   20.50    1.00    2.11    4.31
CBAR            1       1       1       2      1.      0.      0.
```

Listing 2: BDF example code, Elements with I cross-section.

And finally the material and boundary conditions:

```
MAT1            1   72000           0.300
GRID            1               0.00   25.10   50.15
GRID            2               0.00   20.40   40.25
SPC1      1        123456  1
FORCE           1      21       0  1000.0 0.00000 0.00000-1.00000
```

Listing 3: BDF example code, Element Properties and Loading.

4.4.2 INP Output

Very popular and widely spread FEM solver is Abaqus CAE. KuFEM offers an option to generate Abaqus input file. The mathematical procedure is the same as in case of BDF file above. The INP file consist of the following sections:

1. Job information record,
2. Part record (nodes, elements, Elsets),
3. Section and material record,
4. Assembly record (list of active instances),
5. Step record (Nodesets and Elsets, BCs and Loads),
6. Output requests.

The model uses element type B31 (linear 3-dimensional beam element). B31 is an equivalent to CBAR. Material record uses elastic formulation (elastic modulus and Poisson ratio). This formulation is equivalent to NASTRAN.

```
** Section: Section-7-BAR_7  Profile: Profile-7
*Beam Section, Elset=BAR_7, material=MID_7, section=I
** ref.ht., height, width1, width2, t1, t2, t3
5, 10, 20.5, 15.75, 2.11, 4.31, 1.81
1,0,0
** Section: Section-8-BAR_8  Profile: Profile-8
*Beam Section, Elset=BAR_8, material=MID_8, section=RECT
** ref.ht., height, width1, width2, t1, t2, t3
5, 10
1,0,0
```

Listing 4: INP example code, Elements with I cross-section and rectangular cross-section.

```
**  material data from MAT1 with MID = 7
*Material, name=MAT_MID_7
*Elastic
45000,0.28
```

Listing 5: INP example code, Material properties.

```
** STEP: DoGoodJob
*Step, name=DoGoodJob, nlgeom=YES
*Static
0.1, 1., 1e-05, 1.
** LOADS
** Name: Loading   Type: Concentrated force
*Cload
NodeL, 3, -500.0
```

Listing 6: INP example code, Step record with nlgeom parametr.

Interesting option *"nlgeom"* is available in the step option. This option alters the kinematic formulation in order to provide accurate results when large deformations are achieved [23].

4.4.3 IGES Output

In simulation software available today it is not straight forward obtaining deformed geometry for further use. A lot of effort must be undertaken in order to be able to obtain at least the nodes in the deformed position. User can generate an IGES files obtaining both: the un-deformed and deformed geometry.

For the purpose of exporting the geometry an universal 3D geometry file format is used. Most commonly used universal formats are IGES and STEP. IGES format has been chosen for its simplicity.

IGES file is an ASCII record with 80 characters per line of code. The code is divided into the following sections:

1. section S (Start),
2. section G (Global),
3. section D (Directory Entry),
4. section P (Parameter Data) and
5. section T (Terminate).

Each line is identified by one of these letters. The letter is the 73^{rd} character in each line. Sections S and G contain general information about the file origin and settings. Section T is a checksum function that ensures the number of data transmitted and received are of the same length.

Sections D and P contain the actual geometry data. First, the entity (point, line, etc.) is declared in two lines per entity in section D. This entity is later specified in the section P.

KuFEM uses only point and line entities. The following example illustrates a line (defined by point A and B) and a point C. The geometry is shown on figure 4.23 and described in table 4.4. Note that points A and B serve only to define the entity 'Line' and are not explicitly listed in the IGES code.

IGES files use number-codes to describe the entity type. In case of point and a line the code is 110 and 116 respectively.

Point	X [mm]	Y [mm]	Z[mm]
A	0	5.12	9.70
B	0	8.34	2.53
C	0	7.71	3.69

Table 4.4: Example points for IGES output.

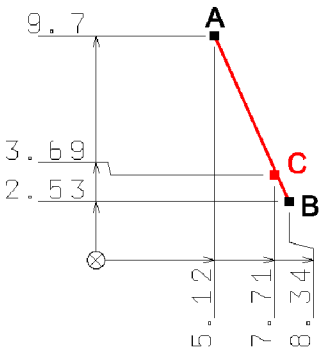

Figure 4.23: Example geometry for IGES code illustration.

Each element is drawn as a box with thickness T and width B. In the middle of the box a line representing mid-fibre is also drawn. In the scene of Bernoulli beam theory, the cross-section of the deformed shape remains perpendicular to the mid-fibre. Geometrical representation of an element is illustrated on figure 4.24.

```
     116       1       0       0   10000       0       0   000000001D       1
     116       0       2       1       0                     Point   0D       2
     110       2       0       0   10000       0       0   000000001D       3
     110       0       2       1       0                      Line   0D       4
116,0.0,7.71,3.69,0,0,0;                                             1P       1
110,0.0,5.12,9.7,0.0,8.34,2.53,0,0;                                  3P       2
```

Listing 7: IGES example code.

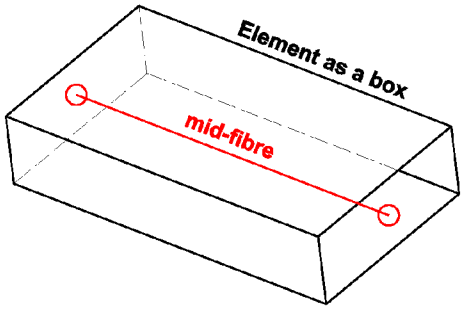

Figure 4.24: Element geometry in the output IGES file.

4.5 Geometrical simplification

The program assumes that the cross-section is a rectangle (or an I shape). This is not necessarily true in all cases, radius edges are usually employed in order to achieve convenient shape of the product. Practical question is when the radius should be considered in the analysis. Omitting the radius of the corners has an impact on the cross-section moment of area. This also stiffens the element.

Following figures (4.25) illustrate the ideal geometry ($R = 0$), mid-size radius and maximum radius $R = \frac{T}{2}$. According to this geometrical idea an error in second moment of are JJ will be determined.

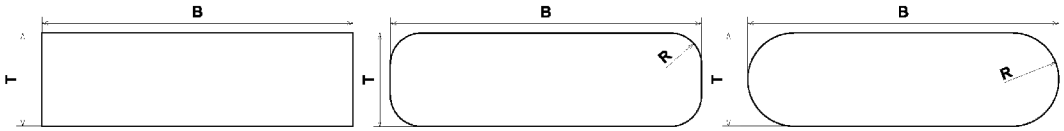

Figure 4.25: Rectangular cross-section without radius, with mid-size radius and with rounded edges (maximum radius).

Investigation of the error, that is associated with the radius omitting will be investigated on a cross-section, which is defined through maximum width B, maximum thickness T and radius R. The interval of investigation is going to be set as follows:

- radius $R \in \langle 0, \frac{1}{2} \cdot T \rangle$,
- cross-section aspect ratio $\frac{B}{T} \in \langle 0.1, 0.5 \rangle$.

By omitting the radius and error in the JJ calculation occurs. The JJ_{IDEAL} is the 2^{nd} moment of area of the rectangle defined by maximum width and maximum thickness of a cross-section. The JJ_{REAL} is the 2^{nd} moment of area of the real cross-section, including the radius. The difference of these two values will define the error:

$$JJError = 100 \cdot \frac{JJ_{IDEAL} - JJ_{REAL}}{JJ_{REAL}}$$

This error has been pre-calculated for the intervals given above. A nomogram 4.26 is pre-calculated to represent this error. Therefore the user can easily quantify the error of omitting the radius. Further more by knowing the error the real 2^{nd} moment of area he can determine.

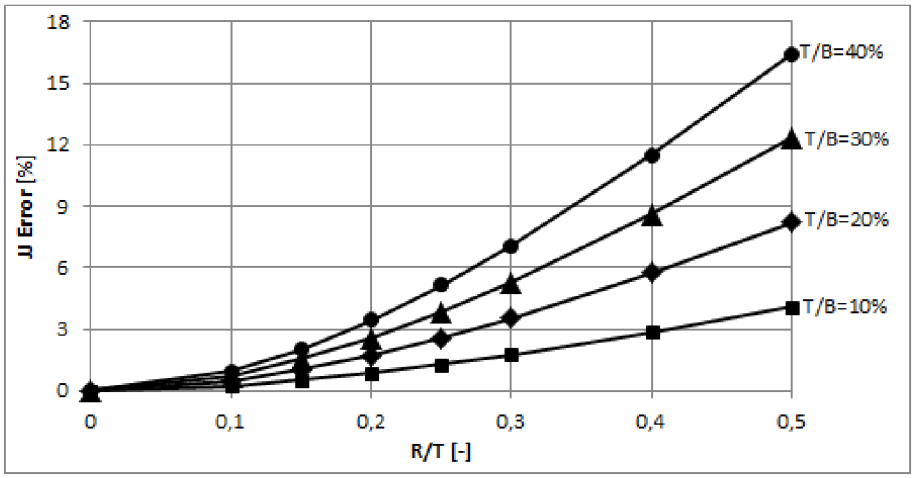

Figure 4.26: An error estimation function of JJ depending on R.

Just like the element density choice is up to user's consideration, so is the the geometry idealization. Flowchart on figure 4.27 shows suggested engineering approach to follow while creating the data inputs for KuFEM.

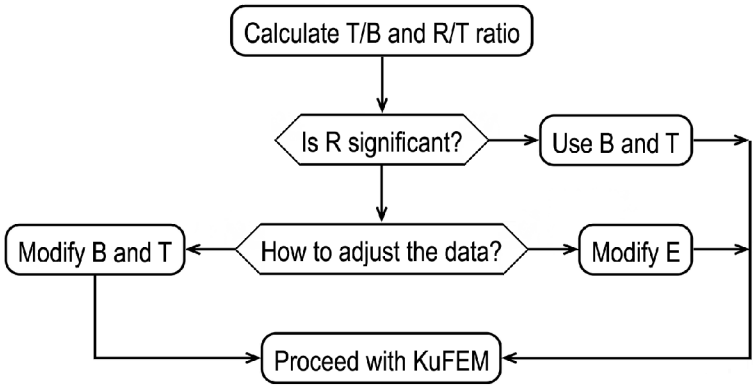

Figure 4.27: Flowchart of radius significance assessment.

4.6 Upper and lower flange determination

There are structures where the core layer is absent ($t_C = 0$). Upper and lower flange are made from the same material, except the material exhibit tension/compression non-linearity ($MR \neq 1$). In this case, user faces a dilemma as to how should be the upper and lower flange thickness determined.

First natural response would be:

$$t_H = t_D = \frac{1}{2} \cdot T$$

This is true only if $E_H = E_D$, that is if the compression and tension has the same moduli. Since it is obvious, that composite material posses different properties in opposite direction, the phenomena should be accounted for. A suggestion is given on figure 4.28 and following equations.

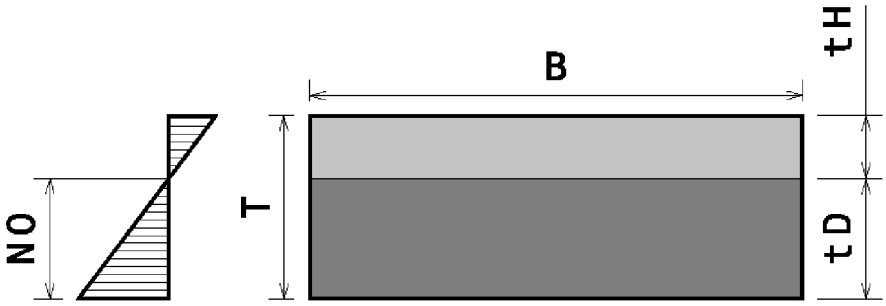

Figure 4.28: Suggestion how to determine t_H and t_D.

The division of the cross-section is based on an assumption, that main loading is bending along the J axis of an element. Therefore the flexural stiffness of upper and lower flange should be equal:

$$E_H \cdot JJ_H = E_D \cdot JJ_D$$

$$E_H \cdot \left[\frac{1}{12} \cdot B \cdot t_H^3 + \left(\frac{1}{2} \cdot t_H\right)^2 \cdot t_H \cdot B\right] = E_D \cdot \left[\frac{1}{12} \cdot B \cdot t_D^3 + \left(\frac{1}{2} \cdot t_D\right)^2 \cdot t_D \cdot B\right]$$

$$E_H \cdot t_H^3 = E_D \cdot t_D^3$$

From here a simple equation is obtained:

$$t_D = T \cdot \frac{\sqrt[3]{\frac{E_H}{E_D}}}{1 + \sqrt[3]{\frac{E_H}{E_D}}}$$

Hence:

$$t_H = T - t_D$$

In practical terms the lower the compression/tensile stiffness ratio, the higher the thickness of the compression part (illustrated on figure 4.29).

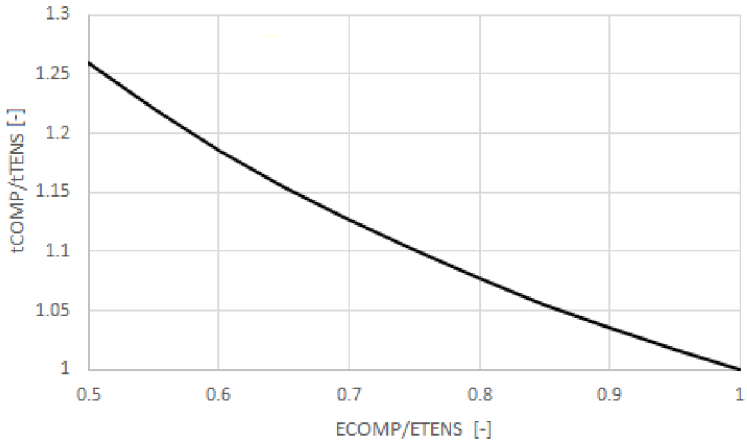

Figure 4.29: Stiffness compression/tensile ratio vs. the thickness ratio.

4.7 Verification Examples

The mathematical apparatus must be verified in order to be trusted in real application. For this reason typical examples, that can be solved analytically, will be presented. Further verification and validation will be shown in the following chapters.

All examples are presented on the same geometry (figure 4.30 and table 4.5) and mechanical properties. Constant cross-section of $B = 20mm$ and $T = 5mm$ with elastic modulus $E = 72GPa$ and wrap thickness $t_O = 2mm$.

Assumptions are that cross-sections remain plane, the material is homogeneous and follows Hooke's law and elastic modulus for tension and compression are the same.

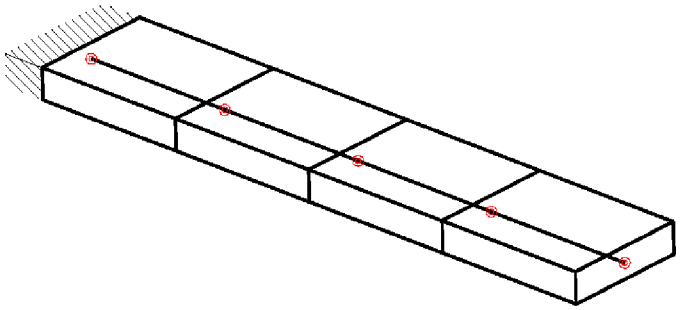

Figure 4.30: Example beam geometry.

Node #	Y [mm]	Z [mm]
1	0	0
2	25	0
3	50	0
4	75	0
5	100	0

Table 4.5: Node coordinates.

4.7.1 Tension

Loading, for achieving only tensional stress, is introduced in the last node (see figure 4.31). The only non-zero force is $F_Y = 500N$. First, analytical solution will be presented and than KuFEM results will be compared with this analytical solution.

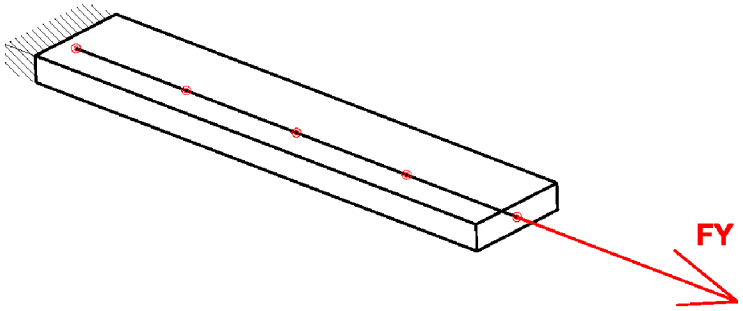

Figure 4.31: Loading by F_Y produces pure tension.

$$\sigma I_i = \frac{F_Y}{B \cdot T} = \frac{5000}{20 \cdot 5} = 50MPa$$

$$\epsilon I_i = 100 \cdot \frac{\sigma}{E} = 100 \cdot \frac{50}{72000} = 0.0694\%$$

$$U1_5 = \frac{F_Y \cdot (Y_5 - Y_1)}{B \cdot T \cdot E} = \frac{5000 \cdot (100 - 0)}{20 \cdot 5 \cdot 72000} = 0.0139mm$$

KuFEM predicts even stress along the whole beam $\sigma I_i = 50MPa$, also constant strain $\epsilon I_i = 0,0694\%$ and last node displacement $U1_5 = 0,0139mm$. These are the same results as given by analytical solution above.

4.7.2 Bending

When $F_Z = 500N$ is introduced, the beam is loaded by shear force and bending moment. This state can be also analysed with analytical equations and compared to KuFEM results. Figure 4.32 shows the example.

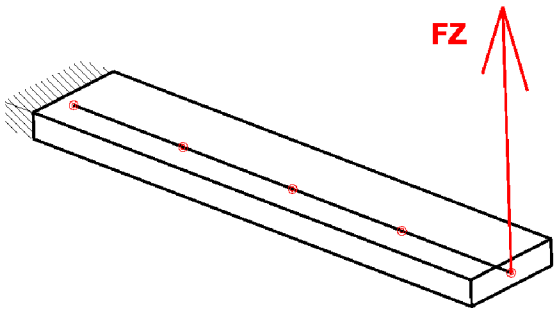

Figure 4.32: Simple bending.

- analytical solution for peaks in normal stress:

$$\sigma I_i = \pm \frac{F_Z \cdot (Y_5 - Y_i)}{JJ} \cdot \frac{T}{2}$$

- analytical solution for displacement:

$$U2_i = \frac{1}{6} \cdot \frac{F_Z \cdot Y_i^2}{6 \cdot E \cdot JJ} \cdot [3 \cdot (Y_5 - Y_1) - Y_i]$$

- analytical solution for peak in shear stress through thickness:

$$\tau_{IK} = \frac{3}{4} \cdot \frac{F_Z}{B \cdot T} = \frac{3}{4} \cdot \frac{500}{20 \cdot 5} = 3.75MPa$$

U_{2i} at node #	1	2	3	4	5
Analytical solution	0	0.95	3.47	7.03	11.11
KuFEM solution	0	0.95	3.47	7.03	11.11

σ_{Ii} at Element #	1	2	3	4
Analytical solution	525	375	225	75
KuFEM solution	525	374	224	74

τ_{IKi} at Element #	1	2	3	4
Analytical solution	3.75	3.75	3.75	3.75
KuFEM solution	7.49	7.46	7.42	7.40
NASTRAN solution	8	6	6	7

Table 4.6: Results for simple bending.

There is a slight differences in the normal stress values (table 4.6). This difference is caused by the fact, that KuFEM calculates stress on deformed shape. The difference is greater near the force introduction, where the displacement is greatest. Therefore it can be concluded, that

KuFEMs' predictions are in agreement with analytical solution.

Significantly different results are presented in the shear-through-thickness. Whereas KuFEM and NASTRAN (figure 4.33) are generally in agreement, the analytical solution tends to underestimate the resulting stress by approximately 50% in the presented example. Further validation is required.

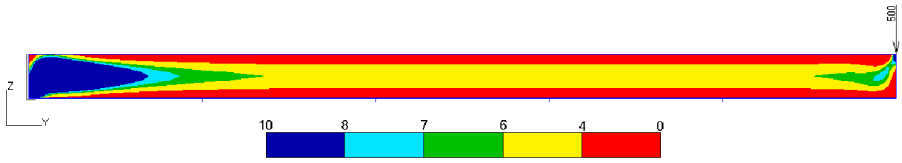

Figure 4.33: Shear through thickness as predicted by NASTRAN.

4.7.3 Torque

Torque is transferred through the wrap layers. The thickness of the wrap in this example is $t_O = 2mm$. KuFEM allows only force loading. But this may be worked around by introducing a force on a lever. This however requires editing the input data by adding one extra node (table 4.7), which will serve as point-connector element (figure 4.34). Also the geometry of the last element will be different in order to ensure stiffness.

Procedure of introducing the torque by a single force, as described above, has an unwanted side-effect: it introduces FJ force and MK moment.

All nodes lie in Y-Z plane. Therefore neither F_Y nor F_Z will produce torque moment. The loading is only the force $F_X = 500N$.

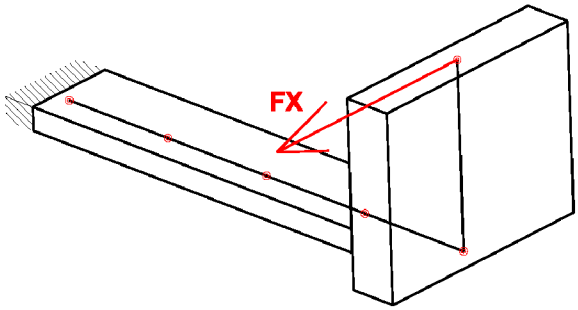

Figure 4.34: Simple torque of a beam with special point-connector element.

Node #	Y [mm]	Z [mm]
4	...	...
5	100	...
6	100	40

Table 4.7: Node coordinates for torque example. 6th node extends those defined in table 4.5

- torque moment:
$$MY = FX \cdot (Z_6 - Z_5) = 500 \cdot (40 - 0) = 20000N \cdot mm$$
- Torque shear flow:
$$q_O = \frac{MY}{2 \cdot B \cdot T} = \frac{20000}{2 \cdot 20 \cdot 5} = 100N/mm$$
- Shear stress in the wrap:

$$\tau_O = \frac{q_O}{t_O} = \frac{100}{2} = 50MPa$$

KuFEM has analysed the same example. As the deformation is calculated only in Y-Z plane and the loading is in X direction, KuFEM shows zero deformation (figure 4.35). However the results exported into TXT (figure 4.36) and CSV files quantify the stresses.

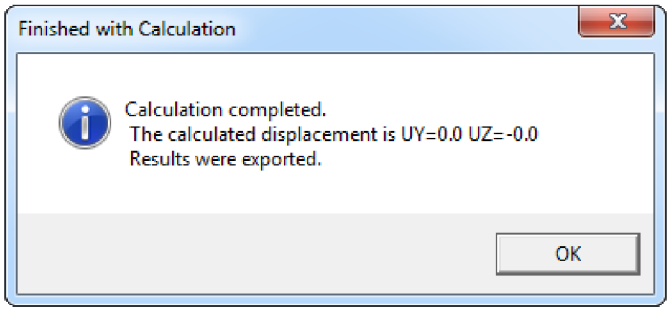

Figure 4.35: No reported deformation when calculation finished.

```
Stresses and Strains:
    TauO[MPa]: 50.0,50.0,50.0,50.0,0.0
```

Figure 4.36: Part of text output file *KuFEMOutput.txt* describing the shear stress in the wrap.

4.7.4 Summary

KuFEM has been verified for three simple cases: tension, bending and twisting in terms of deflection, normal stress, shear stress through thickness and shear stress in the wrap. The verification has been shown against closed-form generally accepted equations and NASTRAN solver. Further verification and validation will be shown in the following chapters.

5 Practical examples of KuFEM results

5.1 HPH Shark Composite Wing

The wing segment, which has been tested at the IAE, is the root section of a full composite wing. Tested segments were not equipped with flaps. Structurally the segments were identical to the wing: main spar made out of a foam core and thick carbon flanges.

The first five specimens were subjected to static tests, on the other four specimens fatigue tests were conducted. Static tests of two whole wings were also carried out. The figure 5.1 shows the fatigue test layout of X06 specimen in 2007. Parts of this chapter were published as

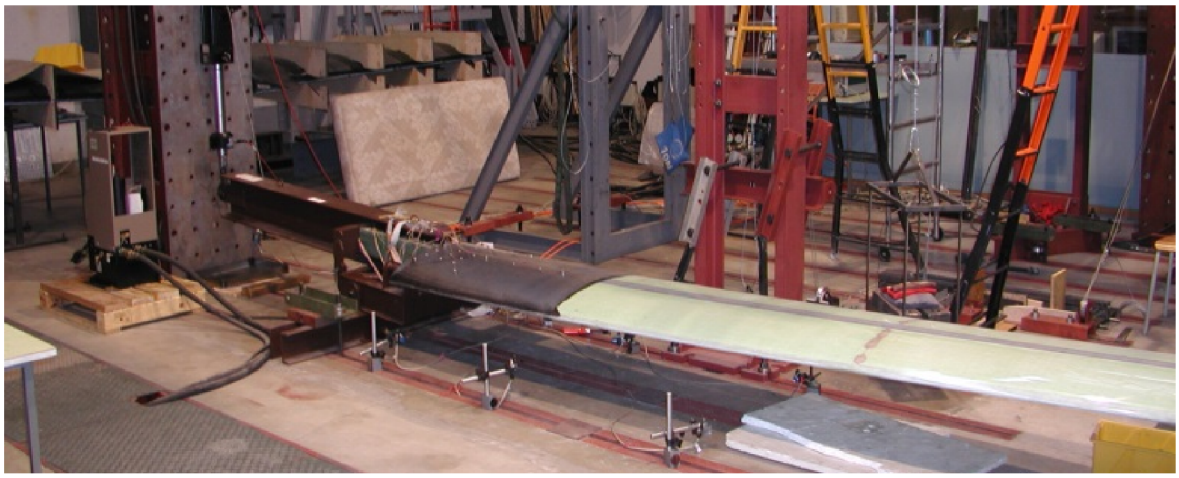

Figure 5.1: Layout of X06 wing segment fatigue test. Archive of IAE.

papers [74] under the title *"Modifications of a simple I-beam and its Effects on the Stress State"* and in [73] as *"Stress-deformation analysis of a composite wing segment"*. The first article has investigated the changes in stresses according to the structure shape and boundary conditions. The other describes simulation of the static wing segment test.

The author has also published an article about acoustic emission as a monitoring method used during the fatigue test of these segments. The article is entitled *"Acoustic Emission Localization in Testing of Composite Structures"* [75].

Three different programs are used to analyse the wing segment. First prediction is obtained from KuFEM (Euler-Bernoulli and Timoshenko, linear and non-linear prediction), then a NASTRAN finite element analysis (1D and 2D analysis), and a quick deformation analysis made in Ministatik. In the summary the deflection, strains and element forces are compared.

5.1.1 Loading

The original geometry and loading has been reduced. Geometrical changes include the removal of skin, rib and rear spar. Loading has reduced the forces (no counter F_Z force in the root rib) and twisting moment at the tip. Boundary conditions changed also. Original boundary conditions are shown on figure 5.2 (left), whereas the reduced boundary conditions are shown on figure 5.2 right). This simplified geometry, loading and boundary conditions will be used in analysis presented here after. Displacement vectors were calculated by three different methods. Firstly in KuFEM. From KuFEM a BDF file has been generated and analysed by NASTRAN. Another NASTRAN analysis using shell elements has been adopted from [74]. For third independent prediction Ministatik has been used.

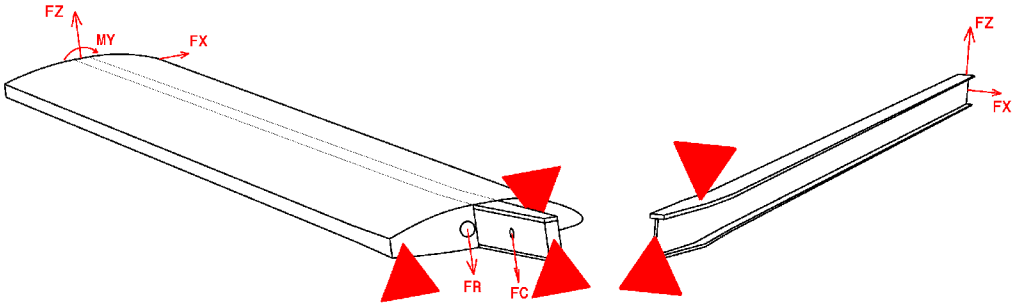

Figure 5.2: Left: original loading of the wing segment. Right: simplified model for verification analysis.

KuFEM results

First, the KuFEM analysis has been performed. Figure 5.3 shows an alert message informing the user about successfully finished calculation. Also last-node deformation is presented as a quick information. KuFEM automatically exports TXT file with detailed description of the

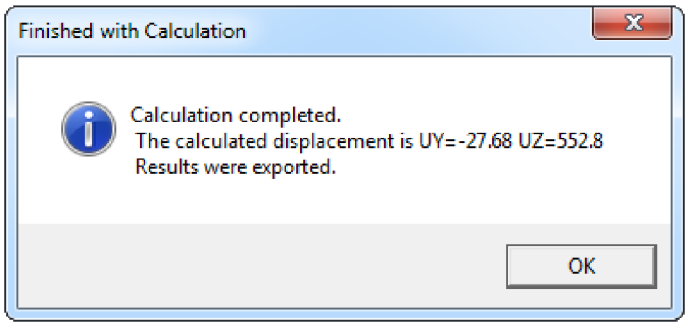

Figure 5.3: KuFEM information message after finished calculation.

task and the results. This file serves as all-in-one information. The data are presented in a way not suitable for further evaluation (plotting graphs, finding extremes, etc.). For this reason CSV output files are also automatically created. These spreadsheets contain original program-precision values, while the TXT file contains rounded values. The complete content of the output folder is presented on figure 5.4.

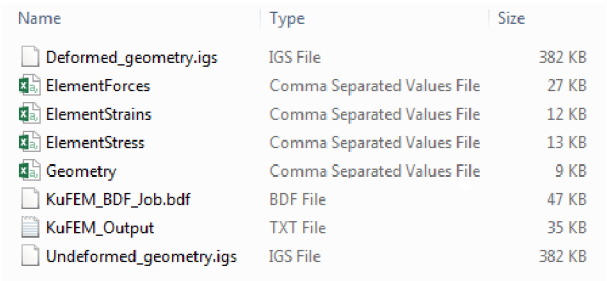

Figure 5.4: KuFEM information message after calculation has finished.

NASTRAN results, 1D model

A BDF file has been generated from KuFEM. This BDF file has been submitted to the NASTRAN solution SOL101 and post-processed in Patran. Because for each element the condition

in equation 51 is fulfilled, all elements are assigned the I-cross-section 5.5.

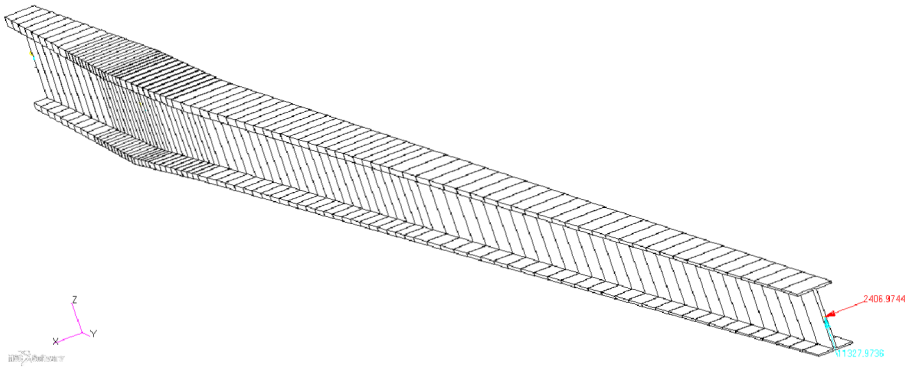

Figure 5.5: NASTRAN 1D model shown with graphical representation of cross-sectional properties.

NASTRAN results, 2D model

Shell element model (figure 5.6) from previous works at IAE is modified according to the scheme shown on figure 5.2. In order to achieve the effect of different flange thickness and yet keep the required work load as low as possible, a step change in the flange thickness is introduced within five intervals. Figure 5.7 shows the comparison between the actual flange thickness distribution along the span and the distribution used in the NASTRAN 2D model. Clearly there is a compromise between the workload and the representativeness of the distribution. In this case a legitimate expectation is that the 2D model is going to be stiffer and the strains will be lower than in case of 1D model, which changes the thickness at each element and therefore the drops are much lower.

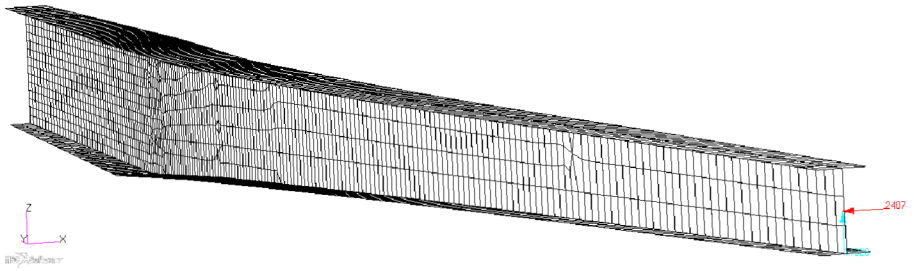

Figure 5.6: NASTRAN 2D model.

Ministatik results

A third, independent, deformation analysis is carried out by Ministatik program. The resulting displacement is calculated only in Z-direction, therefore UY=0. This program does not provide any information on stresses or strains.

5.1.2 Results

Deflection

Table 5.1 summarizes the last node displacement. To each analysis method is presented the Y and Z direction displacement in order to compare the results.

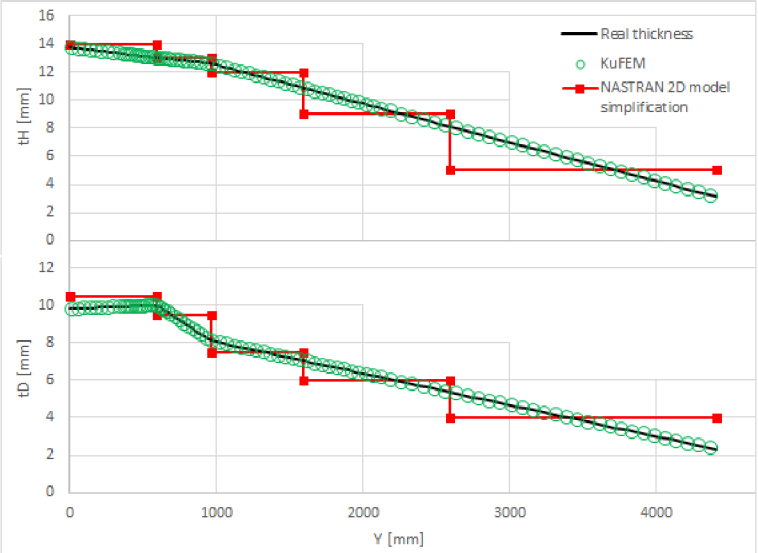

Figure 5.7: Simplification in flange thickness in 2D model.

Analysis	no. of iterations	Displacement UY [mm]	Displacement UZ [mm]
KuFEM Euler	1	-27.7	552.8
KuFEM Timoshenko	1	-29.6	592.3
Ministatik	1	0	684.5
NASTRAN 1D	1	-23.5	469.1
NASTRAN 2D	1	-25.8	511.6
KuFEM Euler	10	-111.0	513.4
KuFEM Timoshenko	10	-122.7	546.1
NASTRAN 2D	10	-64.4	490.5
KuFEM Euler	200	-115.5	504.1
KuFEM Timoshenko	200	-127.3	535.5

Table 5.1: Comparison of last node displacement.

Not only the last node displacement is important. The displacements along the wing span are also important. Following figures 5.8 and 5.9 shows the UZ span-wise displacement function. A special emphasis is given to the linear and non-linear calculation.

Strains

Strains are compared only for linear solutions. Figure 5.10 show the strains of KuFEM Euler-Bernoulli 1 iteration solution, KuFEM Timeshenko 1 iteration solution, NASTRAN 1D and 2D SOL101 solutions.

5.1.3 Summary

Three analysis of a wing segment are presented (KuFEM, NASTRAN and Ministatik). Further more different models and different theories are used. Total of 10 different variants are shown and discussed. The results are compared in terms of displacement and strains.

Comparison of strains on figures 5.8 and 5.9 shows good agreement between all analysis variants. Even more so, the comparison confirmed the claims of [9] that Euler-Bernoulli beam formulation is stiffer than Timoshenko formulation.

A search to lower the work load in modelling the 2D model took it's toll in the strain results (figure 5.10). Not only is the distribution scarred by steps, but also the effect of changing slope

is traceable. Also interesting observation is that the 2D model is stiffer as a result of the method used to replace the real flange thickness distribution.

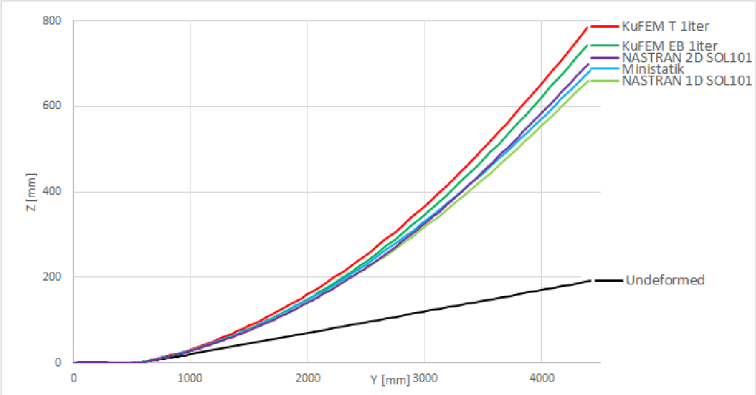

Figure 5.8: Deformed mid-fibre comparison for linear (1 iteration) solutions.

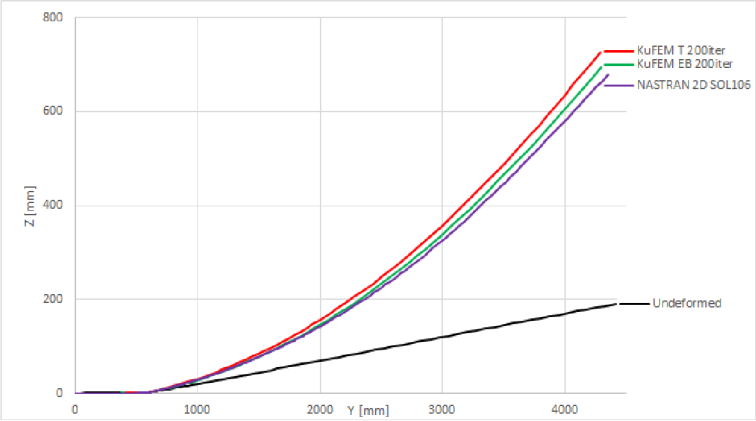

Figure 5.9: Deformed mid-fibre comparison for non-linear (multiple iterations) solutions.

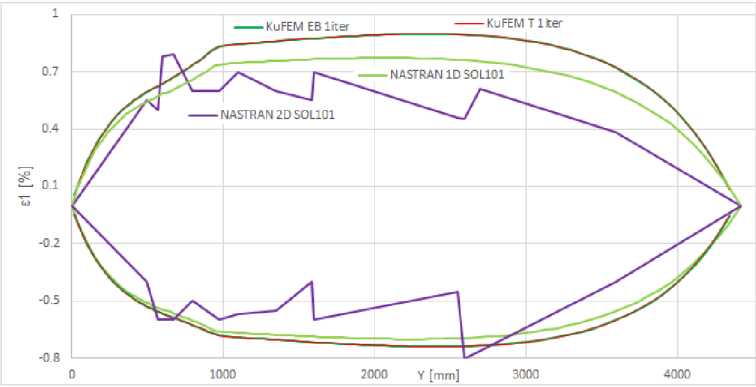

Figure 5.10: Strains in the longitudinal element direction.

5.2 Main Landing Gear Spring of Merlin 103

Merlin 103 is an UL-category airplane with tricycle landing gear. Main landing gear is made of a single composite spring, attached at each side of the fuselage. This type of attachment is called continuous (see figure 4.13). Following paragraphs explain approach adopted during the design phase in slightly broader fashion in order to reveal the philosophy behind using KuFEM.

5.2.1 Design Approach

Approach suggested in this thesis is shown on flowchart 5.11. The design of main landing gear is the most interesting for the loading-deflection dependency. UL2 [65] as well as ASTM 2245 Standard Specification [64] define this dependency.

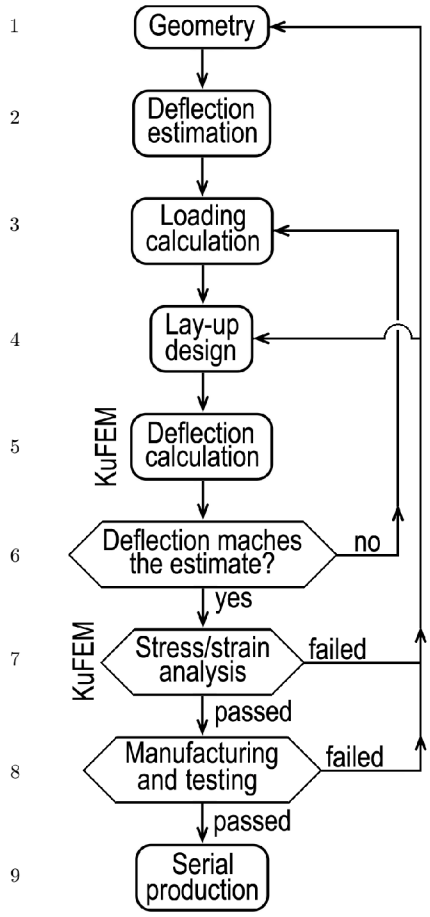

Figure 5.11: Methodology of composite landing gear design.

The designer starts with geometry of the landing gear (step 1). Basic dimensions: width and thickness, position of wheel and the attachments to the fuselage.

In order to calculate the force, landing gear deflection has to be estimated first (step 2). This parameter is expected to dampen the impact during the landing. The larger the deflection, the lower the load factor is obtained (step 3).

Next step is to define the lay-up of the plies. Global characteristics (fibre volume ratio and hence the estimated composite stiffness) are derived from this layup. When the geometry with boundary conditions (loading and attachment) and mechanical properties are known, the deformed shape is calculated (step 5). For this purpose KuFEM can be used.

Usually the displacement is different from that estimated in the beginning. A good approach is to change the estimated valued, based on the newly calculated displacement. This, however,

will influence the loading force, thus changing the final deflection (loop begins at step 6). After several iterations of chasing the combination of deflection and final loading, an agreement between estimated and calculated value is reached. For this final loading the stress-strain analysis can be done (step 7).

It may happen, that the design is not structurally satisfactory. Changing the lay-up and/or geometry is in place. Also a problem may occur at step 8 (workshop is unable to manufacture the required geometry, layup or similar).

Step 8 illustrates the need for a close communication between manufacturing workshop and design / analysis department. Information not only about the manufacturing capability but also about the materials available must be known to the designer. Based on the lamina thickness the number of plies is determined.

KuFEM is easy to use and allows user to quickly change loading and obtaining the deflection. In further sections more detailed description will be given. Example is illustrated on an UL airplane Merlin 103 (figure 5.12), manufactured by TechProAviation, s.r.o.

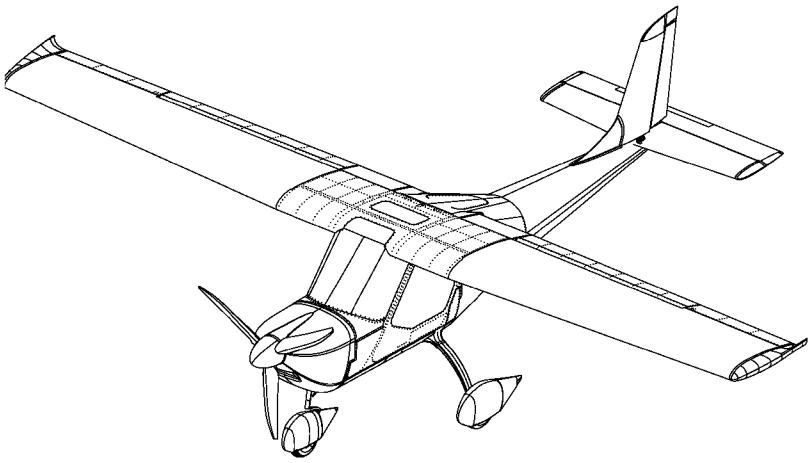

Figure 5.12: Merlin 103, an UL2 airplane. Courtesy of TechProAviation, s.r.o.

5.2.2 Model and Geometry

Geometry of the landing gear has been given as an input (step 1 on the flowchart 5.11). The geometry is given by demands such as wheel track, airframe structure of attachment points and appearance requirement.

First step is to create the mid-fibre curve and parse it to the elements. Total of 42 nodes were created in order to approximate the curved shape of the mid-fibre. Boundary condition of symmetry is applied to node number 1. Support is assigned to node number 5. Width of the support is denoted as R.

As the second step, the thickness of the wrap is estimated (estimation described in the following section). Knowing the manufacturing technology and the wrap thickness, the thickness T and width B of the unidirectional fibre plies is determined for each element. The first loop of calculation may start (step 5). Figure 5.13 shows the main landing gear with it's boundary conditions and loading.

5.2.3 Loading

Description of Iterative Calculation

Parameters of the airplane, relevant to the landing gear design is the take-off weigh $m[kg]$, wing area $S[m^2]$, tyre compression on limit load $Z_{PN}[mm]$, vertical displacement of the landing gear $Z_{TL}[mm]$ (both explained on figure 5.14) and finally the dampening efficiency $\eta_D[\%]$.

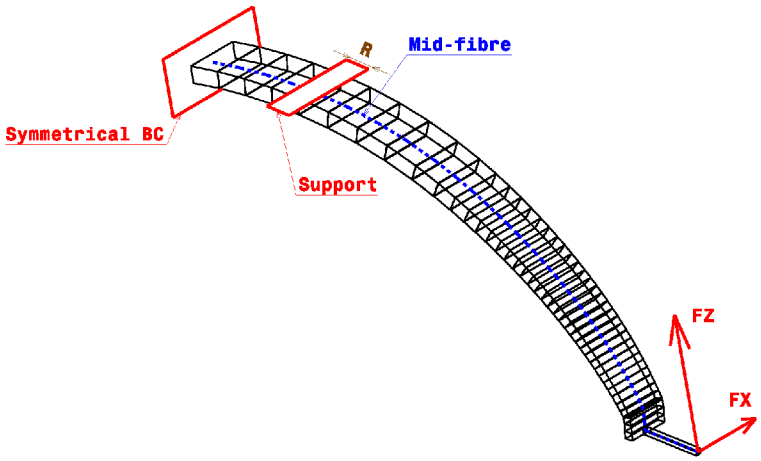

Figure 5.13: Geometry and boundary conditions.

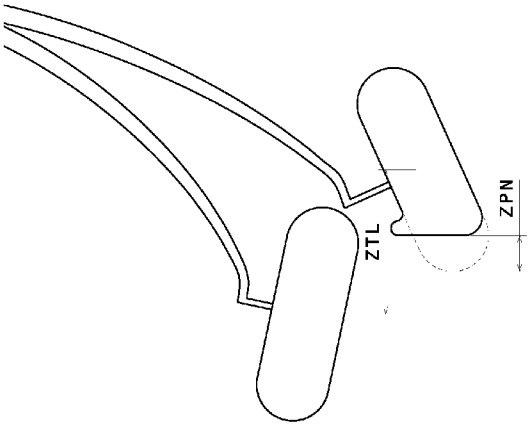

Figure 5.14: Un-deformed and deformed tire and landing gear spring.

The maximum take-off weight and wing area are known exactly. Slightly problematic is the dampening efficiency. As it is not easy to measure, a constant value of $\eta_D = 50\%$ can be accepted as a reasonable value.

Remaining two values - the deformation of the landing gear and the tire are dependent on the loading force. According to the airworthiness regulation [64], [65], the force is dependent on the deformation. This leads to an iterative calculation (described further in the text).

In order to ease the problem, the iteration will focus only on the landing gear. As for the tire deformation, a constant value can be chosen. For example a reasonable value of Z_{PN} can be set to 1/3 of the wheel radius.

The iterative calculation is shown on figure 5.15. Arrow 1 illustrates that for an estimated deflection a force has been calculated. Arrows 2 and 3 calculates actual deflection for given loading.

Calculated deflection 3 is greater than estimated deflection 1. Therefore a new deflection is estimated and the force is calculated accordingly (arrow 4). For the calculated loading a new deflection is calculated (arrow 6). Again, the calculated deflection is greater than the one estimated. Therefore a new iteration starts (arrow 7). This time, however, the estimated deflection matches the one that is calculated.

A reasonable value of estimated deflection to start with, for this kind of landing gear, is the

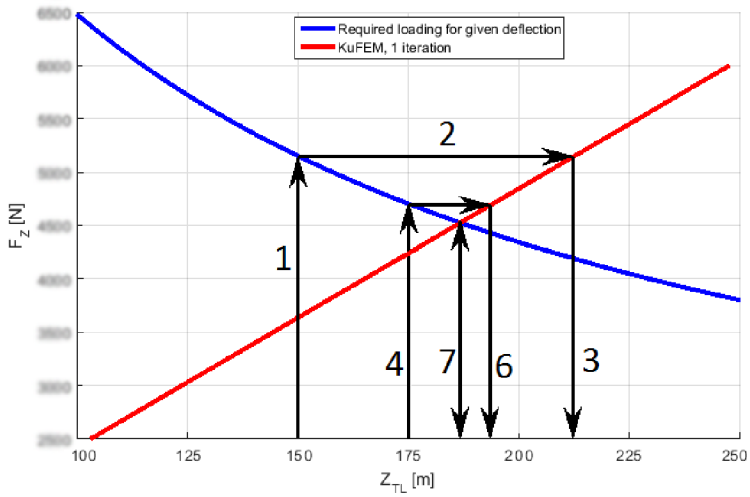

Figure 5.15: Example of iterative calculation: matching the loading and the deflection.

radius of the wheel (in this case the wheel used is 12 inch diameter, therefore the initial value of estimated deflection for the limit load is $Z_{TL} \approx 150mm$) Validity of this approximation is visible on figure 2.16 (a composition of two pictures taken during the drop test).

Equations used

An important note concerning the landing gear arrangement: The worst landing conditions (that is the highest forces) are different for tricycle landing gear and for tail dragger. In case of tail dragger, the worst landing for main gear is the level landing, whereas for tricycle is the landing with nose wheel juts of the ground. These conditions are illustrated on figure 5.16.

However both types of landing gear arrangement are loaded by the force of the same magnitude and orientation. Therefore the equations given in table 5.2 are valid for both: the tricycle and the tail dragger airplanes.

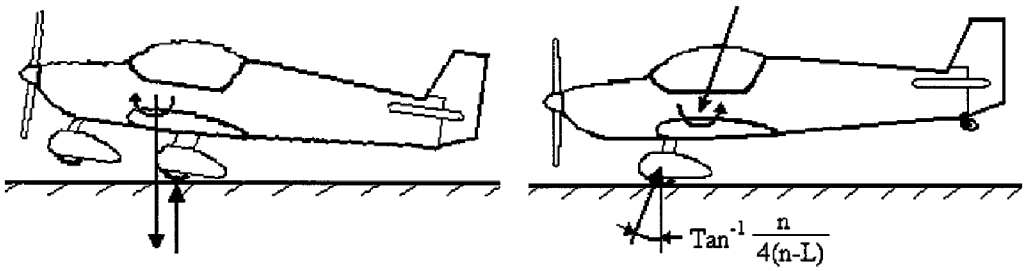

Figure 5.16: Level landing with Nose Wheel just Clear of Ground (tricycle). Level landing (tail dragger). [64]

In order to calculate the landing condition loads, the following parameters must be calculated first:

- drop height

$$h = 13.2 \cdot \sqrt{\frac{m \cdot g}{S}} = [mm]$$

- landing load factor

$$n_Z = \frac{h + \frac{1}{3} \cdot (Z_{PN} + Z_{TL})}{\eta_D \cdot (Z_{PN} + Z_{TL})} = [-]$$

- total load factor

$$n = n_Z + \frac{2}{3} = [-]$$

- main wheels loading

Horizontal force	$\bar{F_X} = \frac{n}{4} \cdot m \cdot g$
Vertical force	$\bar{F_Z} = n_Z \cdot m \cdot g$

Table 5.2: Horizontal and vertical force on main wheels (total on both main wheels).

These equations give two vectors of the force (upwards and backwards). The usual practice is to tilt the landing gear slightly forward (figure 5.17). Therefore a vector re-calculation is necessary:

$$F_Z = \bar{F_Z} \cdot cos\,(\nu) + \bar{F_X} \cdot sin\,(\nu)$$

$$F_X = \bar{F_X} \cdot cos\,(\nu) - \bar{F_Z} \cdot sin\,(\nu)$$

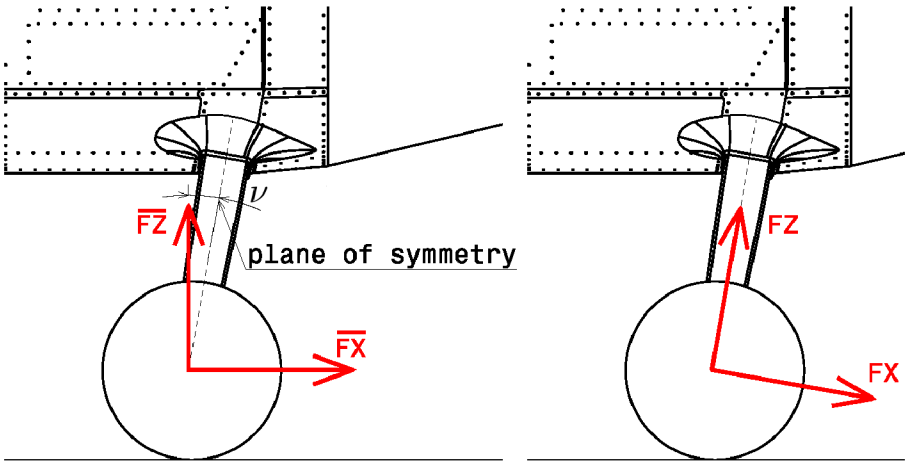

Figure 5.17: Tilting the landing gear in relation to the loading forces.

5.2.4 Models for Verification

For the KuFEM calculation to be verified, two other models are devised. First, the KuFEM-generated 1D NASTRAN model. Then another NASTRAN model, that uses 2D shell elements (figure 5.18). This NASTRAN 2D model will allow to use non-linear solver SOL 106.

5.2.5 Results

Total of 6 calculations were made. Three KuFEM, using linear and non-linear formulation, and linear NASTRAN analysis with 1D elements and finally NASTRAN model with shell elements using linear and non-linear solvers:

- KuFEM: linear
- KuFEM: non-linear, 10 iterations
- KuFEM: non-linear, 100 iterations
- NASTRAN 1D: linear
- NASTRAN 2D: linear
- NASTRAN 2D: non-linear, 10 iterations

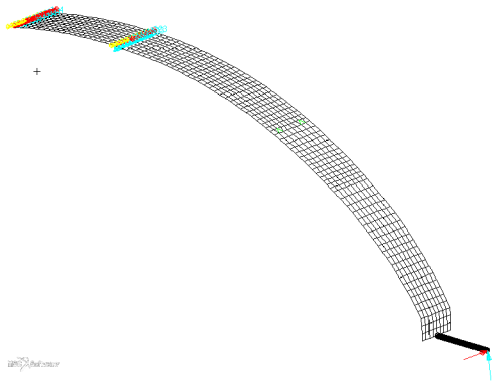

Figure 5.18: 2D model analysed in NASTRAN.

Deflection

Figure 5.19 shows a front view of the landing gear. There is shown the initial un-deformed geometry (black). In green a deformed 2D NASTRAN linear solution is shown. And finally in red the linear KuFEM and NASTRAN beam deformed geometries are presented. The non-linear deformed bodies are not shown on this picture, further discussion on this topic is given in the summary and figure 5.22.

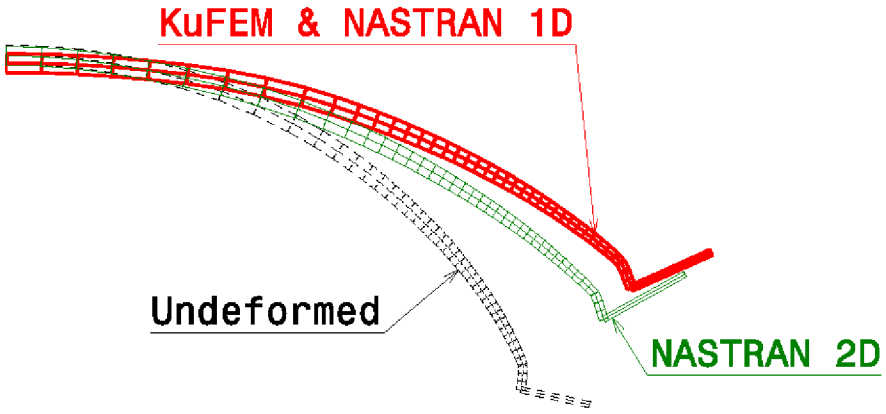

Figure 5.19: Comparison of deformed shapes obtained from KuFEM and NASTRAN (both 1D and 2D).

Results: Strains

Presented strains (figure 5.20) are measured in the element longitudinal axis - ϵ_I for KuFEM and NASTRAN 1D results. The results of NASTRAN 2D model are presented as the major and minor strains.

Strains, predicted by KuFEM are higher than the NASTRAN prediction. At the fuselage attachment, the strain predicted by KuFEM is $\epsilon_{KuFEM} = 1.1\%$. At the same location, the NASTRAN beam model predicts $\epsilon_{NASTRAN} = 0.875\%$. From here, the ratio is:

$$k = \frac{\epsilon_{KuFEM}}{\epsilon_{NASTRAN}} = \frac{1.1}{0.875} = 1.257$$

This difference is largely attributed to the fact, that KuFEM calculates it's stresses and strains using deformed geometry, while NASTRAN uses the geometry un-deformed. The presented

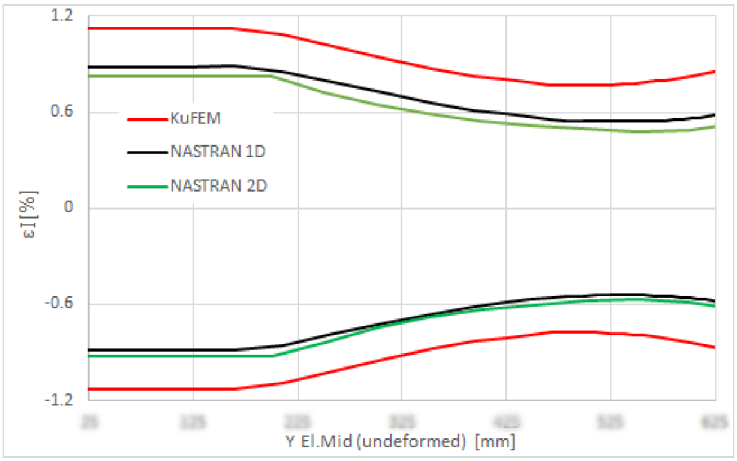

Figure 5.20: Comparison of ϵ_1 strains obtained from KuFEM and NASTRAN.

strains are caused by the bending moment MX, which is mainly caused by the vertical force RF_Z at a distance ΔY. The difference in ΔY of deformed versus un-deformed geometry creates the difference (figure 5.21). In this case, the ratio is:

$$k = \frac{MX_{deformed}}{MX_{undeformed}} = \frac{\Delta YD}{\Delta YU} = 1.276$$

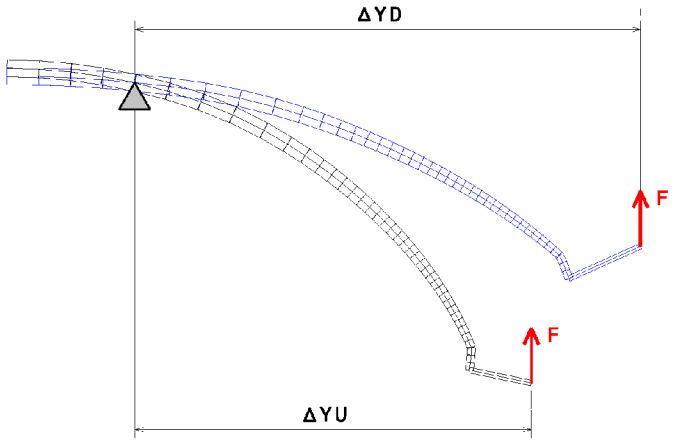

Figure 5.21: Different position of the vertical force.

5.2.6 Summary

In this chapter an approach for the design of main landing gear composite spring is suggested. Further description of the philosophy behind using KuFEM is explained. Another verification of KuFEM code is presented simultaneously.

An iterative determination of the relation between loading forces, given by the airworthiness regulation and deflection obtained as a result of introducing the force is shown on figure 5.22.

Figure 5.22 shows the required force for given landing gear deflection (blue line). Other lines represent the dependency of the spring response to the loading. Force predicted by linear KuFEM solution is within 5.9% agreement with NASTRAN 2D, whereas non-linear predictions

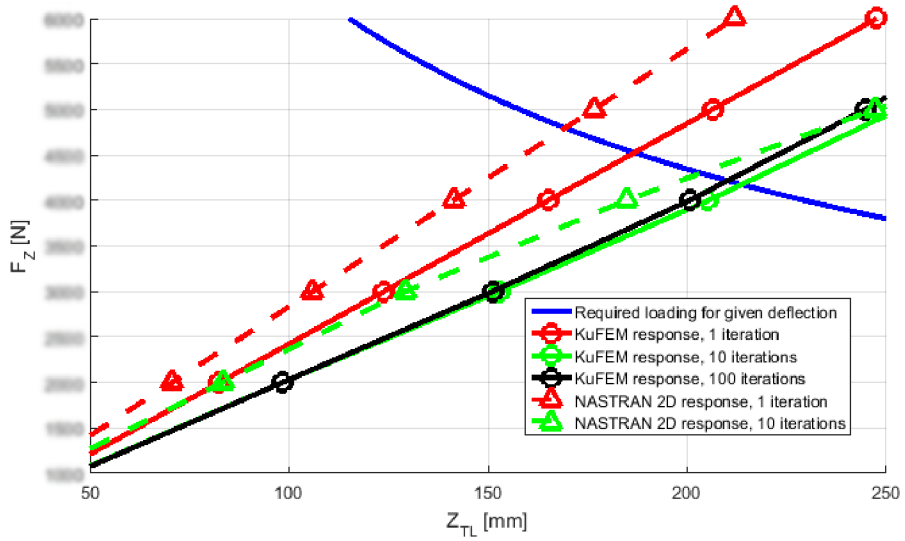

Figure 5.22: Force-deflection dependencies according to KuFEM, NASTAN and airworthiness requirements.

are within 3% and 2.1% respectively. This fact clearly illustrates the importance of the non-linear behaviour of the loading.

5.3 Nose Wheel Spring of Merlin 103

The spring is located on the nose wheel (figure 5.23), connecting lower tube with upper assembly. The most severe loading is caused by horizontal landing. This loading is compressing the nose gear and the spring is loaded by bending momentum and shear force. Other loads may also occur, for example when steering the nose wheel, side loads and so on. These minor loadings are not of interest in terms of spring design.

Figure 5.23: Nose gear spring (shown in colour) on the airplane.

The design aims to create a spring that is linear in compression up to the contact between stops. This should occur at 120% of the limit load. Figure 5.24 shows the desired working diagram of the nose wheel spring.

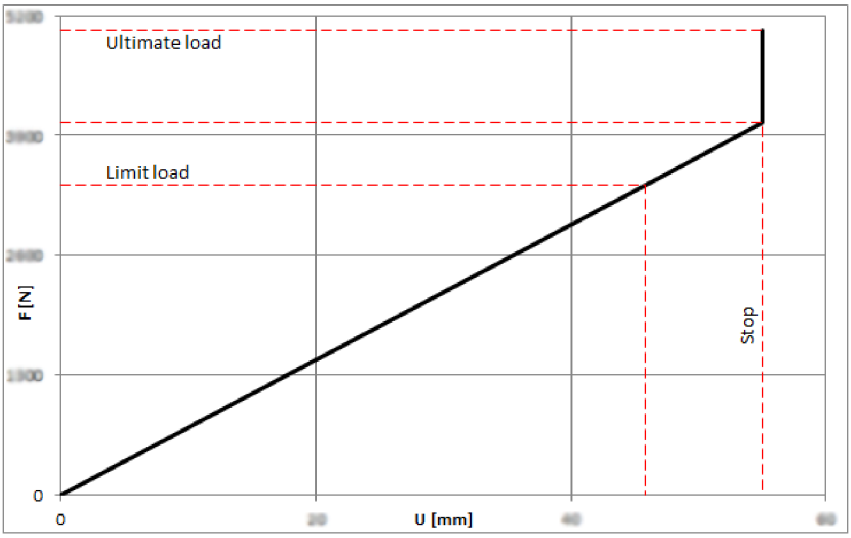

Figure 5.24: Desired working diagram of the nose wheel dampening system.

5.3.1 Geometry and Loading

Geometrically the spring is symmetrical. A divergent U shape has been adopted. The length and height of the spring is given by the wheel cowling. Only the thickness had to be calculated.

From the known un-cured thickness of the composite layer $t_0[mm]$, local mould thickness $T[mm]$, number of layers $n[-]$ and geometrical coefficient $k = 78.5\%$ a volume fracture has been determined at each node (figure 5.25):

$$V_F = k \cdot \frac{n \cdot t_0}{T}$$

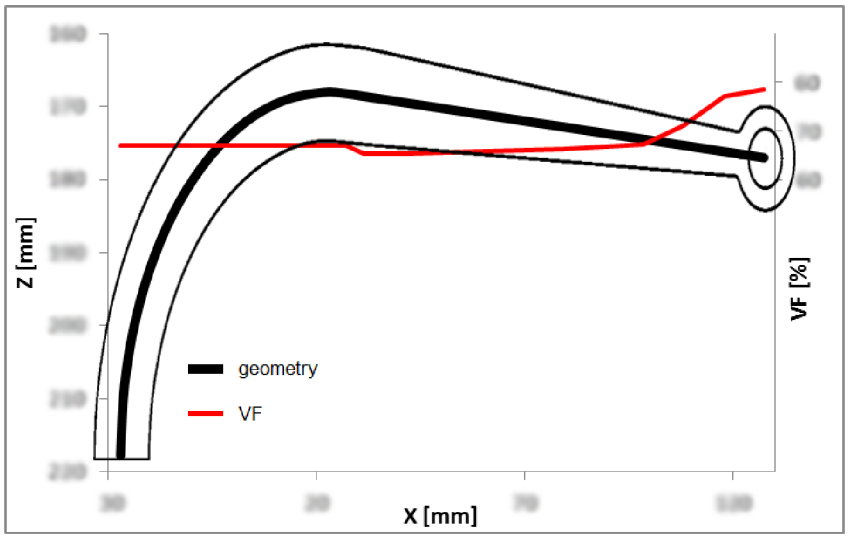

Figure 5.25: Volume fracture along the spring.

Even though the spring is hand-made, the volume fracture is relatively precisely abided because of the geometrically precise mould is used. This is great advantage in the calculation of the stiffness.

Highest loading occurs during level landing on front CG position (figure 5.26). The forces are

redistributed into the desired directions (tangential and normal). Tangential forces are transferred through steel tube contact, whereas the normal load is transferred through the spring.

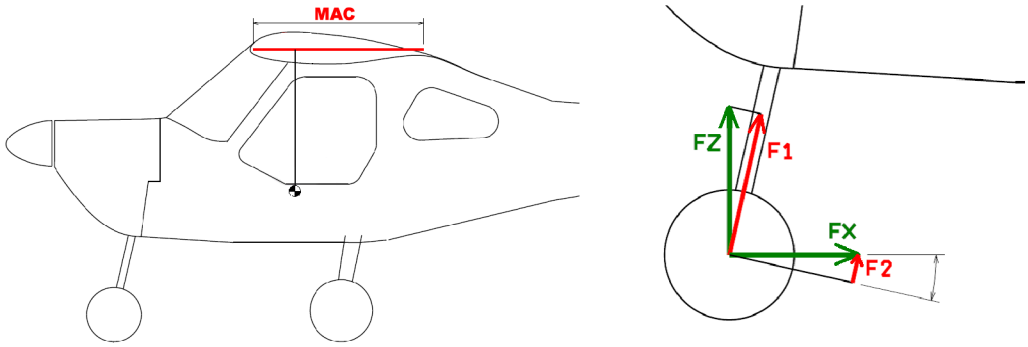

Figure 5.26: Loading of the spring.

5.3.2 KuFEM Analysis

From volume fracture the local stiffness modulus for each element (as an average between each node) has been determined. Both limit and ultimate load has been calculated with linear and 10-iterations non-linear solving methods. Figure 5.27 shows the working diagram calculated by KuFEM.

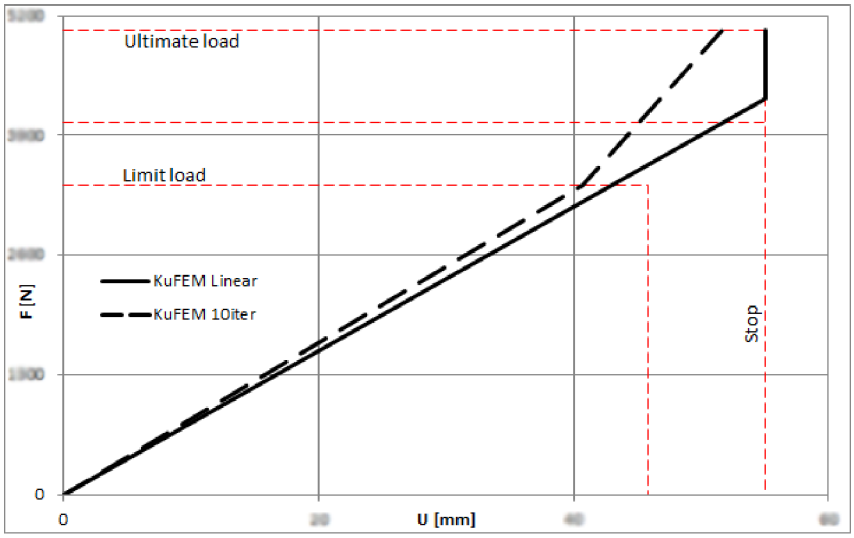

Figure 5.27: Working diagram as predicted by KuFEM models.

5.3.3 NASTRAN Analysis

In order to validate the KuFEM results, another analysis used MSC.Patran/NASTRAN software. First analysis used the BDF file generated by KuFEM with beam elements (figure 5.28, left). The other used 8-node HEX 3D element (figure 5.28, right) based on suggestions from [17]. Both simulations used linear SOL101 solver. Further non-linear SOL106 solver has been used for the CHEXA model. The NASTRAN results are presented on figure 5.29.

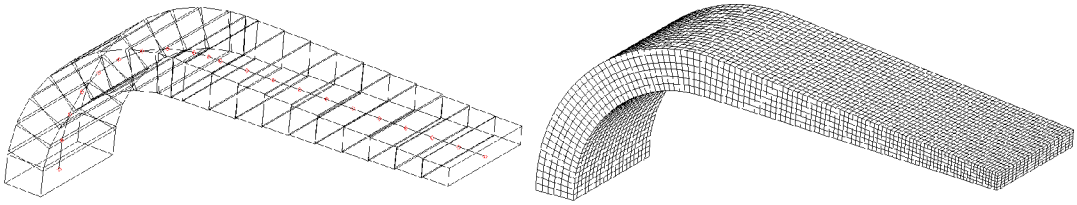

Figure 5.28: NASTRAN finite element model generated from KuFEM BDF file (left) and model made of 3D CHEXA elements (right).

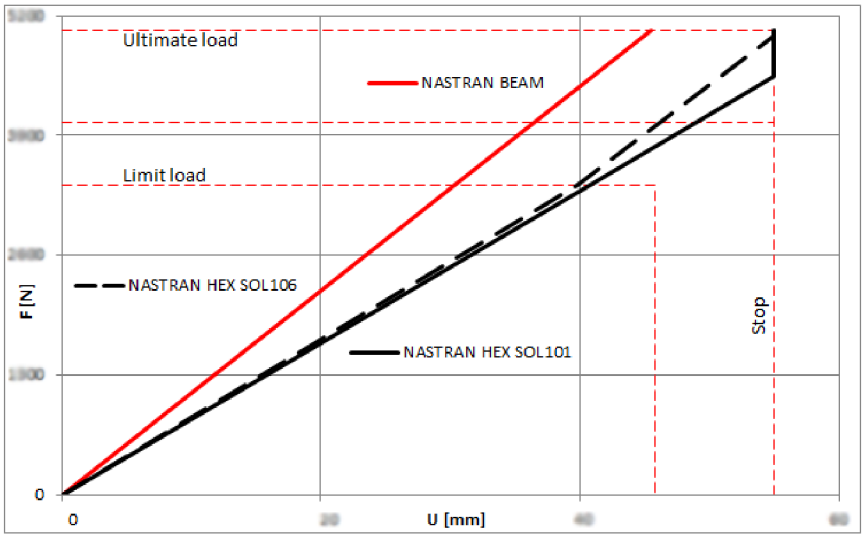

Figure 5.29: Working diagram as predicted by NASTRAN models.

5.3.4 Lab Tests

First thee springs produced were tested in the laboratory (figure 5.30) in order to verify the calculation and establish the manufacturing variance. Each sample had been measured several times close to or slightly above the limit load.

All measured values suggest linear behaviour (diagram 5.31) in the measured range.

Figure 5.30: Spring in the test jig with control marks.

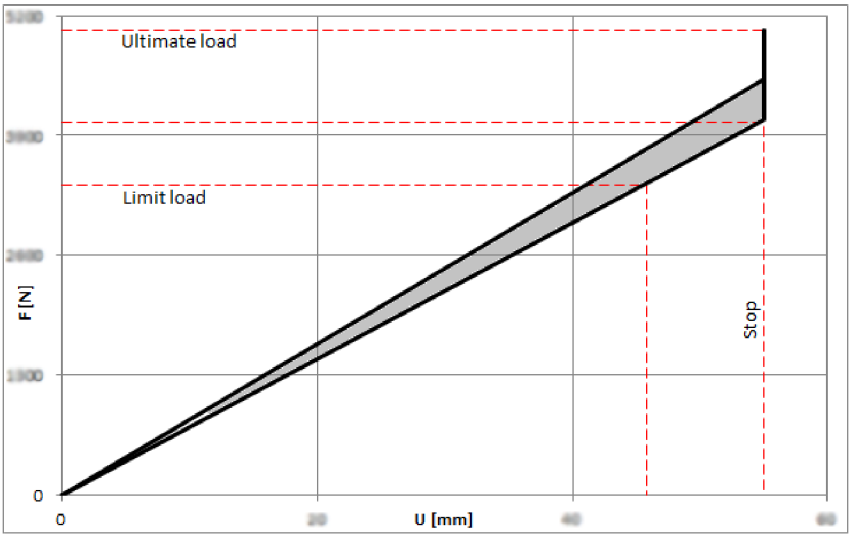

Figure 5.31: Working diagram with manufacturing interval.

5.3.5 Summary

A nose gear spring was designed using KuFEM software. The task was to design a spring for given loading and travel distance. The required working diagram is shown on figure 5.24. Same problem has been analysed in MSC.Patran/NASTRAN with beam and CHEX elements.

When first specimens were available the laboratory tests took place. Total of 9 measurements on three specimens were made. Evaluation of these tests created an interval of working diagram. Figure 5.32 compares the best results obtained from KuFEM and NASTRAN in correlation with the lab results.

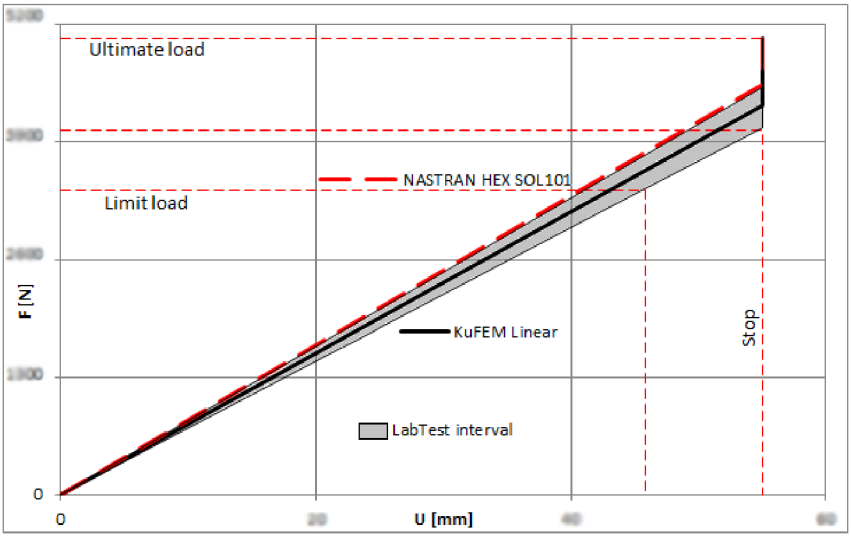

Figure 5.32: Final comparison of the KuFEM, NASTRAN and lab test results.

Linear solution fits the reality the best in both solutions. KuFEM beam model gives the best fit - right in the middle of the interval measured in the lab tests. NASTRAN CHEXA model gives stiffer results.

Very important factor is the manufacturing method, which uses a precise NC machined

pressure moulds. Also the layup is simple (no core or cavities). Another factor is the workmanship (manufacturer has a long years of experience and follows the drawing instructions).

During the tests were reached the stops. No failure has occurred whatsoever. The spring is safe to operate. However no failure data were produced and stress/strain evaluation has not been done.

5.4 Tail Gear Spring of Merlin 110

With development of Merlin's tail gear variant a need to design a composite spring emerged. It has been decided to use glass UD fibres, the same as in nose gear spring (chapter 5.3). Except this time there will be also additional layers of ±45° fabric.

5.4.1 Tail Gear Loading

Merlin 110 is designed under UL2 [65] certification base. In the sense of the landing gear loading the requirements are equal to LSA [64]. The loading, acting on the tail gear, described in the certification specifications are shown on figure 5.33:

1. tail-down landing,
2. up and aft (supplementary condition in tail-down condition) and
3. up and sideways (supplementary condition in tail-down condition).

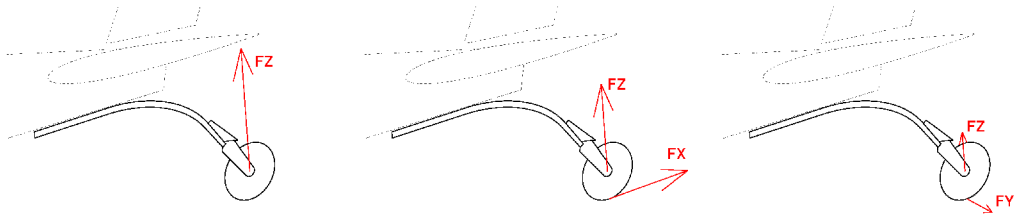

Figure 5.33: Considered types of loading: tail-down landing, supplementary conditions: up + aft and up + sideways.

From the design standpoint view, the most important loading is the one, that causes the largest displacements. The philosophy of design is to set the maximum travel of the wheel, under limit load, to the maximum extent just before hitting the elevator. This is usually the tail-down landing load with largest F_Z force. Yet, the other loads are important as well. In compassion to the nose wheel spring, there is and explicit requirement for the tail spring to withstand out-of-plane force (supplementary condition up and sideways). To counter the effects of side loads, the ±45° layers on top of the UD were used.

5.4.2 Laboratory test

All the described loadings were tested up to the ultimate load. No destruction of the composite has occurred. Therefore no relevant data on the failure were obtained.

Even though the worst loading case is the tail-down landing and the design has used this force, there is no laboratory data on the force / deflection relation because of the way the drop-tests are practised.

However adequate data were obtained during the supplementary up + aft test. For the purpose of evaluating the calculated results these data shall be used.

During the laboratory test a little over limit load is applied in the wheel axis at the defined angle. The displacement has been measured at the same place. Figure 5.34 shows the deformed shape of the tail gear.

A contact between composite spring and the lower side of the fuselage is visible on figure 5.34. This effectively changes the boundary conditions from two supports to three (figure 5.35).

Figure 5.34: Supplementary condition up + aft - limit load.

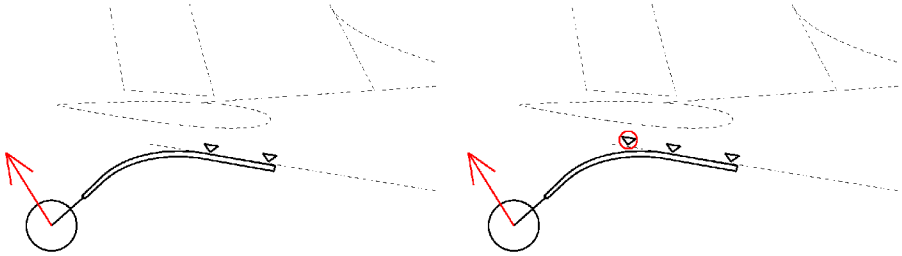

Figure 5.35: Change in boundary condition.

Contact between the tail and the tail gear's spring may not be a great deal in terms of certification, but it is a great deal in terms of predicted behaviour validity. The prediction does not have the ability to introduce additional support during the loading.

5.4.3 Comparison of Test and Prediction

The following analysis is by no means considered a valid proof and no firm conclusions may be taken from this. Only one measurement has been taken and the boundary condition of the test is inconsistent with the numerical analysis. However the comparison is presented to illustrate the difference.

Figure 5.36 shows similar deformed shape obtained from KuFEM and one measured during the limit load test. Worth noting is the fact, that while the real spring stopped upon contact with fuselage, the KuFEM did not have any additional boundary condition at this area and continued through the fuselage.

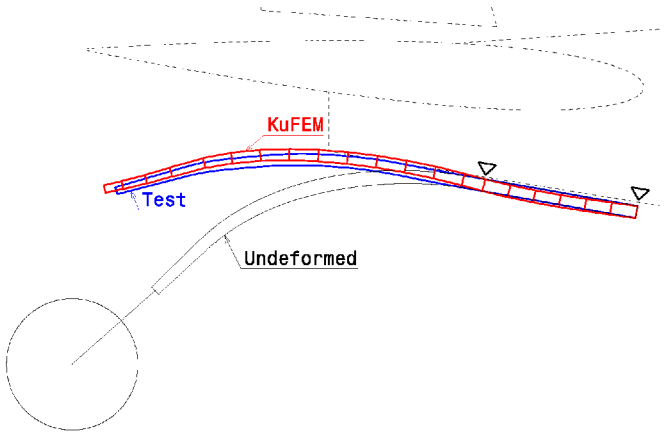

Figure 5.36: Comparison of deformed shapes, KuFEM vs. Limit load test.

6 Summary

6.1 Area of interest

Composites are unique peace of engineering, used in many different branches: from construction industry to aerospace. This thesis focuses on the small sport airplane industry (ultralight category), which has a great history in the Czech Republic as well as bright future.

The author's personal experience from this industry has led to the conclusion, that there is great difference between world-class composites manufactured for the large corporations in business (Airbus, Boeing) and those made for small airplanes.

Typical product of TechProAviation company is an ultralight airplane with metal airframe and minor share of composite components. These components are mostly of non-structural character (wing tips, wing-fuselage transition, etc.). The only structural composite parts are springs used for the landing gear. Whether main landing gear or just a small nose gear spring, all are:

- considered to be thick-wall,
- manufactured in two-sided moulds with exact control over the volume fraction,
- made out of the unidirectional fibre layup[11],
- very similar types of loading and deflection characteristics.

Using this type of moulds ensures minimal deviation in the production. Therefore the influence of the worker's inaccuracies is minimized. Keeping the determined volume fracture ensures a valid way to calculate the stiffness and thus results in a meaningful analysis.

Further advantage is the unidirectional layup of the springs in combination with the loading character. The loading in one direction is relatively insignificant in terms of deflection and stresses in comparison with the other two directions. Therefore some of the stresses are less significant and can be neglected. This leads to homogenisation of the material and therefore this reduces the complexity of the analysis, which in turn lowers the demand on the data input.

Similar problems are encountered in analysing the flanges of the main spar in a composite wing. The flanges are thick-wall. Flanges are manufactured in a way, that the resulting volume fraction is according to the specification. Layup of the flanges consists of unidirectional fibres only. Here is also one dominant force (in case of wing, lift is the dominant force) which causes significant deflection in one plane.

Further observation concerns the quality of analysis that is available to the manufacturer. The procedure of design and analysis of thick composite parts does not seem adequate to the extend of the problem. The design tools, commonly available to the manufacturer, are:

- closed-form beam solutions,
- simple and specialized program tools (such as MiniStatik),
- CAD built-in analysis modules,
- dedicated FEA programs.

Closed-form beam solutions are cheap and fast. Very useful for quick orientation. The great drawback is difficulty in handling curved beams and deflection determination. The results can not be used strait forward in 3D CAD model for assembly clash analysis.

CAD built-in analysis modules and dedicated FEA programs can provide great results. First problem with these solution is the price. Next drawback is the level of user's knowledge (these programs are universal and therefore more misleading options are available for user to choose from).

Simple program tools offer the best ratio of results for a low price. These programs are usually written with specific purpose. For this reason only the necessary inputs are required and the results are easily accessible and understandable. Even to an inexperienced user.

A simple, cheap and yet effective means of thick composite analysis is required. The ambition of KuFEM is to fill this spot.

[11] Main loading is transferred via unidirectional fibres. Some products, where twisting is expected, are equipped with additional layers of wrap plies.

6.2 Meeting the dissertation goals

Chapter 3 has set goals to be met in this dissertation thesis. Main goal was to develop a program, that would help in landing gear spring design. Using the program must be quick and simple with accurate results. The program is required to:

1. analyse typical thick composite parts,
2. predict displacements in one plane,
3. calculate the forces, moments, stresses and strains,
4. export results,
5. allow user to export deformed geometry,
6. allow user to export NASTRAN BDF file.

The inseparable part of KuFEM development is the verification and validation.

Chapter 4 describes the program operation: data input, deflection calculation, force and moment distribution, stress and strain calculation, geometry export and NASTRAN BDF file export functions. There are three verification examples showing the correlation to the closed-form solution of a simple-tension, simple-bending and simple-torque. Further verification and validation are shown in chapters 5.1, 5.2, 5.3 and 5.4.

First example in chapter 5.1 is based on HPH composite wing segment test. KuFEM results were compared to MiniStatik and NASTRAN solutions. Both, deflection and strains were compared. Difference between linear and non-linear solutions were also presented. All results are in excellent agreement and therefore the author considers KuFEM to be verified to produce correct results for this type of analysis.

The simplicity and flexibility of using KuFEM is presented in chapter 5.2. In the design process of a composite landing gear the iteration process is necessary, because the deflection influences the loading force. KuFEM linear and non-linear results are compared to the equivalent 1D and 2D NASTRAN models.

KuFEM analysis gives higher strains compared to NASTRAN (in this case approximately 25% higher). This is due to the fact, that KuFEM calculates the strains on deformed geometry (whereas the NASTRAN uses the un-deformed geometry). The difference is traced to the the arm of the bending moment, which is greater by 27% for the deformed geometry. These results are in agreement and therefore the author considers KuFEM to be verified to produce correct results for this type of analysis.

Different design approach is described in chapter 5.3. KuFEM is used to design the shape and layup of a nose wheel spring according to the required working diagram (force-displacement function). KuFEM is excellent help in this task, because it provides results immediately for the changes in geometry, stiffness and loading.

KuFEM results were verified with the NASTRAN 1D and 3D models. Laboratory tests were conducted on 3 specimens (total 9 measurements). The best results obtained from KuFEM and NASTRAN are from the linear analysis. KuFEM result is in excellent agreement with the measurement. The author considers KuFEM to be verified and validated (only deformation) to produce correct results for this type of analysis. Linear solution is preferred.

Similar design approach has been adopted for the tail gear spring, chapter 5.4. The laboratory test showed similar deflection of the spring as KuFEM did predict.

Spring toughed the tail of the airplane during the test. This contact has changed boundary conditions. Therefore no reasonable data may be compared.

When the KuFEM deformed geometry of the spring has been compared with the tail of the airplane, similar clash has been detected. Because of this event KuFEM has been equipped with geometry output function. Now the user can easily export the deformed geometry. It can be inserted into the assembly and checked for clashes.

KuFEM has shown it's flexibility, simplicity and usefulness in design of thick structural

laminates, such as wing flanges and landing gear springs. The program has been verified and partially validated. Table 6.1 presents the verification and validation status:

KuFEM	Verification	Validation
Deflection	✓	✓
Stress and strains	✓	×

Table 6.1: KuFEM verification and validation status.

The goals, that were set in chapter 3, are fulfilled. The program for analysis of typical thick composite parts has been developed. It calculates loads, stresses and strains in the elements. Using KuFEM is easy and flexible. The results are exported and presented in understandable fashion. Among the results are universal geometry IGES files with un-deformed and deformed geometry and a BDF NASTRAN input file.

6.3 Contribution and novelty of the thesis

The outcome of this dissertation thesis is the development, verification and validation of KuFEM program. It is a simple-to-use program that combines in new original way following key elements:

1. established 2D finite element solution for beam deflection prediction,
2. simple force and moment equilibration in 3D,
3. Euler-Bernoulli and Timoshenko beam theory,
4. geometrically non-linear procedure,
5. composite oriented analysis,
6. 3D deformed geometry CAD output.

Among other FEA and stress analysis software, only KuFEM combines 2D deflection analysis and 3D stress components. Further more KuFEM introduces special element description in the stress analysis. This definition accounts for three different cross-section constituents and their specific material properties (upper and lower flange with core in between, each having it's own elastic modulus). It has been verified, that using this formulation can increase accuracy of the beam deflection prediction to a full HEX NASTRAN model.

Useful KuFEM function is the possibility to export the task into NASTRAN and Abaqus input files (BDF and INP respectively).

Another unique function of KuFEM is the ability to export deformed CAD geometry (in universal IGES file), which can be used in clash analysis. This function is very uncommon even between first class commercial FEA software.

KuFEM program has found it's place in TechProAviation company as a tool for analysis and manual optimization of thick composite structures (landing gears and springs). Program offers user-friendly interface, simple change in the geometry, property and loading.

6.4 Future work: KuFEM V2.x

During the development and practical use of the KuFEM V1.x a number of issues were investigated, but could not be incorporated in the first version. A list of these issues is kept in order to be incorporated into the KuFEM V2.x version. Below are listed just the most important and interesting topics that will be addressed.

Cross-section

Current KuFEM version expects a rectangular cross-section. Yet not all applications are without any radius. Therefore the next version of KuFEM will take into account the radius R_H and R_D as seen on figure 6.1.

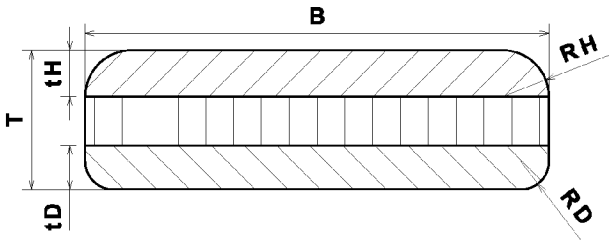

Figure 6.1: Cross-section for KuFEM V2.x.

Data input

Currently there are two input table files. One for nodes, the other for elements. Also the table must contain only numbers.

New version will accept only one table file with all information, including text header. This will decrease the user workload and improve the orientation in the input table for on-spot adjustments.

Element constituents

In the KuFEM V1.x the cross-section is defined by total thickness T, thickness of upper flange t_H and lower flange t_D. Should the element contain core, the core thickness is calculated as

$$t_C = T - (t_H + t_D)$$

In new KuFEM version the input will specifically expect the user to provide the t_C and also E_C. In general the new version will be more oriented on the core problematic. Data will be provided to user in order to evaluate core failure modes such as compressive failure, wrinkling, global buckling and core shear instability.

7 Conclusion

During the past seven years the author has participated on several projects at commercial and academic ground. These projects involved design, optimization, analysis and testing of aeronautical composite components. All these components resembled key similarities in terms of composite structure, manufacturing and loading. Namely these components are thick composite landing gear springs and wing spars.

In order to design, optimize and analyse these components, there were two different roads to go: either to use standard closed-form solution or exploit the hi-tech finite element software. Both options being extremely different with significant advantages and drawbacks. This state of affairs has raised a demand to develop a new program, specifically design to reduce the drawbacks of both previous roads. The requirements for this new program are the goals of this dissertation thesis. These goals are to develop a program, that will:

- be used in design and analysis of typical thick composite parts,
- predict displacements in one plane,
- calculate the element loads, stresses and strains,
- export these results in understandable fashion,
- be easy and flexible to use,
- allow user to export geometry of deformed body,
- allow user to export NASTRAN BDF file.

Further more this software must be verified and validated.

This dissertation thesis begins with overview of current trends in the field of composite part analysis and summarises the relevant research to be incorporated into the developed software. This new software is called KuFEM.

KuFEM is a software tool with own graphical user interface. Data inputs are made with spreadsheet tables, therefore in a very simple, understandable and user-friendly way, which allows dynamic and flexible workflow. Managing data inputs in this way saves time and allows user to efficiently try out number of simulations in order to achieve desired results.

Solution for deformed shape calculation is based on a scripts in Matlab programming language, provided by Antonio Ferreira [1]. These codes were modified (cross-section homogenization and multiple beam theory incorporation) and translated to Python programming language, exploiting numpy package. Using Python offers significant advantages: final program can have efficient graphical user interface, can be distributed freely and as a stand-alone executable file.

Further code determining the internal forces, moments stresses and strains are author's original work. So is the non-linear sequence and element description formulation and data export functions (IGES geometry, NASTRAN BDF and Abaqus INP files).

Products, based on KuFEM design, optimization and strain analysis were manufactured as prototypes and tested at TechProAviation s.r.o. First product was nose gear spring (shown in green on figure 7.1). This horse-shoe-shaped spring has been designed, manufactured and tested for stiffness (discussed in chapter 5.3). The product has met the requirements and is now in serial production.

Another product, where KuFEM contributed in design process is tail gear spring. It has been also tested and declared to comply with the requirements. This spring is used on two types: Merlin 110 and Merlin Sportster (shown in green on figure 7.2).

Last product, KuFEM has been used for, is landing gear for an ultralight helicopter called Dropper. The landing gear (shown in green on figure 7.3) has been manufactured and first testing is expected in Q2 of 2018.

Goals, that were set in chapter 3 were met: a software has been developed, verified and validated. Practical results were presented on products of TechProAviation company. Software, that is outcome of this dissertation thesis, is user-friendly, stand-alone and distributed free of

charge as an open source project[12]. Intended target users are mainly small companies, developing aeronautical composite components. Other use of KuFEM software can be found in similar applications: automotive industry (leaf springs), sport equipment (bows, jumping stilts) and maritime industry (mast, boom and oar).

A list of further enhancements and potential issues is kept for future development of KuFEM program, which still goes on.

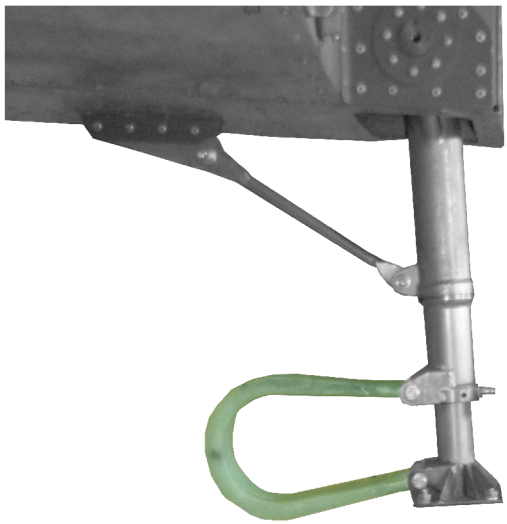

Figure 7.1: Nose gear spring (in green) on Merlin 105 airplane. Courtesy of TechProAviation, s.r.o.

Figure 7.2: Tail gear spring (in green): Merlin Sportster. Courtesy of TechProAviation, s.r.o.

[12]Available at author's personal web page `http://www.cejpek.eu/KuFEM`

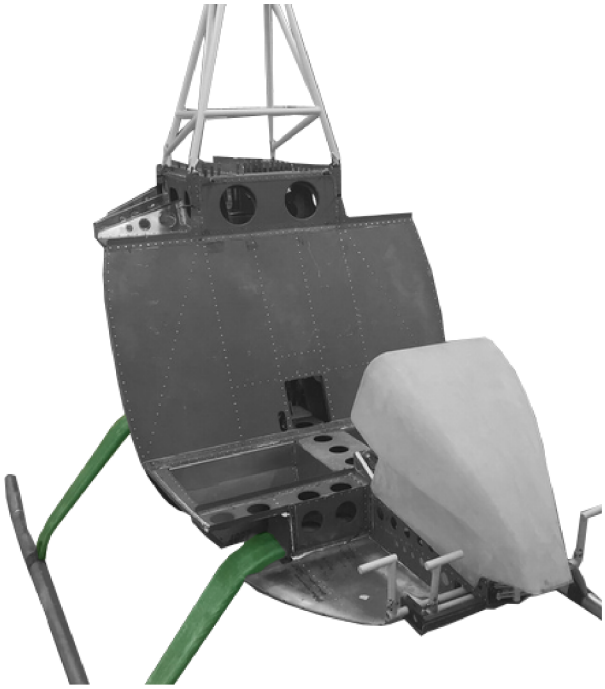

Figure 7.3: Main landing gear (in green) of a helicopter. Courtesy of TechProAviation, s.r.o.

References

Solid Structure Analysis

[1] Ferreira A., *MATLAB CODES FOR FINITE ELEMENT ANALYSIS*: Solids and Structures. Springer Science & Business Media - Technology & Engineering. 235 pages. 2008. ISBN 1402092008.

[2] Janíček, Ondráček, Vrbka. *PRUŽNOST A PEVNOST I.* VUT v Brně. 1992.

[3] MSC.Software. *MSC NASTRAN 2014*: Quick reference guide. 3854 pages. 2014.

[4] Torstenfelt B., *FINITE ELEMENTS*, Preliminary edition LiU-IEI-S–08/535–SE. Linköping universitet. 2008.

[5] Liu Y. *INTRODUCTION TO THE FINITE ELEMENT METHOD.* 188 pages. CAE Research Laboratory. 2003.

[6] Petersson, H. *THE ENGINEERING DESIGNER IN THE ROLE OF A DESIGN ANALYST – AN INDUSTRIAL SURVEY.* 23 pages. NWC15 – NAFEMS World Congress 2015, San Diego, California, USA, 21-24 June, 2015.

[7] Aberdeen Group. *ENHANCE ENGINEERING*: Reduce Time and Optimize Products with Simulation Best Practices. Boston, 2013.

[8] Bathe K., *FINITE ELEMENT PROCEDURES FOR SOLIDS AND STRUCTURES.* RES.2-002 Spring 2010. Massachusetts Institute of Technology: MIT OpenCourseWare, https://ocw.mit.edu. License: Creative Commons BY-NC-SA.

[9] Gavin H. *STRUCTURAL ELEMENT STIFFNESS, MASS, AND DAMPING MATRICES.* CEE 541. Structural Dynamics, Duke University, 2016. 33 pages.

[10] Munoz H. *ELASTIC SECOND-ORDER COMPUTER ANALYSIS OF BEAM-COLUMNS AND FRAMES.* Master thesis at The University of Texas at Austin. 1991. 140 pages.

[11] Matthews B. *APPLIED STRESS ANALYSIS* Section XI: Composite Materials (Analysis). General Dynamics, Convair Division, 92 pages.

[12] Cowper, G.R. *SHEAR COEFFICIENT IN TIMOSHENKO BEAM THEORY.* J. Appl. Mech 33(2), 335-340. 1966. 6 pages.

[13] Gruttmann F., Wagner W. *SHEAR CORRECTION FACTORS IN TIMOSHENKO'S BEAM THEORY FOR ARBITRARY SHAPED CROSS–SECTIONS.* Computational Mechanics, 27, 199-207. 2001. 20 pages.

[14] Wanga C., Lima G., *RELATIONSHIPS BETWEEN BENDING SOLUTIONS OF REISSNER AND MINDLIN PLATE THEORIES*, Engineering Structures, Volume 23, Issue 7, Pages 838–849, July 2001.

[15] ANSYS, Inc. *ANSYS 17 Update.* 66 pages. 2016.

[16] Voyiadjis G., Kattan P. *Mechanics of Composite Materials with MATLAB.* Louisiana State University. ISBN-10 3-540-24353-4. 337 pages. 2005.

[17] Goering J., Kim H. *HIGHER ORDER FINITE ELEMENT ANALYSIS OF THICK COMPOSITE LAMINATES.* NASA Act NAS1-18862, McDonnell Douglas Corp., St. Louis.

[18] Zhang Y., Yang C. *RECENT DEVELOPEMENTIN FINITE ELEMENT ANALYSIS FOR LAMINATED COMPOSITE PLATES.* Composite Structures 88 (2009) 147-157.

[19] Bednarcyk B., Aboudi J. *SIMPLIFIED SHEAR SOLUTION FOR DETERMINATION OF THE SHEAR STRESS DISTRIBUTION IN A COMPOSITE PANEL FROM THE APPLIED SHEAR RESULTANT*. American Institute of Aeronautics and Astronautics. 25 pages. 2008.

[20] Yildiz H., Sarikanat M. *FINITE-ELEMENT ANALYSIS OF THICK COMPOSITE BEAMS AND PLATES*. Composites Science and Technology 61, 1723–1727. 2001.

[21] Liu Y. *LECTURE NOTES: INTRODUCTION TO THE FINITE ELEMENT METHOD*. CAE Research Laboratory, University of Cincinnati. 2003. 188 pages.

[22] Xiao J., Gilhooley D. *ANALYSIS OF THICK COMPOSITE LAMINATES USING A HIGHER-ORDER SHEAR AND NORMAL DEFORMABLE PLATE THEORY (HOSNDPT) AND A MESHLESS METHOD*. Composites: Part B 39 (2008) 414–427.

[23] Dassault Systemes SIMULIA. *Abaqus CAE 6.14*: Reference guide. HTML version. 2014.

[24] Bathe K. *INTRODUCTION TO NONLINEAR ANALYSIS*. [online 2017-01-13] available at `https://youtu.be/TJh7KPABk6I`

[25] Euler–Bernoulli beam theory [online 2017-04-16] available at `https://en.wikipedia.org/wiki/Euler-Bernoulli_beam_theory`

[26] Timoshenko beam theory [online 2017-04-16] available at `https://en.wikipedia.org/wiki/Timoshenko_beam_theory`

[27] Element aspect ratio [online 2016-12-20] available at `https://upload.wikimedia.org/wikipedia/commons/a/a6/Aspect_ratio_grid.PNG`

[28] Common Methods for Laminating Composite Fabrics [online 2017-02-06] available at `http://www.sollercomposites.com/fabricstechniques.html`

[29] Quora *What is the difference between displacement, deflection and deformation?*. [online 2017-03-10] available at `https://www.quora.com/What-is-the-difference-between-displacement-deflection-and-deformation`

[30] Plate theory [online 2017-08-17] available at `https://en.wikipedia.org/wiki/Plate_theory`

[31] Kirchhoff–Love plate theory [online 2017-08-17] available at `https://en.wikipedia.org/wiki/Kirchhoff-Love_plate_theory`

[32] Mindlin–Reissner plate theory [online 2017-08-17] available at `https://en.wikipedia.org/wiki/Mindlin-Reissner_plate_theory`

Materials

[33] Department of Defense Handbook*COMPOSITE MATERIALS HANDBOOK*: volume 3. polymer matrix composites materials usage, design and analysis. Washington D.C. 2012. 693 pages. MIL-HDBK-17-3F.

[34] Lo K., Chim E. *COMPRESSIVE STRENGTH OF UNIDIRECTIONAL COMPOSITES* . Journal of Reinforced Plastics and Composites. Vol 11, Issue 8, pages 838-896. 1992.

[35] Chamis Ch., *ANALYSIS OF THREE-POINT-BEND TESTS FOR MATERIALS WITH UNEQUAL TENSION AND COMPRESSION PROPERTIES*. 36 pages. NASA technical note TN D-7572, 1974.

[36] Daniel I., Abot J. *THREE-DIMENSIONAL CHARACTERIZATION OF CONSTITUTIVE BEHAVIOR AND FAILURE OF TEXTILE COMPOSITES*. 6 pages. ICF11, Italy 2005.

[37] Harris B., *ENGINEERING COMPOSITE MATERIALS*. 193 pages. The institute of Material, London, 1999. ISBN 0901462284.

[38] Hussain S., *PREDICTION OF ELACTIC PROPERTIES OF FRP COMPOSITE LAMINA FOR LONGITUDINAL LOADING*. 6 pages. ARPN Journal of Engineering and Applied Sciences, 2008.

[39] Samborsky D., *3-D STATIC ELASTIC CONSTANTS AND STRENGTH PROPERTIES OF A GLASS/EPOXY UNIDIRECTIONAL LAMINATE*. 26 pages. Montana State University, Bozeman, MT 59717.

[40] Roeseler, W., Sarh, B., *COMPOSITE STRUCTURES: THE FIRST 100 YEARS*. Proceedings of the 16th International Conference on Composite Materials, Kyoto, Japan, July 2007.

[41] Kaw A., *MECHANICS OF COMPOSITE MATERIALS*. 473 pages. Florida 2006. ISBN 0-8493-1343-0.

[42] He Y., Makeev A., *NONLINEAR SHEAR BEHAVIOR AND INTERLAMINAR SHEAR STRENGTH OF UNIDIRECTIONAL POLYMER MATRIX COMPOSITES: A NUMERICAL STUDY*. 11 pages. International Journal of Solids and Structures 51 (2014) 1263–1273.

[43] Azzi V., Tsai S., *ANISOTROPIC STRENGTH OF COMPOSITES*. Experimental mechanics, 5, 283-288, 1965.

[44] Thirumalai R., Andersen L. *TENSILE AND COMPRESSION PROPERTIES OF HYBRID COMPOSITES – A COMPARATIVE STUDY*. In Proceedings of the 19th International Conference on Composite Materials (ICCM19). (pp. 1029-1035). Canadian Association for Composite Structures and Materials. 2013.

[45] O'Brian D., *CURE-DEPENDENT VISCOELASTIC POISSON'S RATIO OF EPOXY*. 13 pages. Experimental mechanics, 2007.

[46] Zimmermann K., Zenkert D., *TESTING AND ANALYSIS OF ULTRA THICK COMPOSITES*, Composites Part B: Engineering, 41(4): 326-336. 2010.

[47] Davallo M., Pasdar H. *EFFECTS OF LAMINATE THICKNESS AND PLYSTACKING SEQUENCE ON THE MECHANICAL PROPERTIES AND FAILURE MECHANISM OF UNIDIRECTIONAL GLASS-POLYESTER COMPOSITES*. International Journal of ChemTech Research, Vol.2, No.4, pp 2118-2124. ISSN : 0974-4290. 2010.

[48] Almeida J., Angrizani C. *EFFECT OF FIBER ORIENTATION ON THE SHEAR BEHAVIOR OF GLASS FIBER/EPOXY COMPOSITES*. Materials and Design 65 (2015) 789–795.

[49] Swamy M., Patil P. *EFFECT OF FIBER ORIENTATION ON INTERLAMINAR SHEAR STRENGTH OF GFRP COMPOSITES*. International Journal of Advancement in Engineering Technology, Management and applied Science, Vol.3, Issue 1. 2016. ISSN 2349-3224. 10 pages.

Failure Theories

[50] Talreja R. *ASSESSMENT OF THE FUNDAMENTALS OF FAILURE THEORIES FOR COMPOSITE MATERIALS*. Composites Science and Technology, 105, 190-201, 2014.

[51] Altenbach H., Sadowski T., *FAILURE AND DAMAGE ANALYSIS OF ADVANCED MATERIALS*. 278 pages. Springer, 2015. ISBN 9783709118344.

[52] Lutz G. *THE PUCK THEORY OF FAILURE IN LAMINATES IN THE CONTEXT OF THE NEW GUIDELINE VDI 2014 PART 3*. 12 pages. VULKAN Kupplungs- und Getriebebau. 2014.

[53] Pinho T., Dávila C., *FAILURE MODELS AND CRITERIA FOR FRP UNDER IN-PLANE OR THREE-DIMENSIONAL STRESS STATS INCLUDING SHEAR NONLINEARITY*. 69 pages. NASA/TM-2005-213530.

[54] FEA code with different tension / compression Young's moduli, thread 727-253779 [online 2017-08-27] available at `http://www.eng-tips.com/viewthread.cfm?qid=253779`

[55] Different elastic modulus in tension and compression direction [online 2017-08-27] available at `https://community.plm.automation.siemens.com/t5/3D-Simulation-Simcenter-3D-Forum/Different-elastic-modulus-in-tension-and-compression-direction/td-p/331293`

Composite Products

[56] Airbus A350 XWB [online 2017-04-29] available at `https://en.wikipedia.org/wiki/Airbus_A350_XWB`

[57] [online 2017-04-29] available at `https://en.wikipedia.org/wiki/Boeing_787_Dreamliner`

[58] Spencer E. *A NOVEL OPTIMIZATION STRATEGY FOR COMPOSITE BEAM TYPE LANDING GEAR FOR LIGHT AIRCRAFT*. 24 pages. United Technologies Aerospace Systems, [online 2016-12-16] available at `http://pages.mscsoftware.com/rs/mscsoftware/images/Paper_ANoveOptimizationStrategyforCompositeBeamTypeLandingGearforLightAircraft.pdf`

[59] Goyal A., *DESIGN, ANALYSIS AND SIMULATION OF A COMPOSITE MAIN LANDING GEAR FOR A LIGHT AIRCRAFT*. 6 pages. MSRSAS Bangalore. 2002.

[60] Ilic I., *STRENGTH ANALYSIS OF MAIN LANDING GEAR TYPE LAYERED COMPOSITE LEAF SPRING FOR UNMANNED AERIAL VEHICLE*. 4 pages. Military Technical Institute, Belgrade. 2012.

[61] Akshay Kumar A., Shinde V., *DESIGN, ANALYSIS, MANUFACTURING AND TESTING OF MONO COMPOSITE LEAF SPRING USING UD E-GLASS FIBER/EPOXY*, International Journal of Advanced Technology in Engineering and Science, Volume No.02, Issue No. 12, December 2014, Pages 112-121, ISSN 2348–7550.

Validation and Verification

[62] Conover D., *VERIFICATION AND VALIDATION OF FEA SIMULATIONS*, ANSYS presentation. 19 pages. Cornell University. 2008.

[63] Sargent R., *VERIFICATION AND VALIDATION OF SIMULATION MODELS*, 16 pages. Proceedings of the 2011 Winter Simulation Conference. 2011.

Airplane Certifiation Specifications

[64] ASTM Int., *F 2245-07*. Standard Specification for Design and Performance of a Light Sport Airplane.

[65] Letecká amatérská asociace ČR, *UL2 - I. ČÁST*. Požadavky letové způsobilosti SLZ. 51 pages. 2002.

[66] Deutsche Flugsicherung, *NACHTRICHTEN FUR LUFTFAHRER*, teil II. 42 pages. 2003.

[67] EASA, *CS-22*, Certification specifications for sailplains and powered sailplanes. 140 pages. 2003.

Technical University Brno

[68] Juračka J. *REFERENČNÍ STATICKÁ ZKOUŠKA SEGMENTU KŘÍDLA*.34 pages. Brno University of technology, IAE Report. 2007.

[69] Juračka J. *KOMPOZITNÍ KONSTRUKCE V LETECTVÍ*. 103 pages. Brno University of technology, 2007. LU31-2007-OST.ST.

[70] Matěják V. *LABORATORY STRENGTH TEST METHODOLOGY OF 304S WING*. 13 pages. Brno University of technology, 2010.

[71] Institute of aerospace engineering *G304S*. [online 2014-03-23] available at `http://lu.fme.vutbr.cz/vysledky.php?projekt=g304s&full=`

[72] Schoř P. *ADVANCES IN COMPOSITE STRUCTURES DESIGN AND SIMULATION*, training modules for Researchers, Volume 3. Brno University of technology. 60 pages. 2015.

[73] Cejpek J. *NAPĚŤOVĚ-DEFORMAČNÍ ANALÝZA SEGMENTU KOMPOZITOVÉHO KŘÍDLA*. 10 pages. Setkání uživatelů MSC.Software s.r.o. 2013. ISBN 978-80-260-4173-3.

[74] Cejpek J., Juračka J. *MODIFICATIONS OF A SIMPLE I- BEAM AND ITS EFFECTS ON THE STRESS STATE*. Aviation, 2016, 20, 4 pages 168-172. ISSN: 1648-7788.

[75] Cejpek J., Weis, M., Juračka, J. *ACOUSTIC EMISSION LOCALIZATION IN TESTING OF COMPOSITE STRUCTURES*. Applied Mechanics and Materials, Vol. 821, pp. 405-411, 2016

Software

[76] Počítačová podpora navrhování - GLAUERT III [online 2017-03-03] available at `https://www.vutbr.cz/vyzkum-a-vyvoj/publikace?action=detail&pub_id=31776`

[77] Numpy comunity *NUMPY REFERENCE RELEASE 1.11.0*. [online 2016-12-18] available at `https://docs.scipy.org/doc/numpy-1.11.0/numpy-ref-1.11.0.pdf`

[78] wxpython [online 2016-12-18] available at `https://wxpython.org/`

[79] py2exe [online 2016-12-18] available at `hhttp://www.py2exe.org/`

[80] How to Decrypt the MSC Nastran .bdf or .dat Input File [online 2016-07-29] available at `http://mscnastrannovice.blogspot.cz/2013/10/how-to-decrypt-msc-nastran-bdf-or-dat.html`

[81] Humusoft *CENÍK PRODUKTŮ SYSTÉMU MATLAB*. [online 2016-12-18] available at `http://www.humusoft.cz/DOCS/matlab.pdf`

[82] Production processes [online 2017-02-06] available at `http://www.composites.ugent.be/home_made_composites/organizing_your_composite_workshop.html`

List of Symbols

The lists of denotations is given only for symbols used in enumerated equations in chapter 4.

Denotation	Unit	Meaning
cos	$[-]$	cosin value of element geometry
no_{DOF}	$[-]$	number of Degrees of Freedom of the model
$noEl$	$[-]$	number of elements in the model
$noNod$	$[-]$	number of nodes in the model
q_{IK}	$[N/mm]$	shear flow from through thickness
q_O	$[N/mm]$	shear flow from torsion
r	$[mm]$	radius of gyration of the cross-section
sin	$[-]$	sinus value of element geometry
t_C	$[mm]$	core thickness
t_H	$[mm]$	upper flange thickness
t_D	$[mm]$	lower flange thickness
t_O	$[mm]$	wrap thickness
A	$[mm^2]$	cross-section area
B	$[mm]$	width
B_D	$[mm]$	lower flange width
B_H	$[mm]$	upper flange width
E_C	$[MPa]$	core stiffness
E_H	$[MPa]$	upper flange stiffness
E_D	$[MPa]$	lower flange stiffness
E_{EF}	$[MPa]$	element effective elastic modulus
FI	$[N]$	element longitudinal force
FJ	$[N]$	element lateral force
FK	$[N]$	element through-thickness force
JJ_C	$[mm^4]$	2^{nd} moment of area, core to neutral axis
JJ_H	$[mm^4]$	2^{nd} moment of area, upper flange to neutral axis
JJ_D	$[mm^4]$	2^{nd} moment of area, lower flange to neutral axis
JJ	$[mm^4]$	total 2^{nd} moment of area to lateral axis
JK	$[mm^4]$	2^{nd} moment of area to through-thickness axis
L	$[mm]$	length of an element
MI	$[N \cdot mm]$	element twisting moment
MJ	$[N \cdot mm]$	element lateral bending moment
MK	$[N \cdot mm]$	element bending moment
M_X	$[N \cdot mm]$	moment to X axis
M_Y	$[N \cdot mm]$	moment to Y axis
M_Z	$[N \cdot mm]$	moment to Z axis
NO	$[mm]$	position of neutral axis
R	$[mm]$	radius of the cross-section
R	$[mm]$	width of fuselage support
RF	$[-]$	reserve factor
S_K	$[mm^3]$	1^{st} moment of area at K
T	$[mm]$	thickness
T_X	$[N]$	shear force in X direction
T_Y	$[N]$	shear force in Y direction
T_Z	$[N]$	shear force in Z direction

Denotation	Unit	Meaning
α	$[-]$	shear correction factor
ϵ	$[\%]$	strain
μ	$[-]$	Poisson's ratio
σ_{TT}	$[MPa]$	through-thickness stress
σ_C	$[MPa]$	total stress at point C
σ_D	$[MPa]$	total stress at point D
σ_E	$[MPa]$	total stress at point E
σ_F	$[MPa]$	total stress at point F
σI	$[MPa]$	normal tensile/compression stress
σJ_{CD}	$[MPa]$	bending stress at CD edge
σJ_{EF}	$[MPa]$	bending stress at EF edge
σK_{CF}	$[MPa]$	bending stress at CF edge
σK_{DE}	$[MPa]$	bending stress at DE edge
τ_{IK}	$[MPa]$	shear stress trough thickness
τ_O	$[MPa]$	shear stress from torsion
ΔS_Ω	$[mm^3]$	slice addition to the 1^{st} moment of area
Φ	$[-]$	relative importance of the shear deformations
Θ	$[rad]$	characteristic angle of an element

List of Arrays

Denotation	Meaning
$[GS]$	Global Stiffness Matrix of an Element
$[GSM]$	Global Stiffness Matrix of the Model
$[LS]$	Local Stiffness Matrix of an Element
$[T]$	Transformation Matrix of an Element
$\{F\}$	vector of loading
$\{R\}$	vector of reactions
$\{U\}$	vector of displacements
$\{\epsilon\}$	vector of strains

List of Abbreviations

Abbreviation	Meaning
A	denotation of first node in the model
ASCII	American Standard Code for Information Interchange
ASTM	American Society for Testing and Materials
BDF	MSC.Nastran input data file
EL	element
C	compression
CAD	Computer Aided Design
CAE	Computer Aided Engineering
CFD	Computational Fluid Dynamics
CFRP	Carbon Fibre Reinforced Plastics
CLT	Classical laminate theory
CS-22	certification base issued by EASA for gliders
CSV	Comma-Separated Values data file
DB	database, MSC.Patran main data file
DOF	Degree Of Freedom
ESL	Equivalent Single Layer theories
F	Fibre
F	Force
FEA	Finite Element Analysis
FEM	Finite Element Model or Method
FI	Failure Index
FSDT	First-Order Shear Deformation Theory
GCS	Global Coordinate System
GFRP	Glass Fibre Reinforced Plastics
GUI	Graphical User Interface
HEX	Six-Sided Solid Element
HM	High Modulus
HS	High Strength
HSDT	Higher order Shear Deformation Theory
L	node where the loading is introduced
LLT	Layer-wise Lamination Theory
LSA	Light Sport Aircraft
IAE	Institute of Aeronautical Engineering
IGES	Initial Graphics Exchange Specification, CAD file format
ILSS	Inter-Laminar Shear Stress
INP	Abaqus input data file
MBS	Multi-Body System analysis
MCS	Material coordinate system
N	denotation of supported node
OPT	Optimisation
R	displacement: rotation
SOL	Solver of NASTRAN
STEP	CAD file format
STL	stereo-lithography CAD file format
T	Tensile
TXT	text file format
U	displacement: translation
UD	Uni-Directional
UAV	Unmanned Areal Vehicle

Glossary

- Deflection

Deflection is the distance that an object bends or twists from its original position.

- Deformation

Deformation is a resulting distortion in the material. It is the result of the externally introduced force.

- Displacement

Displacement is a vector that describes and quantifies the deflection.

- Mid-fibre

The mid-fibre is an intersection of two planes representing geometrical centre of the thickness and width along the length of an element.

- Validation

Validated data provides accurate and reliable information.

- Verification

Verification is a process of confirming that the process is correct.